STUDY OF RHEOLOGICAL PROPERTIES OF BIODEGRADABLE POLYESTERS

STUDY OF RHEOLOGICAL PROPERTIES OF BIODEGRADABLE POLYESTERS

By

DAMYAN KANEV, M.Eng.

A Thesis

Submitted to the School of Graduate Studies

In Partial Fulfillment of the Requirements

for the Degree

Master of Applied Science

McMaster University

Master of Applied Science (2007) McMaster University
(Chemical Engineering) Hamilton, Ontario

TITLE: Study of rheological properties of biodegradable polyesters

AUTHOR: Damyan Kanev
M.Eng. (UCTM, Bulgaria)

SUPERVISOR: Dr. John Vlachopoulos

NUMBER OF PAGES: xxi, 177

ABSTRACT

Biodegradable polyesters are considered as one of the most cost effective and environmentally friendly solutions to waste-disposal problems associated with traditional thermoplastics. The technologies for converting the resins into useful items require knowledge about the rheological properties of these materials. Adequate rheological models are essential for the design and optimization of the process technologies.

Rheological properties of two commercial biodegradable polyesters– poly(lactic acid) (PLA) and aliphatic-aromatic co-polyester (AAC) Ecoflex – have been investigated using parallel plate and capillary rheometers. Results from a study on the extrusion instabilities of biodegradable polymers are reported for the first time.

The experimental studies found that the biodegradable polyesters exhibit pseudo-plastic (shear-thinning) behaviour and the Cox-Merz rule is obeyed. A Cross model was proposed to describe their shear-thinning behaviour. The viscosity of both PLA grades is more temperature sensitive than the viscosity of Ecoflex. It was observed that the extensional viscosity of Ecoflex is larger than that of PLA and that the extensional viscosity of biodegradable polymers is similar to that of LLDPE.

The experimental results indicate that biodegradable polymer melts slip at the die wall. It was observed that with increasing shear rate PLA exhibits sharkskin and gross melt fracture while Ecoflex exhibits only gross melt fracture. With regards to flow instabilities PLA behaves like linear polyolefins, however without exhibiting stick-spurt phenomenon. While Ecoflex behaves like branched LDPE, its gross melt fracture starts at higher values of wall shear stress than LDPE. Both biodegradable materials exhibit small extrudate swell: up to 28% for PLA and up to 34% for Ecoflex, which is comparable to that of rigid PVC.

It was observed that biodegradable polymers substantially degrade during extrusion processing. It was also found that blending PLA and Ecoflex produced immiscible blends. Melts of these blends exhibited sharkskin and gross melt fracture at

higher shear stresses than the neat resins. This effect was attributed both to degradation during blending and to some sort of lubricating effect.

ACKNOWLEDGMENTS

I would like to express my most sincere thanks to:

Dr. John Vlachopoulos for his support, encouragement and guidance.

Velichko Hristov, for his advice and help in various areas of studies

Elizabeth Takacs for her support in the experimental procedures and for the helpful discussions

My wife, Margarita for her patience, understanding and love

Ghodratollah Hashemi, Xiaonan Qin, Hector Larrazabal, and Karen Rogers for the helpful discussions and sparks of humour which made the hard work enjoyable

All "the guys in the office" who were cooperative and understanding

My parents and brothers in Europe for their encouragement

My friends from 1st CRC – Hamilton who supported my family in various ways

TABLE OF CONTENTS

LIST OF FIGURES

LIST OF TABLES

NOMENCLATURE

Symbols

ϕ_0	angular amplitude
Ω	angular velocity in parallel plate rheometer
$\dot{\varepsilon}$	apparent extensional rate of strain
$\dot{\gamma}_T$	true shear rate without slip
$\dot{\gamma}_a$	apparent shear rate
b	temperature coefficient
D	diameter of the die in capillary rheometer
e	Bagley correction factor
F_z	total thrust in z direction in parallel plate rheometer
G'	storage modulus
G''	loss modulus
h	gap between the discs of parallel plate rheometer
L	length of a die in capillary rheometer
L/D	aspect ratio of a die in capillary rheometer
m	consistency index
m_0	consistency index at a reference temperature T_0
M_0	torque in parallel plate rheometer
M_n	number average molecular weight
M_w	weight average molecular weight
n	power law exponent
N_1	first (primary) normal stress difference ($\tau_{11} - \tau_{22}$)
N_2	second (secondary) normal stress difference ($\tau_{22} - \tau_{33}$)
Q	volumetric flow rate through a capillary
R	radius
T_g	glass transition temperature

T_m crystalline melting temperature

V_s slip velocity

V_s slip velocity

$\dot{\gamma}_w$ true (Rabinowitch corrected) shear rate

δ phase shift or "mechanical loss angle" in parallel plate rheometer

ΔP_{ent} entrance pressure drop

ΔP^L_{total} total pressure drop measured at the ends of the long die in capillary rheometer

ΔP^O_{total} total pressure drop measured at the ends of the orifice die in capillary rheometer

ΔP_{total} total pressure drop measured in capillary rheometer

η shear viscosity

η^* complex viscosity

η_e extensional viscosity

τ_w wall shear stress

$\tau_{w(true)}$ true (Bagley corrected) wall shear stress

Ψ_1 first normal stress difference coefficient

ω circular frequency in parallel plate rheometer

Abbreviations

AAC aliphatic-aromatic copolyester

DSC differential scanning calorimetry

GMF gross melt fracture

HDPE high density polyethylene

LDPE low density polyethylene

LLDPE linear low density polyethylene

MWD molecular weight distribution

PET poly(ethylene terephthalate)

PLA poly(lactic acid)

PMMA poly(methyl methacrylate)

PP	poly(propylene)
PS	poly(styrene)
PTFE	poly(tetrafluoroethylene)
PVC	poly(vinyl chloride)
SEM	scanning electron microscopy
SS	sharkskin
TTS	time-temperature superposition
WLF	Williams-Landel-Ferry model

CHAPTER 1

INTRODUCTION

1.1 Background

Plastics and polymers have become an integral part of the modern life. Annual worldwide production of polymers from fossil fuels is estimated to be more than 170 million tons (Vink et al., 2003). This fact raises concerns about the availability of the raw-materials for commodity plastics production and about the disposal of plastic waste. It is estimated that each year over 70 million tons of plastic are discarded into the global waste stream. One half of all discarded plastics comes from packaging, 60% of that being single-use packaging (Stevens, 2002). Biodegradable polymers, i.e. polymers which fully decompose under environmental factors and/or microbial attack are seen as a viable solution to the waste-disposal problems of traditional plastics. This is why a considerable amount of research effort has been channelled towards development of polymers which are biodegradable and synthesized from renewable sources. Today, biodegradable polymers from the polyester family are considered as a cost effective and environmentally friendly solution to waste-disposal problems associated with traditional thermoplastics. Although two biodegradable polyesters - poly(lactic acid) NatureWorks™ (PLA) and the aliphatic - aromatic copolyester (AAC) Ecoflex ™ – are commercially available, there is limited information about their rheological properties. This is a major non-cost related obstacle to the development and mass production of biodegradable plastic products.

1.2 Objectives and motivation

This research project is directed to meet the needs of the polymer processing science and industry for a systematic study of the rheological properties of biodegradable

polymers. Our rheological study focuses on the flow instabilities, which are critical for the industrial applications – wall slip, sharkskin, melt fracture and extrudate swell [Migler, 2005]. To our knowledge, there are no publications on the processing instabilities of the biodegradable polyesters. Hence, we believe that our project will contribute to the engineering of a more sustainable future for the humankind without sacrificing the achieved quality of life.

CHAPTER 2

LITERATURE REVIEW

2.1 Introduction to Biodegradable Polymers

The growing significance of biodegradable polymers both to industry and academia is reflected in a quickly expanding number of published papers and books. In his recent book Smith (2005) makes an excellent review of the state of the art in the field of research and application of biodegradable polymers. Mohanty *et al.* (2000) reviewed some mechanical properties and the market potential of various biodegradable plastics, biofibres and biocomposites. They also discussed the definitions of biodegradable polymers and the fact that a standard world-wide accepted definition has not been developed. Generally, biodegradation of polymers can be defined as a process of thorough chemical decomposition which is a result of enzymatic action or is associated with metabolic processes of living organisms (bacteria, fungi, etc.). It might also be accompanied or preceded by abiotic degradation reactions like hydrolysis, photodegradation and oxidation, which are due to environmental factors. Hence, biodegradation of a material is strongly influenced by polymer chemical structure and the environmental conditions (Mohanty *et al.*, 2000).

Unlike biodegradation, compostability of polymeric materials is a well defined standard concept. Main criteria for a polymer to be classified as a compostable are: 1) Complete biodegradability of the material in terms of standard tests such as ASTM D5338-98, ISO/CD 14855 etc. during the specified time period (usually 2-6 months). 2) No harmful effects of the compost on the aquatic and terrestrial organisms. (Mohanty *et al.* 2000).

A summary of ASTM testing methods for determining biodegradability is shown in Table 1.1.(adapted from Bhattacharya *et al.* 2005)

Table 1.1. Standard methods for estimating biodegradation of plastic materials

Test	Environment	Property Measured
ASTM D 5209-92	Aerobic sewage sludge	Carbon dioxide
ASTM D 5210-92	Anaerobic sewage sludge	Carbon dioxide, methane
ASTM D 5247-92	Aerobic specific microorganism	Molecular weight
ASTM D 5271-93	Activated sewage sludge	Oxygen, carbon dioxide
ASTM D 5338-92	Controlled composting	Carbon dioxide
ASTM D 5509-94	Simulated compost	Physical properties
ASTM D 5511-94	High solids anaerobic digestion	Carbon dioxide, methane
ASTM D 5512-94	Simulated compost using external heated reactor	Physical properties
ASTM D 5525-94	Simulated landfill	Physical properties
ASTM D 5526-94	Accelerated landfill	Carbon dioxide, methane
MITI Test	Mixed microbial	Oxygen

As all polymeric compounds, biodegradable polymers can be classified on the basis of their origin. We can distinguish completely biosynthetic, such as proteins, polysaccharides, starch plastics and polyhydroxyalkanoates (PHA), which are naturally produced by living organisms. At the other extreme are completely synthetic (chemosynthetic) degradable polymers (polybutylene succinate (PBS), polybutylene succinate adipate (PBSA), modified polyethylene terephthalate (PET)). In addition, there are polymers obtained from chemical polymerisation of precursors of which at least one is biosynthetic; these are classified as semibiosynthetic (i.e. polylactides (PLA)) (Steinbuchel, 1995).

Another important classification of biodegradable plastics is based on the age of their constitutive carbon atoms. Biobased plastics are defined as plastics in which carbon

comes from contemporary renewable resources. Plastics, which are synthesized from fossil resources, are considered non-biobased. Biobased content is determined according to ASTM D 6866 – 05 using radioactive C^{14} and Isotope Ratio Mass Spectrometry Analysis.

Polymers from the polyester family play a predominant role as biodegradable plastics due to their potentially hydrolysable ester bonds. Based on their molecular structure they are classified in two major groups – aliphatic (linear) and aromatic (containing aromatic rings) polyesters. Classified by their origin, aliphatic polyesters can be biosynthetic, semibiosynthetic and chemosynthetic, while the aromatic polyesters are completely synthetic.

Aliphatic polyesters are readily biodegradable but usually exhibit poor mechanical properties in comparison to their aromatic cousins. On the other hand, aromatic polyesters such as PET exhibit excellent material properties but they prove to be almost totally resistant to microbial attack. All polyesters degrade eventually, with hydrolysis (polymer chain scission induced by water) being the dominant mechanism.

There is a third group available – aliphatic-aromatic copolyesters(AAC), which are classified as chemosynthetic. AAC combine the biodegradable properties of aliphatic polyesters with the strength and performance properties of aromatic polyesters. Such a AAC is produced by BASF AG Germany, which is marketed under the trade name Ecoflex®.

2.2 Poly(lactic acid)

2.2.1 Structure and Commercial Production Methods

The most prominent aliphatic polyester is the polylactic acid (PLA). It has championed the researchers' interest because it is biodegradable aliphatic polyester, which can be produced from renewable resources (corn). In addition, its production requires 25-55 % less fossil fuel than conventional plastics and its properties are comparable to those of some petroleum-based polymers (Dorgan *et al.,* 2000; Lunt, 1998; Sinclair, 1996).

Poly(lactic acid) resin is produced by polymerizing of lactic acid (2-hydroxypropanoic acid). Lactic acid exists in two optically active isomers – L (or S)- and D (or R) –lactic acid. While mammalian organisms metabolize only L-lactic acid, bacterial systems produce both stereoisomers (Sodergard and Stolt, 2002). Lactic acid synthesized by bacterial fermentation of carbohydrates is mainly L- optical isomer. As a contrast, petro-chemically derived lactic acid is a racemic mixture of the two stereo isomers, which is optically inactive (Lunt, 1998). When polymerized, the dual chiral structure of lactic acid monomer allows for control over the stereochemical composition of the resultant polylactic acid. There are three technologies for industrial production of high molecular weight PLA resins: direct condensation polymerization, azeotropic dehydrative condensation and ring-opening polymerization of lactides. Most widely used is the ring – opening polymerization method, which permits tailoring the properties of the final product by controlling the ratio and the chain sequencing of L- and D- lactic acid units. (Auras *et al.*, 2004). The ring-opening polymerization method is patented by Cargill Inc. (US Patent 5142023, 1992). PLA produced by this technology is offered commercially by Nature Works LLC, USA.

PLA is normally a linear polymer (Auras *et al.*, 2004). However, branching can be introduced during polymerization or processing. Nature Works LLC use low levels of epoxidised natural oil during polymerization to produce branched PLA (Lunt, 1998).

Poly(lactic acid) molecule structure is shown on Figure 1.1.

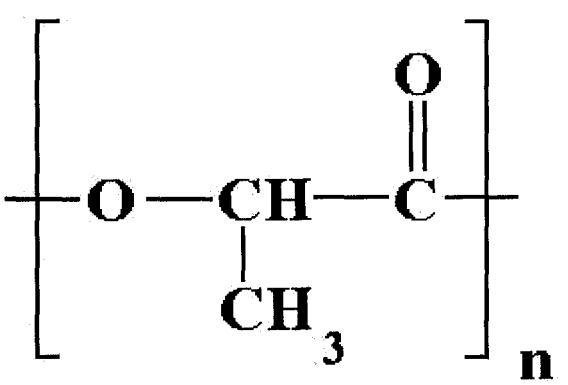

Figure 1.1. Structure of PLA molecule

2.2.2 Thermal and Thermodynamic Properties of Poly(lactic acid)

The effects of stereochemical composition on thermal, rheological and mechanical properties of PLA resins are well reported in the literature. The ratio of L-, D- and *meso-* lactides affects the percent of crystallization, its rate, and consequently, the crystalline melting point of the poly(lactic acid) polymers (Kolstad, 1996). Both pure L- and D- poly(lactic acid) homopolymers are semicrystalline. The reported values of their equilibrium crystalline melting point are about 207°C, but practically they melt at around 170 - 180°C due to presence of impurities, slight racemization and small and imperfect crystallites (Garlotta, 2002). Another interesting characteristic of PLA is the formation of a racemic crystallite (stereocomplex) when pure poly (L-lactide) and poly(D-lactide) are mixed in 50:50 ratio in solution or in melt. This stereocomplex has crystal melting point of 230°C and superior mechanical properties than either pure polymer. However, the stereocomplex formation in melt polymerization or crystallization is limited to low molecular weights of up to 6000 (Fukushima and Kimura, 2006, Tsuji, 2005).

Depending on the stereochemical composition, high molecular weight poly(lactic acid) can be produced either totally amorphous or up to 40% crystalline. PLA resins are semicrystalline when the L-lactic acid content is more than 95%. The resins are amorphous if PLLA content is in the range of 50-90% (Auras *et al.*, 2004). From design and processing point of view, one of the most important thermal characteristics of the amorphous polymers is their glass transition temperature, T_g because in the vicinity of T_g occur substantial changes in the polymer chain mobility. For semicrystalline PLA resins both T_g and the crystalline melting point are of utmost importance. Witzke (1997) investigated the thermal behaviour of high molecular weight amorphous polylactic acids. He observed that T_g of these polymers is around 58 °C. At temperatures below 58 °C, these polymers were brittle with signs of creep (physical ageing) in the range of -45 °C to 58 °C. For temperatures above T_g, the polymers became ductile and the transition region to viscous liquid was between 110 °C and 150 °C. Finally, it was observed that the amorphous PLA polymers decompose at temperatures of 215 – 285 °C.

Detailed knowledge about both the T_g and T_m of semicrystalline PLA resins is important for identifying their industrial applications. The glass transition temperature for semicrystalline PLA indicates the transition from brittle to ductile material properties. While the glass transition temperature depends on the inherent chemical structure of the amorphous phase, the crystalline melting temperature depends on both the stereochemical composition and the thermal history, i.e. the processing condition for producing the PLA resin. The maximum T_m of optically pure polylactides (both L- and D-), which could be practically obtained is around 180°C with an enthalpy of 40 to 50 $J.g^{-1}$ (Auras *et al.*, 2004). Presence of even small amounts of *meso*-lactide produced substantial reduction in the T_m of semicrystalline poly(lactic acids), which followed the rule: T_m (°C) ≈ 175 °C – $300W_m$, where 175°C is the T_m of pure poly-L-lactic acid, and W_m is the weight fraction of *meso*-lactide, introduced during polymerization (Auras, 2004; Witzke, 1997). By this method can be obtained reduction of the crystalline melting point to as low as 130°C (Lunt, 1998). Introducing of D-lactide to the polymer structure can easily depress the melting point by 20 to 50 °C (Auras, 2004). Thermal properties of two commercial PLA resins were studied through Differential Scanning Calorimetry (DSC) by Fang and Hanna (1999). The amorphous grade (of stereochemical composition 82% L-lactide and 18% D-lactide) had T_g of 58°C and T_m of 148°C. The T_g and T_m of the semicrystalline resin (L- to D- lactide ratio 95:5) were 62°C and 151°C, respectively. Dorgan *et al.* (2000) reported the thermal properties of linear and branched PLA commercial polymers with L- to D-lactide ratio 96:4. The crystalline melting temperature was 152.6 ± 0.3 °C and the glass transition temperature was found to be 58.4 ± 0.3°C. It was also concluded that the chain architecture did not significantly affect the transition temperatures. However, it did affect the rate of crystallization – the branched material crystallized faster than the linear. Four commercial polylactide grades were studied by Cooper-White and Mackay (1999) and the T_g reported were in the range of 54 - 60°C, and the T_m ranged from 178 to 186°C. The authors also calculated the percent crystallinity of the PLLA samples subjected to DSC scans using a reference heat of fusion ($\Delta H'_m$) of 93.1 J/g for 100% crystalline PLLA.

Using adiabatic calorimetry and DSC, Pyda *et al.* (2004) investigated the thermodynamic properties of three commercial semi-crystalline PLA resins with L- to D-ratios of 98.5: 1.5, 92:8 and 84:16. They reported T_g values of 57 – 60°C and equilibrium melting temperature of 207°C. The experimental heat capacity of liquid state PLA was expressed as a linear function C_p(liquid) = 120.17 + 0.076T [$J.K^{-1}.mol^{-1}$], where T > T_g is the temperature in Kelvin. Tabulated values for C_p(solid) are also reported. The changes of heat capacity (ΔC_p) at T_g = 60°C for 100% amorphous PLLA was reported to be 38.4 $J.K^{-1}.mol^{-1}$. For 100% crystalline PLLA the heat of fusion ($\Delta H'_m$) of 91±3 J/g was reported. Auras and coworkers (2004) reported the thermodynamic properties of two commercial grades polylactides with optical isomer ratio L-lactide to D-lactide of 98:2 and 94:6. For grade PLLA 98% and 40% crystallinity, were reported T_g = 71.4°C, T_m = 163.4°C, $\Delta H'_m$ = 37.5 J/g. For PLLA resin (94% L-stereoisomer) and 25% crystallinity, were reported T_g = 66.1°C, T_m = 140.8°C, $\Delta H'_m$ = 21.9 J/g.

2.2.3 Rheological Properties of Polylactides

Rheological properties of PLA polymers affect the choice and design of methods for their melt processing as well as the mechanical properties of the final product (Dealy and Wissbrun, 1990). Generally, the rheological behaviour of polylactides is similar to that of polystyrene (Auras *et al.*, 2004). Fang and Hanna (1999) reported results of shear viscosity measurements for an amorphous (L-PLA to D-PLA ratio of 82:18) and a semicrystalline (containing 95% L-PLA) commercial PLA resins. Shear viscosity as a function of shear rate and at 150°C and 170°C was measured by tube rheometer attached to a laboratory extruder. They observed that both PLA grades behave as pseudoplastic (shear-thinning) non-Newtonian fluids and fitted the experimental data to a power law model. The authors reported that the semicrystalline PLA had lower viscosity than the amorphous grade and that shear viscosity of both grades decreased as the temperature increased. Ramkumar and Bhattacharya (1998) studied the steady and dynamic rheological properties of two commercial grades of PLA with varying degree of crystallinity (L-PLA and D,L-PLA). Using cone and plate rheometer they measured steady shear viscosity (η), first normal stress difference (N_1), dynamic moduli (G', and

G"), and complex viscosity (η^*) at temperatures 170°C, 180 °C and 190 °C. Thermal degradation rate constants of PLA at each temperature were determined using the time sweep mode of the cone and plate rheometer. High shear rate measurements of the steady shear viscosity were measured with capillary rheometer at temperature 170 °C. It was reported that D,L-PLA (lower L-lactic acid content) had higher values of all rheological properties (η, Ψ_1, G' and G"), which was attributed to the higher molecular weight of the D, L resin. Although no data for Ψ_1 was provided, it was stated that the D,L- PLA exhibited more elasticity than the high L-content grade. Validity of the Cox-Merz rule was reported based on the overlap of viscosity curves obtained by steady and dynamic cone and plate measurements after correcting for thermal degradation. The capillary viscosity data presented suggested that validity of the Cox-Merz rule could not be implied. Palade *et al.* (2001) performed a comprehensive study on melt rheology of commercial PLA high L-content (L:D ratio 96:4 and 98:2). Using capillary, parallel plate and cone and plate rheometers, they measured steady, dynamic and transient shear viscosities. They investigated the effects of thermal degradation and chemical stabilization on rheological properties of PLA. Contrary to the conclusions of Ramkumar and Bhattacharya (1999), Palade *et al.* observed that the samples having higher content of the D-PLA were characterized with lower zero shear viscosity than those with less or zero D-content PLA. These authors reported that plateau modulus G_N^0 value approached $5x10^5$ Pa. Extensional viscosity data was presented for the first time. It was observed that PLA exhibited strain hardening of the extensional viscosity by two orders of magnitude and an ability to draw samples without melt breaking to Hencky strains of 10, which are unusually large for linear polymers. This extensional phenomenon was explained with presence of a small fraction of high molecular weight PLA. An attempt to model the nonlinear rheological behaviour of PLA was made by using a truncated K – BKZ constitutive equation. The model reportedly predicted well the experimental values of the steady state viscosities. However, it did not produce adequate predictions for the extensional viscosity.

Dorgan *et al.* (1999) reported that PLLA melts with 98% L-content have a critical molecular weight for entanglement M_e of approximately 9000 g/mol and the molecular weight for branch entanglement M_b of around 34 600 g/mol. The dependence of the zero shear viscosity η_0 on the molecular weight was found to be increasing to the power of 4.6. On the other hand, for commercial PLLA resins it was found that M_e is about 16 000 g/mol, and the dependence of η_0 on molecular weight to the fourth power (Cooper-White and Mackay, 1999).

Rheological study of the melt properties of poly(lactic acid) with L-content ranging from 50% to 100% and different molecular weight distributions was conducted by Dorgan *et al.* (2005). It was concluded that PLA behaves as a typical linear glass-forming polymer. The authors argued that the PLA brittleness is a result of rapid physical aging of the PLA polymer during cooling from melted state, since room temperature is only about 25°C below its glass transition temperature. It was reported that for reference temperature 180°C and weight average molecular weight range of 10^5-10^6 [g/mol], the zero-shear viscosity is independent of stereochemical composition and might be modeled by the equation $\log(\eta_0)= -14.26+3.4 \log(M_w)$. The plateau modulus was measured to be 1.0±0.2 MPa, the average WLF parameters were $c_1= 3.24$ 1/K and $c_2= 164.9$ K. The critical molecular weight for entanglement, M_c was reported to be near 9000 g/mol and the molecular weight between entanglements, M_e was around 4000 g/mol.

Time Temperature Superposition (TTS) Principle was employed to capture the flow behaviour of PLA melts over wider ranges of frequency and temperatures than those of the rheometers used in the experiments (Cooper-White and Mackay (1999), Palade *et al.* (2000), Lehermeier and Dorgan (2001), Dorgan *et al.* (2005)). Then, the horizontal a_T and the vertical b_T temperature shift factors, calculated from the TTS procedure were used to calculate the flow activation energies E_H and E_V for the studied PLA polymers from Arhenius-type equations.

Yamane *et al.* (2004) studied the effect of introducing small amounts of D-poly(lactic acid) in a matrix of commercial L-PLA. They conducted dynamic and steady rheological experiments using parallel plate rheometer. It was observed that the addition

of D-PLA isomer resulted in increase of steady zero shear viscosity, complex viscosity, G', and G". Yamane and coworkers also measured biaxial extensional viscosities of the PLLA/PDLA blends. Again, addition of PDLA caused increase in the strain hardening behaviour of the blends compare to the neat PLLA resin. Based on the rheological measurements, the authors suggested that addition of D-stereoisomer of PLA to matrix of poly(L-lactic acid) produces a stereocomplex crystallite, which acts as a crosslinking point of PLLA chains causing increase in the apparent molecular weight, broadening of the molecular weight distribution and introducing of long chain branching.

Effects of blending linear and branched commercial grades of PLA (containing 96% L- enantiomer) on their rheological behaviour were investigated by Lehermeier and Dorgan (2001). The authors used both parallel plate and capillary rheometers. It was observed that while the Cox-Merz rule is valid for the linear molecular architecture and most of the blends, it does not hold for the branched grade. It was reported that when branched content was increased, both the elasticity (i.e. the recoverable shear compliance) and the zero shear viscosity were also increased. Apparent shear viscosity of the blends approximately followed a log additivity mixing rule. TTS plots of the stress relaxation modulus showed that introducing branched content increased the time for reaching a plateau modulus value. Results from tensile testing of the blends showed no statistically significant difference between the branched, the linear and the blended samples. In another paper Dorgan *et al.* (2000) reported that the branched PLA (L-content 96%) had larger zero shear viscosity compared to same stereochemical composition linear material but exhibited larger degree of shear thinning. Based on the viscoelastic behaviour was suggested that the branched PLA structure can be modeled by a four-arm star with asymmetric arms (i.e. possessing large difference in arms' molecular weight).

Lunt (1998) reported that some increase in PLA melt elasticity could be achieved by controlling the molecular weight distribution of PLA polymers. When polydispersity (measured as Mz/Mn) varied from 3.8 to 6.1, die swell ratio ranged from 1.28 to 1.4.

2.3 Aliphatic-aromatic copolyester Ecoflex

2.3.1 Structure and Commercial Production Methods

Ecoflex is a biodegradable aliphatic-aromatic copolyester (AAC) based on the monomers:1,4- butanediol, adipic acid, terephtalic acid and modular units of sebacic acid, succinic acid and 1,3 propanediol (Yamamoto *et al.*, 2002). Ecoflex has properties similar to low density polyethylene (LDPE) because of its high molecular weight and its branched molecular structure (BASF, 2005). Its production is based on conventional bulk condensation polymerization of aliphatic diols with a controlled mixture of aliphatic dicarboxylic acids and terephthalic acid (Bhattacharya *et al.*, 2005). There are several international patents regarding the biodegradable copolyester of BASF (WO 96/15173; 96/15174; 96/21689). BASF implemented a modular approach for adding hydrophilic monomer components as branches to the linked statistical copolyester units of 1,4-butanediol, adipic acid and terephthalic acid. Thus, not only control over the molecular weight, the morphology and the properties of the aliphatic-aromatic copolyester, is achieved but also successful integration in BASF's manufacturing system and economies of scale (Yamamoto *et al.*, 2002). A representative molecular structure is shown on Fig 1.2, which is adapted from (Witt *et al.*, 2001)

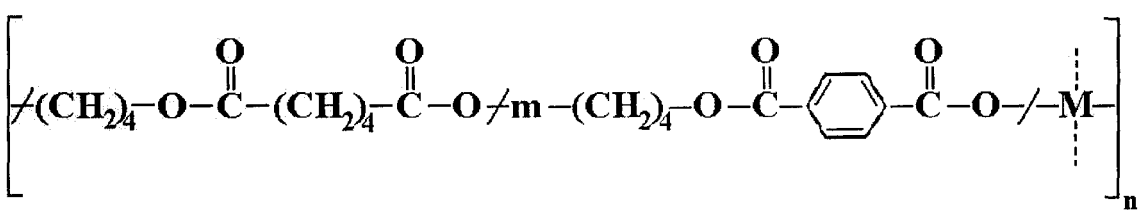

Figure 1.2. Structure of Ecoflex F BX 7011. M and m represent monomers with branching and chain extension effect, respectively.

2.3.2 Thermal and Rheological Properties of Ecoflex

While there are numerous publications concerning PLA, there are just a few on the aromatic-aliphatic copolyesters (AAC) probably because those are obtained from

non-renewable fossil fuel resources. Yet, plastics based on AAC may stir the researcher's interest in the near future since there are reports on various synthesis routes to produce them from totally renewable resources like glucose and saccharose (Heufel, 2005). In addition, they have certain properties, which make them more easily processable than their aliphatic counterparts. Hence, they can also serve as performance enhancers for other biodegradable plastics from renewable resources (Heufel, 2005; Scherzer, 2005)

Yamamoto *et al.* (2002) reported DSC obtained values for the glass transition temperature of Ecoflex® - T_g= -30°C. The crystalline melting temperature T_m of Ecoflex was reported to range from 110°C to 115°C. Jiang *et al.* (2006) measured T_m of a commercial film grade Ecoflex by applying different heating rates. It was found that at heating rate 10°C/min, T_m was approximately 122°C. T_m=120°C was measured at heating rate 5°C/min.

To our knowledge, there are no comprehensive publications on the rheological properties of AAC but one can obtain some rheological data (i.e. viscosity curves at different processing temperatures) from the manufacturer of Ecoflex – BASF AG. A representative plot of viscosity as a function of shear rate (from $0.1 s^{-1}$ to $100 s^{-1}$) at temperatures 140 °C, 160 °C, 180 °C, 200 °C and 230°C is presented by Yamamoto *et al.* (2002). As part of their study on the polylactide/ Ecoflex blends, Jiang *et al.* (2006) presented limited steady and dynamic rheological data obtained by parallel plate rheometer at temperature 180°C. The authors observed that Ecoflex does not exhibit typical relaxation behaviour. Instead of being function of squared frequency, the Ecoflex storage modulus G' was function of frequency to power 1.24 ($G' \sim \omega^{1.24}$), which was explained with the broad molecular weight distribution of Ecoflex. Only one steady viscosity curve at shear rates from $0.05 s^{-1}$ to $50 s^{-1}$ was reported. Neither investigation of validity of Cox-Merz rule (Cox and Merz, 1958) was done, nor study on the effect of temperature on rheological properties was performed.

Although some literature sources state that the aromatic polyester monomers are resistant to microbial attack (Ki and Ok Park, 2001), the aliphatic-aromatic copolyester Ecoflex is totally biodegradable and compostable. The biodegradation of Ecoflex was

studied by U. Witt *et al.* (2001) who found that it depolymerises by 99.9% during 22 days of degradation and it does not incur ecological risks on the composting process or environment.

2.4 Biodegradable PLA blends

With regards to its mechanical properties, PLA resembles polystyrene. PLA has good strength (i.e. high modulus) but low toughness (characterized by low elongation at break) (Dorgan *et al.*, 2001). Figure 1.3 presents a comparison of the mechanical properties of PLA with those of some commodity plastics. Its brittleness is due to its inherent structure and to its rapid physical ageing (Dorgan *et al.*, 2005). Several strategies are being employed to increase the toughness of PLA: plasticizing PLA with biocompatible plasticizers, blending PLA with other polymers (both common and biodegradable) or copolymerizing PLA with suitable monomers. Making PLA nanocomposites is another venue for modifying PLA mechanical properties. Using fillers for improving PLA strength is also largely investigated area.

Various chemicals were used as plasticizers to modify PLA properties: citrate esters, poly(ethylene glycol), glucosemonoesters, partial fatty acid esters, oligomeric lactic acid and glycerol . Toughness and resilience of plasticized PLA were improved in comparison with the neat PLA resins (Martin and Averous, 2001). Since plasticization of PLA is beyond the scope of the present work, several papers are referred: (Labrecque *et al.* 1997; Martin and Averous, 2001; Ljungberg and Wesslen, 2002; Pillin *et al.*, 2006; Ren *et al.*, 2005; Zhang and Sun, 2005).

Grijpma *et al.* (1991) and Hiljanen-Vainio *et al.* (1996) demonstrated that copolymerizartion of PLA and ε-caprolactone produced significant increase in elongation

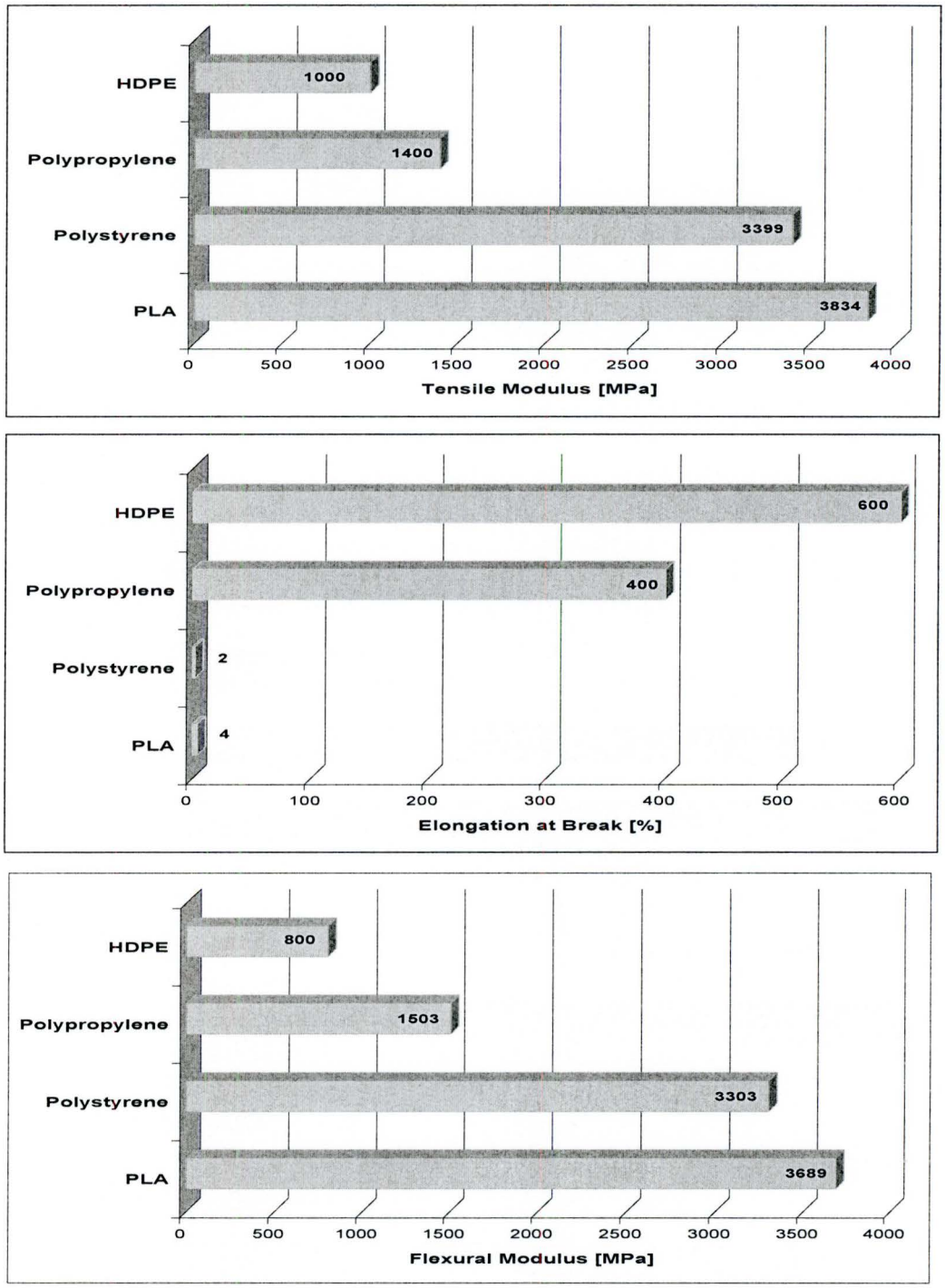

Figure 1.3. Comparison of the mechanical properties of PLA with some conventional plastic packaging materials, adapted from Dorgan *et al.* (2000)

at break, which depended on the amount of ε-caprolactone. Buchholz (1993) reported that copolymers of PLA and trimethylene carbonate are characterized with reduced modulus and tensile strength but elongation of the copolymer reached up to 900%. By ring-opening copolymerization. of L-lactide (LA) with DL-b-methyl-d-valerolactone (MV) Nakayama *et al.* (1995) synthesized new biodegradable polyesters for medical applications. It was observed that when L-lactide content was below 80% the copolymer films were as flexible as natural rubber. Extensive toughening was reported as a result of copolymerizing poly[(trimethylene carbonate)-co-(e-caprolactone)] and lactide (Joziasse *et al.*, 2000). Storey *et al.* (1994) synthesized PLA based poly(ester-uretane)s, which were characterized with improved toughness in comparison to neat PLA – ultimate elongation at break reached up to 600%.

Another approach to improving the mechanical and gas barrier properties of PLA is to produce nanocomposites using nanoclays, organically modified layered silicate, synthetic mica, and microcrystalline cellulose. The reader is referred to several papers, which give an in depth look into the broad and exciting field of PLA nanocomposites (Ray *et al.*, 2003; Petersson and Oksman, 2006; Di *et al.*, 2005; Lewitus *et al.*, 2006; Ray and Bousmina, 2005). An excellent review on the use of inorganic or organic fillers, as well as various fibers in order to modify PLA material properties is presented by Zhang and Sun (2005). Additional information on PLA/natural fiber composites can be found in Huda *et al.* (2006), Oksman *et al.* (2003), Shanks *et al.* (2006), Serizawa *et al.* (2005) and Yu *et al.* (2006). Study of the reactive compatibilization of PLA and cellulosic fibers and properties of the formed microcomposites was reported by Braun *et al.* (2006).

Blending with other polymers is an approach, which is of particular industrial interest. Attempts to develop low cost, degradable thermoplastics with properties similar to those of conventional thermoplastics by blending PLA and nonbiodegradable polymers resulted in immiscible or partly miscible systems, which needed morphology stabilization by compatibilizers. Blending of PLA and LDPE or LLDPE produced improved toughness of PLA matrix, especially when block copolymers (PE-*b*-PLLA) were used as compatibilizers (Wang and Hillmyer, 2001; Anderson and Hillmyer, 2004; Omura *et al.*,

2006; Anderson *et al.*, 2003). Sheth *et al.* (1997) reported that blends of PLA and poly(ethylene glycol) (PEG) range from miscible to partially miscible, depending on the fraction of PEG added and that in amounts smaller than 50% PEG acts as plasticizer, improving the elongation at break of PLA. Polylactide blends with other nonbiodegradable polymers – polystyrene (Biresaw and Carriere, 2002), polyethylene oxide (Nakafuku *et al.*, 1993), poly(vinyl acetate), poly(4-vinilphenol), poly(ethylene-*co*-vinyl alcohol) and polyacrylates are also reported in the literature (Jiang *et al.*, 2006; Zhang and Sun, 2005; Lee *et al.*,2005). It is important to note that commercial application of blends of polylactides and nonbiodegradable polymers is likely be very limited due to the fact that partially degraded conventional polymer chains showed elevated eco-toxicity, according to resent research (Narayan, 2006).

Blends of poly(lactic acid)s with different stereo-isomeric composition or structure were extensively studied. Zuideveld *et al.* (2006) reported that blends of linear and branched (dendritic) PLLA exhibit complete miscibility. However the mechanical properties of the blends are reduced with the increase of the degree of branching or the amount of the dendritic PLLA component. It is also known that when PLAs with different stereoisomer proportions are blended, stereocomplex crystallites are formed. This phenomenon results in improved mechanical properties and an increase in crystalline melting temperature (Jiang *et al.*, 2006;Tsuji and Fukui, 2003; Tsuji, 2005).

Blends of poly(lactic acid) with other biodegradable polymers has attracted both commercial and academic attention. Morphology of melt-mixed blends of PLA and poly(butylene succinate) (PBS) were studied by Park and Im, (2002). They reported that the blends are miscible in the amorphous phase. However, they also observed that crystallization induced phase separation occurs for PBS content of more than 40%. Recently, Ma *et al.* (2006) reported that blends of PLA and the aliphatic biodegradable polypropylene carbonate (PPC) are partially miscible. Based on tensile mechanical testing, DSC, DMA and SEM, it was concluded that the blends are compatible, exhibit strong interfacial adhesion and phase separation occurs when PLA content is between 60 and 70 wt%. Partial miscibility was suggested for blends poly(lactic acid)/ poly(glycolic

acid) (PGA) (Nakafuku andTakehisa, 2004). Wu and Liao (2005) studied blending of PLA and hyaluronic acid, which they found are immiscible and the mechanical properties of the blends were worse than those of PLA It is reported that PLA/poly(ε-caprolactone) (PCL) blends are immiscible but compatibilizers as poly(LA-*co*-εCL) effectively stabilize the morphology of the blends (Kim *et al.*, 1999; Jiang *et al.* ,2006). It was also observed that elongation at break of PLA was substantially increased, even when small amount of PCL was introduced (Zhang and Sun, 2005). Another group of biodegradable polyesters, which has been extensively studied with regards to blending with PLA is that of polyhydroxyalkanoates, which are biologically synthesized in bacterial cultures (Chen, 2005; Satkowski *et al.*, 2002). Blends of PLAs and commercially available PHAs are of particular interest because PHAs can improve the ductility of PLA. Noda *et al.* (2004) investigated properties of PLA/PHA (Nodax^{TM}) blends by a standard set of polymer characterization procedures. Tensile mechanical tests showed improved toughness (measured as energy to break) of the blends containing up to 20 wt% PHA. When PHA fraction was increased to 30 wt% and more, rapid drop in toughness was observed. These results were explained with the amount of PHA crystalline fraction. When PHA was less than 20 wt%, it remained in amorphous state, even at room temperatures. The increase in PHA content lead to formation of PHA crystallites, which reduced ductility of the blends (Noda *et al.*, 2004). Dynamic and extensional rheological properties of PLA/PHA blends (PHA content up to 20 wt%) were studied by Eickhoff and Harrison (2006). The blends were prepared in twin screw extruder without using compatibilizers. Complex viscosity curves of the blends obtained at temperatures 165°C were compared with complex viscosity curves of neat PHA (at T=155°C) and of neat PLA (at T=180°C). It was concluded that the increase of PHA content results in stronger shear thinning, and that PLA/PHA 90/10 viscosity curve has similar slope as PLA. The extensional behaviour of both PLA/PHA blends resembled that of neat PLA, which is characterised with a large degree of strain hardening (Eickhoff and Harrison, 2006).

In quest for obtaining low cost biodegradable plastics with satisfactory properties, poly(lactic acid) polymers are blended with starches. Since there is vast amount of

information available, and this topic is beyond the scope of the present work, the reader is referred to several excellent review articles on PLA/starch blends: (Yu *et al.*, 2006; Halley, 2005, Zhang and Sun, 2005), and several recent publications (Zhang and Sun, 2004; Ohkita and Lee, 2006; Chapleau *et al.*, 2006; Huneault and Li, 2006)

Jiang *et al.* (2006) produced PLA/PBAT (i.e. Ecoflex) blends using a twin screw extruder. Ecoflex content of the blends was from 5 wt% to 20 wt%. They investigated the thermal properties of the blends by using dynamic mechanical analysis (DMA) and differential scanning calorimetry (DSC). Results of DMA showed that all the blends form two-phase systems characterized with two glass transition peaks: -30°C for Ecoflex and 60°C for PLA. Varying PBAT concentration did not substantially influenced glass transition temperatures, which indicated insignificant interaction between polymers. Based on the DSC analysis using heating rates of 5 °C/min and 10°C/min the authors concluded that the presence of PBAT increased the crystallization rate of PLA but did not increase the amount of PLA crystallinity in the blends. It was also observed that at the lower scanning rate, the blends have bimodal melting peak while at rate of 10°C/min only PBAT 5% blend exhibited two melting peaks. The DSC thermograms showed that the PLA/PBAT blends have narrower cold crystallization peaks and lower peak temperatures than pristine PLA, suggesting accelerated cold crystallization of PLA. Jiang *et al.* (2006) presented steady and dynamic rheological data obtained by parallel plate rheometer at temperature 180°C. It was observed that PLA/PBAT blends were characterised with higher shear viscosities and smaller Newtonian regions than the neat PLA. The tensile mechanical testing of injection molded specimens demonstrated improved toughness of the blends (measured as strain at break) from 3.7% for neat PLA to 200% for PBAT 20% blend. While the tensile strength and modulus decreased, the impact strength of the blends raised with the increase of PBAT content. Fractured by tensile stress samples were subjected to scanning electron microscope (SEM) analysis to study the toughening mechanism of PLA/PBAT blends. It was suggested that the tensile stress induced debonding of the round PBAT particles from the PLA matrix, which resulted in ductile instead of brittle fracture; thus increased toughness was observed.

2.5 Flow Induced Instabilities during Polymer Extrusion

2.5.1 Introduction

During extrusion polymer melts are subjected to large stresses which give rise to various instabilities phenomena. The occurrence of processing instabilities is not only limiting the production rates in industrial operations but also imposes constraints on the development and market acceptance of new polymer resins (Hatzikiriakos and Migler, 2005). Although polymer flow instabilities have been extensively studied for more than 60 years (Tadmor and Gogos, 2006), they still represent one of the unresolved issues in viscoelastic fluid mechanics (Denn, 2001).

When polymers are extruded through a die at low throughput rates, the resultant extrudates have smooth surface. However, extrudate irregularities appear when throughput rates are increased. Usually, the first melt flow instability occurs at some critical value of the wall shear stress (around 0.14 MPa) and it manifests itself as surface distortion, mattness or loss of glossiness of the extrudate (Vlachopoulos, 2005). Sometimes this low stress instability, called "sharkskin", is accompanied or followed by oscillating flow (Denn, 2001), which produces the so called "stick-spurt" extrudate defect, characterized by alternating smooth and rough regions (Agassant *et al.*, 2006). When the throughput rate is further increased, the extrudate distorts heavily. This phenomenon is called gross melt fracture (Dealy and Kim, 2005; Agassant *et al.*, 2006). It is important to note that not all polymers exhibit sharkskin instability. Branched polymers, and some linear polymers, (for example, PS) develop periodic instabilities immediately after the smooth extrudate region. Characterised with periodicity and helical shape, these instabilities appear different from sharkskin and stick-spurt. They are called upstream or volume instabilities (Agassant *et al.*, 2006, Dealy and Kim, 2005).

Polymer melts are non-Newtonian liquids, which exhibit viscoelastic behaviour High viscosity, normal stress and elasticity, dependence of viscosity on rate of deformation, strong extensional viscosity and tendency to slip at wall surface are some of the characteristic phenomena observed in polymer flows. During extrusion polymer liquids are subjected to large and rapid deformations (for example, when entering or

leaving a capillary die) and the viscoelastic polymer nature is considered as the root cause of the above mentioned flow instabilities (Dealy, 2005).

2.5.2 Wall Slip

One of the phenomena, which distinguish polymer from Newtonian fluids, is wall slip (Vlachopoulos, 2005). Wall slip is a violation of the classical assumption that at static solid surfaces the fluid velocity is of zero magnitude. While violations of no-slip boundary condition have been rarely observed in simple liquids, it is common for polymer fluids (Hatzikiriakos and Migler, 2005). Archer (2005) reviewed the state of the scientific knowledge in measuring and characterising the wall slip phenomenon in polymer flows. He classified the slip violations as true slip, which is due to adhesive failure at polymer-solid interface, and apparent slip, which is due to failure at polymer-polymer interface at distance one or more molecular diameters away from the polymer-solid boundary. Near two decades of research on the relation between wall slip and extrusion instabilities was discussed in a review article by Denn (2001). He concluded that although violation of no-slip condition accompanies or precedes onset of sharkskin, there is no convincing evidence that there is cause-and-effect relationship between slip and polymer processing instabilities.

2.5.3 Sharkskin and Stick-Spurt Instabilities

The actual cause of sharkskin is still a controversial topic (Migler, 2005). However, it is widely accepted that this instability is a die exit effect, which is caused by a localised stress concentration (Agassant *et al.*, 2006). According to Agassant *et al.* (2006) there are two major schools of thought explaining the mechanism of sharkskin. The first of them was started by Cogswell (1977) who proposed that the surface of the polymer melt fractures due to development of large extensional stresses, which result from rapid acceleration of the surface polymer layer from near zero velocity to the final extrudate velocity. In order to obtain fractured extrudate surface, these stresses should be larger than a characteristic for the tested polymer tensile strength value. When the polymer surface is fractured, a momentary stress relaxation occurs, which explains the

cyclic appearance of sharkskin (Agassant *et al.*, 2006). References of papers which are consistent with the Cogswell analysis and discussion on the method may be found also in Migler (2006). Resent results from laser-Doppler velocimetry with slit dies are reported in (Agassant *et al.*, 2006), which suggest that not only the absolute magnitude of the exit acceleration but also its localisation are important for the obtaining of fractured extrudate surface. The authors also concluded that partial wall slip will reduce the intensity of sharkskin but cannot eliminate it thoroughly.

The second theory about sharkskin mechanism is that of local stick-slip at die exit. It was originally proposed by Vinogradov *et al.* (1972) (Migler, 2005). The original theory stated that since stress at die exit is larger than wall shear stress, it more rapidly reaches a critical value above which slip occurs. This slip is only localised in the exit of capillary die and causes less swell of the extrudate. Hence, in local slip regime a valley in the extrudate surface is observed and a stress relaxation occurs until stick regime returns. Stresses at die exit are being built up again, which causes increase in swell, and the system oscillates between the two regimes of localised stick and slip (Migler, 2005). The latest development in this theory considers sharkskin instability as a result of exit slip-stick phenomena, due to melt/wall interactions on a molecular level (Agassant *et al.*, 2006). It is proposed that at die exit the adsorbed polymer molecules are being stretched and they disentanlgle from the bulk polymer molecules, which produces periodic stick to slip transitions (Agassant *et al.*, 2006). A discussion on the advantages and the limitations of exit stick-slip theory can be found in Migler (2005) who seems to favour a theory, which is a blend of the Cogswell and exit stick-slip ideas.

The effects of the molecular interactions at polymer/die interface on the onset of extrusion instabilities were investigated in detail by Larrazabal *et al.* (2006). The authors studied a large number of polymer/die interfaces to determine a relationship between the work of adhesion and the critical shear stress for the onset of flow instabilities. It was found that for work of adhesion less than approximately 30 mN/m (corresponding to polyolefin/ Teflon, boron nitride, chromium and nickel coated steel systems), there is a linear relationship between the two parameters, and that adhesive failure at the interface

represents the underlying mechanism of the instabilities phenomena. For values of work of adhesion larger than 30 mN/m (corresponding to dies made from steels and brasses) the relationship between work of adhesion and the critical shear stress is non-linear. In these cases, cohesive failure mechanism (Migler *et al.*, 2001), which considers chemisorption and mechanical interlocking at the interface will be more suitable for explanation of the onset of flow instabilities.

In a resent article, Son and Migler (2002) studied the hypothesis that sharkskin fracture results from a cavitation due to negative stresses developed in the melt near the three phase line polymer-wall-air. They observed that cavitation occurs only in gross melt fracture regime and that the die exit region serves as an initiation site.

The stick-spurt instability is characterised by a unstable flow in which the flow rate and the wall shear stress oscillate substantially and the extrudate is characterized by alternating smooth and distorted regions. It is considered to result from wall slip along the die land (Agassant *et al.*, 2006). An excellent summary on this instability can be found in (Georgiou, 2005).

The methods of minimizing sharkskin and stick – spurt instabilities are reviewed in (Agassant *et al.*, 2006; Hatzikiriakos and Migler, 2005). While introducing curvature at die exit and coating the die with low surface energy coatings such as PTFE are reported in the literature, the most effective method to obtain extrudate without surface defects is the utilization of processing additives such as fluoropolymers and Boron Nitride (Agassant *et al.*, 2006). The traditional processing aids – fluoropolymers and stearates act as lubricants at polymer/die interface and postpone sharkskin and stick-spurt instabilities to higher shear stresses (Kharchenko *et al.*, 2005).

2.5.4 Volume and Gross Melt Fracture Instabilities

It is widely recognized that volume instabilities (gross melt fracture being a specific case) result from severe flow destabilization at die entrance and other factors. Gross melt fracture (GMF) was observed even when no capillary was attached to a converging die and die material did not have substantial effects on the onset of GMF (Dealy and Kim, 2005). It is reported in the literature, that GMF onset depends on die

geometry (die aspect ratio and convergence angle) and molecular structure of the polymer (presence of long-chain branching and polydispersity index M_w/M_n) (Dealy and Kim, 2005). The exact mechanism for volume instabilities (including GMF) is still debatable and the three possibilities discussed in the literature are associated with upstream vortices, with high elongational deformations and large viscoelastic stress level in the convergent die entry, and with mechanical rupture of the polymer melt in the entrance zone (Agassant *et al.*, 2006). Techniques to suppress or postpone GMF include increasing the temperature, tailoring polymer molecular structure, using of filters and tapering the die entry. The only known additive which can successfully suppress GMF is boron nitride, which plausibly acts to decrease the extensional viscosity of polyethylenes by providing numerous sites for micro cracks, thus preventing build up of stress field of sufficient magnitude to produce substantial extrudate rupture (Sentmanat and Hatzikiriakos, 2004, Hatzikiriakos, 2005).

CHAPTER 3

EXPERIMENTAL PROCEDURES

3.1 Introduction

Experimental rheological methods aim at determining characteristic physical properties of polymer solutions or melts. These properties are expressed as material functions, for instance, shear viscosity as a function of rate of shear strain. The rheological experiments for measuring polymer material functions are based on the generation of controllable flow, in which the streamline pattern and hence, the deformations are known a priori (Dealy, 2005). Controllable shear deformations of polymer liquids are created by drag flow and pressure driven flow in a capillary or slit. Capillary rheometry is based on the latter and parallel plate rotational rheometry is based on the former. In this work both capillary and parallel plate rotational rheometers are used for rheological characterization of biodegradable polymers and their blends. In addition, optical microscopy was used for study of the extrusion instabilities. Scanning electron microscopy was utilized to gain insight about the morphology developed during extrusion of PLA/AAC blends.

3.2 Materials and sample preparation

Two commercial poly(lactic acid) resins and one commercial aliphatic-aromatic copolyester resins were studied to determine their rheological properties and the types and the occurrence of extrusion instabilities. Summary of their physical characteristics, provided by the resin manufacturers is presented in Table 3.1

Table 3.1. Material properties of the biodegradable polymers used in the present study

Material	Manufacturer	Density [g/cc]	T_g [°C]	T_m [°C]
PLA 4042 D	Natureworks LLC, USA	0.919	60	130-160
PLA 7000 D	Natureworks LLC, USA	1.25-1.28	55-60	145-155
Ecoflex F 7011 BX	BASF AG, Germany	1.25-1.27	-30	110-115

Biodegradable polymer blends were prepared from PLA 7000 D and Ecoflex F 7011 BX to study the effect of blending on the rheological properties and on the flow instabilities. The blending ratios were: (PLA/Ecoflex, wt%): 90:10 and 10:90. The dried polymer resins were weighed using electronic scale and were manually premixed before feeding into the batch mixer. Melt blending was conducted in Haake Rheomix 3000 Internal Mixer at T=190°C, 60 RPM, for t = 10 min using roller rotor blades. After accomplishing the blending process the temperature was set to 170°C to minimize possible thermal degradation during the recovery of material.

PLA is a hygroscopic material. In order to reduce the relative moisture below the advised by the manufacturer 250ppm, and to avoid hydrolytic degradation, the neat polymer granules were dried for 24 hours under vacuum at temperature 45°C prior to preparing the discs for the dynamic measurements, prior to capillary viscometer tests, and prior to blending with Ecoflex. Ecoflex does not need preliminary drying and in most cases it was used as delivered by the manufacturer. However, before melt blending with PLA, Ecoflex resin was dried at the conditions presented above. Flakes of the biodegradable polymer blends were dried using the same protocol as for poly(lactic acid). Sample discs with diameter 25mm and thickness 2mm were prepared by compression molding using the procedure outlined in Table 3.2.

Table 3.2. Protocol for preparing compression molded specimens with disc shape

Material	Preheat Time [min]	Pressing Time [min]	Cooling Time [min]	Mold Temperature [°C]
PLA 4042 D	3	3	2	165
PLA 7000 D	3	3	2	165
Ecoflex F- BX	2	1	3	180
PLA/Ecoflex. blends	3	3	2	165

The PLA and PLA/Ecoflex blend discs were dried for 24 hours in a vacuum oven at temperature 145°C and were held in desiccator before being used in rheological testing.

3.3 Rheological Testing in Parallel Plate Rotational Rheometer

Measurements in dynamic oscillatory mode under strain-controlled conditions were performed on a parallel plate *TA Instruments ARES* rheometer. The diameter of the plates was 25 mm and the gap between the plates was set to 1.5 mm. The test discs were put between the plates and heated to the test temperature in order to eliminate previous deformation and thermal history. After adjusting the gap to 1.5 mm the molten polymer sample was trimmed off for attaining smooth edge surface and right cylindrical sample form. At least 3 runs were performed for each material and the experimental results were averaged. The first experimental step was determining the strain in the linear visco-elastic region at frequency 1 rad/s by strain sweeps (range 0.1-100%). Then, dynamic frequency sweeps were carried out in the interval 0.1-100 rad/s. The storage modulus G', the loss

modulus G'' and the complex viscosity η*, were calculated from the following equations (Dealy and Wissbrun, 1990):

$$G' = \frac{2M_0 h}{\pi R^4 \phi_0} \cos\delta \tag{3.1}$$

$$G'' = \frac{2M_0 h}{\pi R^4 \phi_0} \sin\delta \tag{3.2}$$

$$\eta^* = \sqrt{\left(\frac{G'}{\omega}\right)^2 + \left(\frac{G''}{\omega}\right)^2}, \tag{3.3}$$

where M_0 is the torque, h is the gap between the plates, R is the radius of the discs, ϕ_0 is the angular amplitude, and δ is the phase shift or "mechanical loss angle", and ω is the circular frequency.

Measurements of shear viscosity and normal stresses as functions of shear rate were made by operating the parallel disk rheometer in steady rate mode during which the shear rate was varied between $0.1 s^{-1}$ and $5 s^{-1}$.

Shear viscosity and normal stresses were calculated according to the following equations (Macosko, 1994):

$$\dot{\gamma}_R = \frac{R\Omega}{h} \tag{3.4}$$

$$\tau_w = \frac{2M_0}{\pi R^3} \tag{3.5}$$

$$\eta = \frac{\tau_w}{\dot{\gamma}_R} \tag{3.6}$$

$$N_1 - N_2 = \frac{F_z}{\pi R^2}\left[2 + \frac{d\ln F_z}{d\ln \dot{\gamma}_R}\right], \tag{3.7}$$

where $\dot{\gamma}_R$ is the apparent shear rate at $r = R$, R is the radius of the discs, τ_w is the apparent shear stress, M_0 is the torque, h is the gap between the discs, Ω is the angular velocity, η is the shear viscosity, F_z is the total thrust, N_1 is the first normal stress difference ($\tau_{11} - \tau_{22}$) and N_2 is the second normal stress difference ($\tau_{22} - \tau_{33}$).

It should be mentioned that PLA resins, when melted, are very vulnerable to hydrolytic degradation. Therefore, it is desirable that all rheological measurements be conducted in inert atmosphere, e.g. nitrogen. Our equipment has the limitation that it operates at the ambient air in the lab, which by necessity introduces some degree of degradation. In order to reduce the effect of degradation on the obtained test data, we decided to work at temperatures not exceeding 200°C. Also, we conducted preliminary tests to optimize the time frame of the tests. When we took the measurements, no visual signs of degradation (e.g. color change or increase in stickiness) were observed. Yet, we noticed that the result data from experiments with PLA had standard deviation of up to 10% (in some cases), which is larger than the standard deviation of Ecoflex (up to 6%), or of polyethylenes (up to 5%). We contribute this to the "lurking variable"(Box *et al.*, 1978) of PLA degradation.

3.4 Rheological Testing in Capillary Rheometer

The shear viscosity at apparent shear rates ranging from 20 to 5000 s^{-1} was measured on a two bore rheometer *Rosand Capillary Precision Series 700* equipped with a 1 mm diameter die with L/D = 16 and 180° entry angle. "Zero" length die with 1 mm diameter and 0.25 mm length was used for making the entrance pressure drop correction. The total pressure drop ΔP_{total} and the volumetric flow rate through the capillary Q are used to determine the shear viscosity according to the equations, which follow below. These equations can be found in (Mackley, 1988) and in (Dealy, 1990).

The apparent (Newtonian) shear rate and the apparent wall shear stress are defined by:

$$\dot{\gamma}_a = \frac{4Q}{\pi R^3}, \tag{3.8}$$

$$\tau_w = \frac{\Delta P_{total}}{2\left(\frac{L}{R}\right)}, \tag{3.9}$$

where L and R are correspondingly the die length and radius

The true, or Rabinowitch corrected shear rate is calculated from:

$$\dot{\gamma}_w = \dot{\gamma}_a \left(\frac{3}{4} + \frac{1}{4} \frac{d(\log \dot{\gamma}_a)}{d(\log \tau_w)} \right) \tag{3.10}$$

The true (Bagley or entrance pressure drop corrected) shear stress is determined from:

$$\tau_{w(true)} = \frac{\Delta P_{total}}{2\left(\frac{L}{R} + e \right)}, \tag{3.11}$$

where the Bagley correction e is determined from pressure drop measurements at certain shear rate values using capillary dies with different aspect ratios L/D. A more accurate method is when an orifice die is used in a double barrel rheometer (Mackley, 1988), which is the method we used. In this case the equation for calculating the true shear stress becomes:

$$\tau_{w(true)} = \frac{\Delta P^{L}_{total} - \Delta P^{O}_{total}}{\frac{2L}{R}}, \tag{3.12}$$

where ΔP^{L}_{total} and ΔP^{O}_{total} are the total pressure drops measured correspondingly at the ends of the long and the orifice dies.

Shear viscosity values are then determined from the following equation:

$$\eta = \frac{\tau_{w(true)}}{\dot{\gamma}_w} \tag{3.13}$$

The extensional viscosity of the polymers studied was determined from the entrance pressure drop, following the method of Cogswell (1972). The following formulas, developed by Cogswell were used for calculating the apparent extensional rate of strain and the apparent extensional viscosity (Dealy, 1990):

$$\dot{\varepsilon} = \frac{4\eta\dot{\gamma}^2}{3(n+1)\Delta P_{ent}} \tag{3.14}$$

$$\eta_e = \frac{9(n+1)^2(\Delta P_{ent})^2}{32\eta\dot{\gamma}^2} \qquad (3.15)$$

where η is the true shear viscosity, $\dot{\gamma}$ is the apparent shear rate, n is the power law exponent, and ΔP_{ent} is the entrance pressure drop

Wall slip measurements were carried out on the same rheometer at 180°C according to the Mooney method (Mooney, 1931; Dealy, 1990). Three dies with aspect ratio L/D = 16, entry angle of 180° and diameters 1.0, 1.5 and 2.0 mm were used for the wall slip analysis. The die aspect ratio was kept constant so that the effect of pressure on viscosity be the same (Hatzikiriakos and Dealy, 1992). Measured data are analyzed on the base of the Mooney equation (Dealy, 1990):

$$\dot{\gamma}_a = \dot{\gamma}_T + \frac{8V_s}{D}, \qquad (3.16)$$

where $\dot{\gamma}_a$ is the measured apparent shear rate at certain stress level, $\dot{\gamma}_T$ is the true shear rate without slip, V_s is the slip velocity, and D is the diameter of the die. The analysis was performed in the following way: first, the curves of apparent wall shear stress versus apparent shear rate are plotted for the three dies. From these plots, the corresponding apparent shear rate values were determined by maintaining the stress constant. Then, plots of the apparent shear rate versus the ratio 1/D are constructed. The wall slip velocity V_s for a certain shear stress level is calculated by dividing the slope of the curves by eight.

Polymer extrudates at high and low shear rates were collected and, after solidification in air, examined by an *Olympus CZ-60* light microscope equipped with *Panasonic BP-310* digital camera for the purpose of photographing the surface irregularities (sharkskin and gross melt fracture) of the studied biodegradable polymers.

Extrudate swell ratio – i.e. the ratio of the diameter of the extrudate to that of the die lip – was measured using one of the most commonly used laboratory method, which is also found in the international standard ISO 11443. It involved extruding into air, cutting a strand, letting it air cool and measuring directly the frozen extrudate diameter by a micrometer (Dealy and Saucier, 2000). For each data point (i.e. value of the apparent

shear rate) at least four extrudates of approximately the same length were taken. Then the diameter of each extrudate was measured at 4 points. Finally, statistical average was taken to determine the mean value of extrudate diameter for the corresponding shear rate.

It is appropriate to note that the capillary rheological measurements of PLA are subjected to the same experimental limitations as the parallel disc rheometry mentioned above. Additional sources of variation are also caused by the viscous dissipation and the pressure dependence of shear viscosity.

3.5 Scanning Electron Microscopy of PLA/Ecoflex blends

Samples for scanning electron microscopy (SEM) characterization were prepared from each blend by extrusion from the capillary rheometer into the air using 1 mm die at 180°C and shear rates 750 – 1000 s^{-1}. Since blends with Ecoflex content of more than 50% are very ductile, fractured cross section of the test specimens was obtained by first slightly notching the extrudate by using a sharp razor, followed by an immersion in liquid nitrogen for more than10 min, and finally, by snapping the specimen in the notched area. All the fractured surfaces were coated with gold prior to loading into SEM machine. The SEM observations were performed with Phillips SEM 515 machine equipped with LAB 6 gun.

CHAPTER 4

RESULTS AND DISCUSSION

4.1 Rheological Characterisation of PLA 4042D

This section presents results obtained by using a parallel plate and a capillary rheometer for resin PLA 4042D. These include results for loss and storage moduli, normal stresses and elongational viscosity. Results from tests for wall slip, extrudate swell, sharkskin and melt fracture are also presented and discussed.

4.1.1 Shear Viscosity of PLA 4042D

Figures 4.1.1 and 4.1.2 explore the validity of the experimental Cox-Merz rule (Cox and Merz, 1958) at low and high circular frequencies and shear rates. Cox-Merz rule states that shear viscosity function $\eta = \eta(\dot{\gamma})$, obtained under steady shear conditions and complex viscosity function $\eta^* = \eta^*(\omega)$, obtained in oscillatory shear flow are nearly identical (Dealy and Wissbrun, 1990). Figure 4.1.1 shows results at low frequencies and shear rates. It is obvious that for temperatures 180°C and 190°C the Cox-Merz rule holds very well. At 200°C some deviation from the Cox-Merz rule is observed. It might be explained with some hydrolytic or thermal degradation of the resin during the experiment.

Figure 4.1.2 presents results of complex viscosity measurements done in parallel plate rheometer operated in oscillatory mode together with shear viscosity, which was measured in capillary rheometer at high shear rates. It is seen from Figure 4.1.2 that for temperature 180°C there are some deviations from the Cox-Merz rule at shear rates 60 to 100 s^{-1}. However, the results show that at higher temperatures the Cox-Merz rule holds for PLA 4042D.

From the above discussion it can be concluded that although there are some discrepancies between results from the different experimental methods, the Cox-Merz

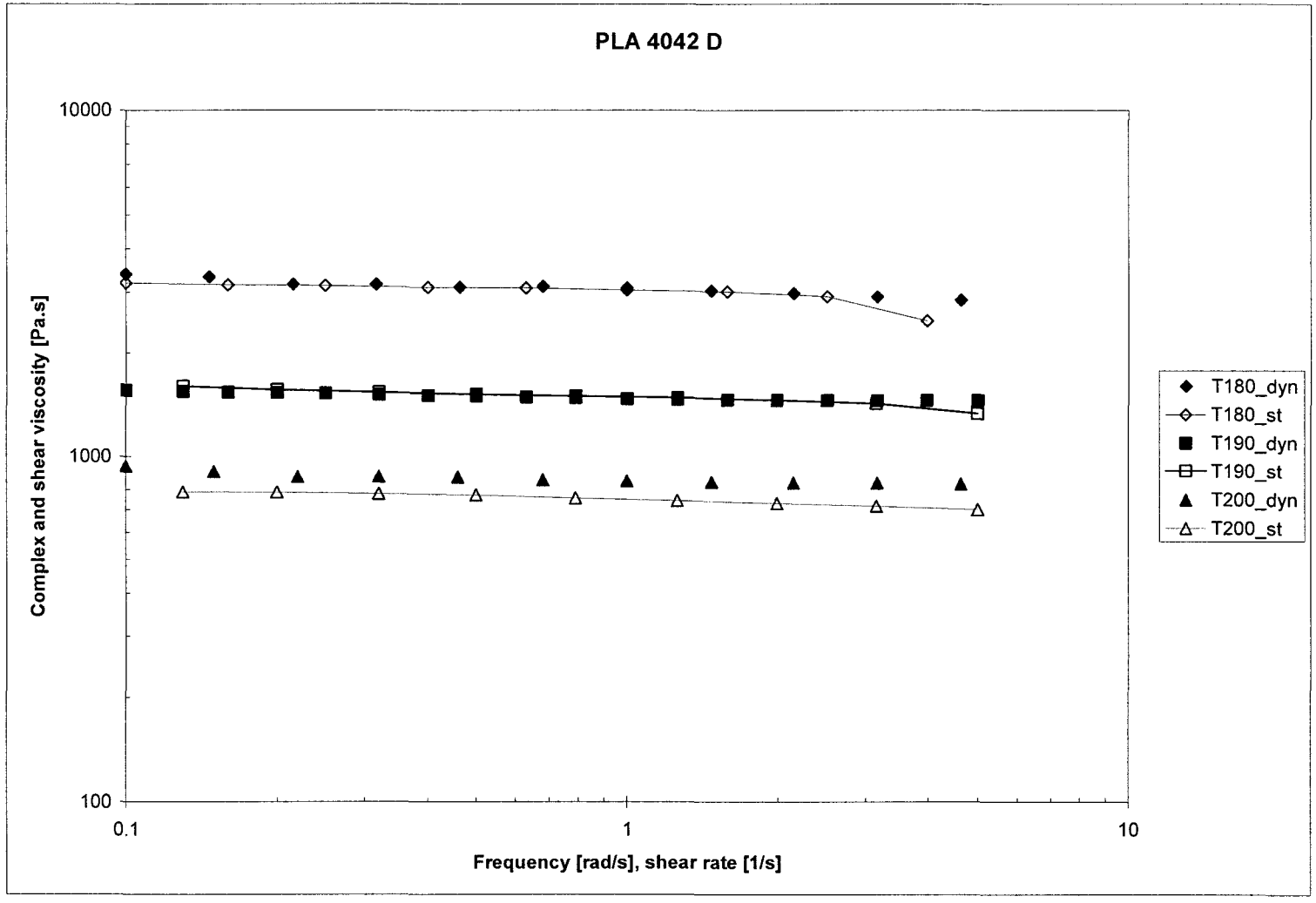

Figure 4.1.1. Complex and shear viscosity curves for PLA 4042D obtained in parallel plate rheometer at 180°C,190°C , and 200°C. Open symbols represent steady shear data. ("dyn" refers to dynamic and "st" to steady state measurements)

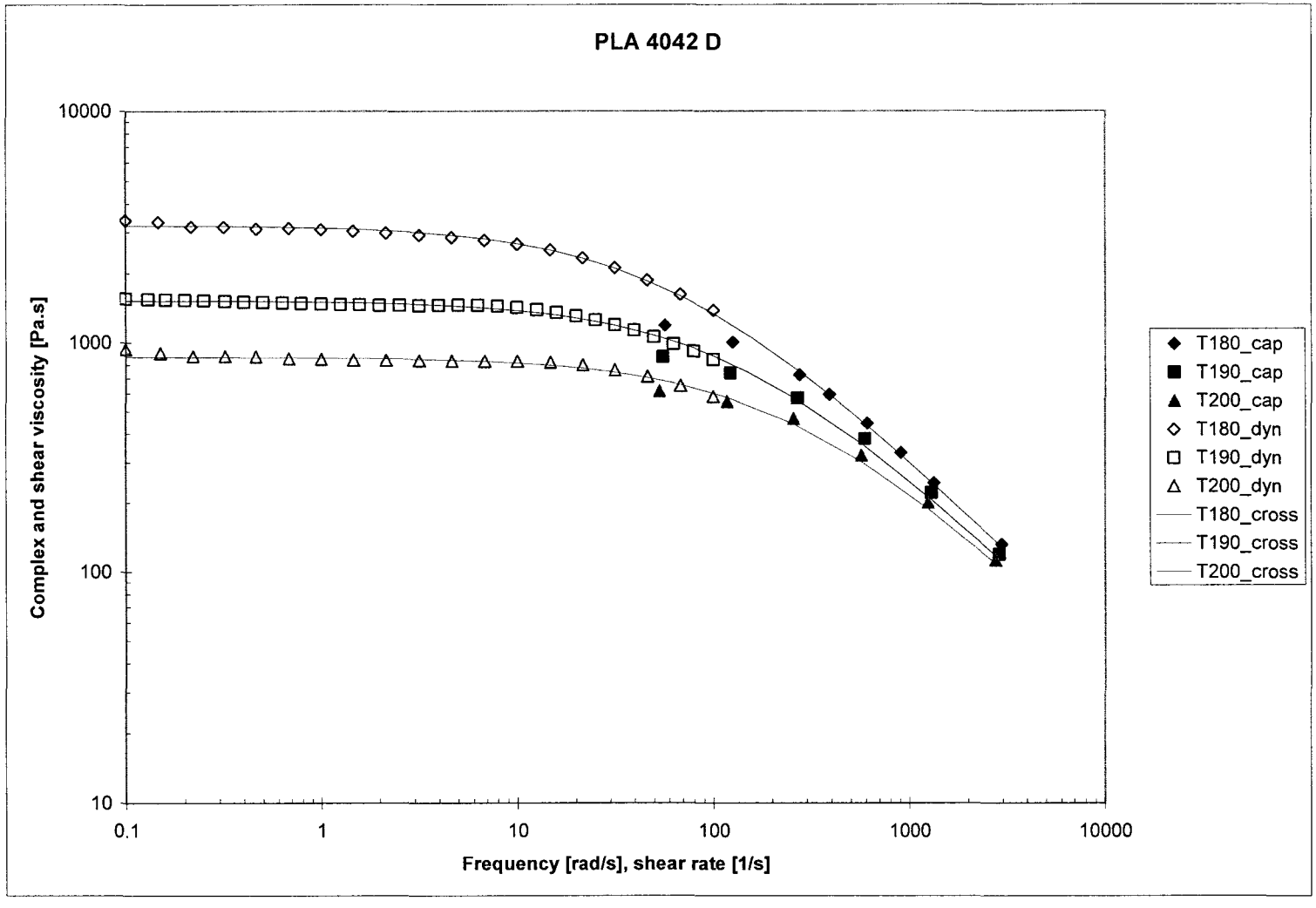

Figure 4.1.2. Complex and shear viscosity curves obtained correspondingly in parallel plate and capillary rheometers at 180, 190, and 200°C. Solid symbols represent capillary data. Lines represent Cross model fitted values.

rule holds for PLA 4042D. The discrepancies could be explained with the differences and the limitations of the experimental techniques, which have been already discussed in Chapter 3.

It can be seen from Figures 4.1.1 and 4.1.2 that the viscosity of PLA 4042D is sensitive to temperature and it exhibits rapid shear-thinning. Usually, fitting to power law and to Cross model equations are employed to quantify the dependence of viscosity on shear rate and on temperature. The power law equation has the form:

$$\tau = K\,\dot{\gamma}^{n}, \qquad (4.1)$$

where τ is the wall shear stress, K is the consistency index, $\dot{\gamma}$ is the shear rate, and n is an exponent, which presents the degree of deviation from Newtonian behaviour (Dealy and Wissbrun, 1990).

Fang and Hanna (1999) used the power-law model to present the results from their viscosity measurements of an amorphous and a semicrystalline commercial PLA resins. It is worth noting that their rheological experiments were done using a tube rheometer attached to the barrel extension of a laboratory single screw extruder, and were conducted for shear rates from 200 to 1000 s^{-1}. However, in extrusion processing the melt is subjected to shear rates in much larger interval of variation (0 – 2000s^{-1}). As can be seen from Figure 4.1.2, at low shear rates PLA exhibits a large region of Newtonian behaviour. The power low model can only fit well PLA viscosity data in the high shear rate region and hence, its use for representation and design purposes is not appropriate. On the other hand, the Cross equation gives satisfactory fitting for the entire range of shear rates.

Figure 4.1.2 shows the viscosity curves of PLA 4042 D at three different temperatures. The lines represent viscosity values which are predicted by a fitted to the experimental data Cross model of the form (Dealy and Wissbrun, 1990)

$$\eta = \eta_0[1+(\lambda\dot{\gamma})^{1-n}]^{-1}, \qquad (4.2)$$

where η_0 is the zero shear viscosity, λ is a characteristic relaxation time, n is the power-law exponent, and $\dot{\gamma}$ is the true shear rate, determined according to the procedure outlined in Chapter 3.. It was observed that PLA 4042D exhibits typical pseudoplastic behaviour. At low shear rates this PLA resin has a well defined Newtonian region and at higher shear rates its shear viscosity declines rapidly. It is seen from Figure 4.1.2 that Cross model fits the experimental data well.

The temperature coefficient *b* for the Cross law model has been calculated from the equation:

$$\eta_0 = \eta_{0ref}\exp[-b(T-T_0)], \qquad (4.3)$$

where η_0 is the zero shear viscosity at certain temperature *T*, and η_{0ref} is the zero shear viscosity at a reference temperature T_0 (Vlachopoulos and Wagner, 2001)
The results of the temperature sensitivity and shear rate dependence are summarized in Table 4.1.1.

Table 4.1.1 Cross model parameters: zero shear viscosity η_0, relaxation time λ, power-law exponent **n**, and temperature coefficient **b** for PLA 4042D, $T_{ref} = 180^{\circ}C$:

Polymer	T [°C]	Zero shear viscosity η_0 [Pa.s]	Relaxation time λ [s]	Power-law exponent *n*	Temperature coeff. *b* [$^{\circ}C^{-1}$]
PLA 4042D	180	3212	0.016	0.16	n.a.
	190	1499	0.0067	0.16	0.071
	200	876	0.0037	0.16	0.071

The above presented results show that viscosity of PLA 4042 D is very sensitive to temperature variations (b = 0.071). In comparison with some conventional polymers, PLA 4042D has temperature sensitivity similar to PMMA and rigid PVC, however more than polyethylenes (b = 0.01-0.03) (Vlachopoulos and Wagner, 2001).

4.1.2 Storage and Loss Moduli of PLA 4042D

Storage (G') and loss (G'') moduli are material functions which are obtained from small amplitude oscillatory shear experiments, in which the specimen is subjected to harmonic shear stress. They are used to characterize the linear viscoelastic properties of polymer melts (Dealy and Wissbrun, 1990). The storage and the loss moduli are calculated using the equations (3.1) and (3.2), listed in Chapter 3.

Figure 4.1.3 shows the G' and G'' curves of PLA 4042D at temperatures 180°C, 190°C, and 200°C. It can be seen that at all temperatures the storage modulus curve lies below the loss modulus curve (i.e. $G'' >> G'$). Hence, for the temperature range 180°C – 200°C PLA4042D exhibits liquid type viscoelastic behaviour (i.e. can be modelled as elastic liquid). The slope of the storage modulus curve on the log-log graph changes from 1.33 for 180°C, through 1.67 for 190°C, to 2.00 for 200°C. This behaviour shows the diminishing elastic contribution of the polymer chain entanglements with the temperature increase. The slopes of the loss modulus for 180°C, 190°C, and 200°C are correspondingly 0.95, 0.97, and 0.96.

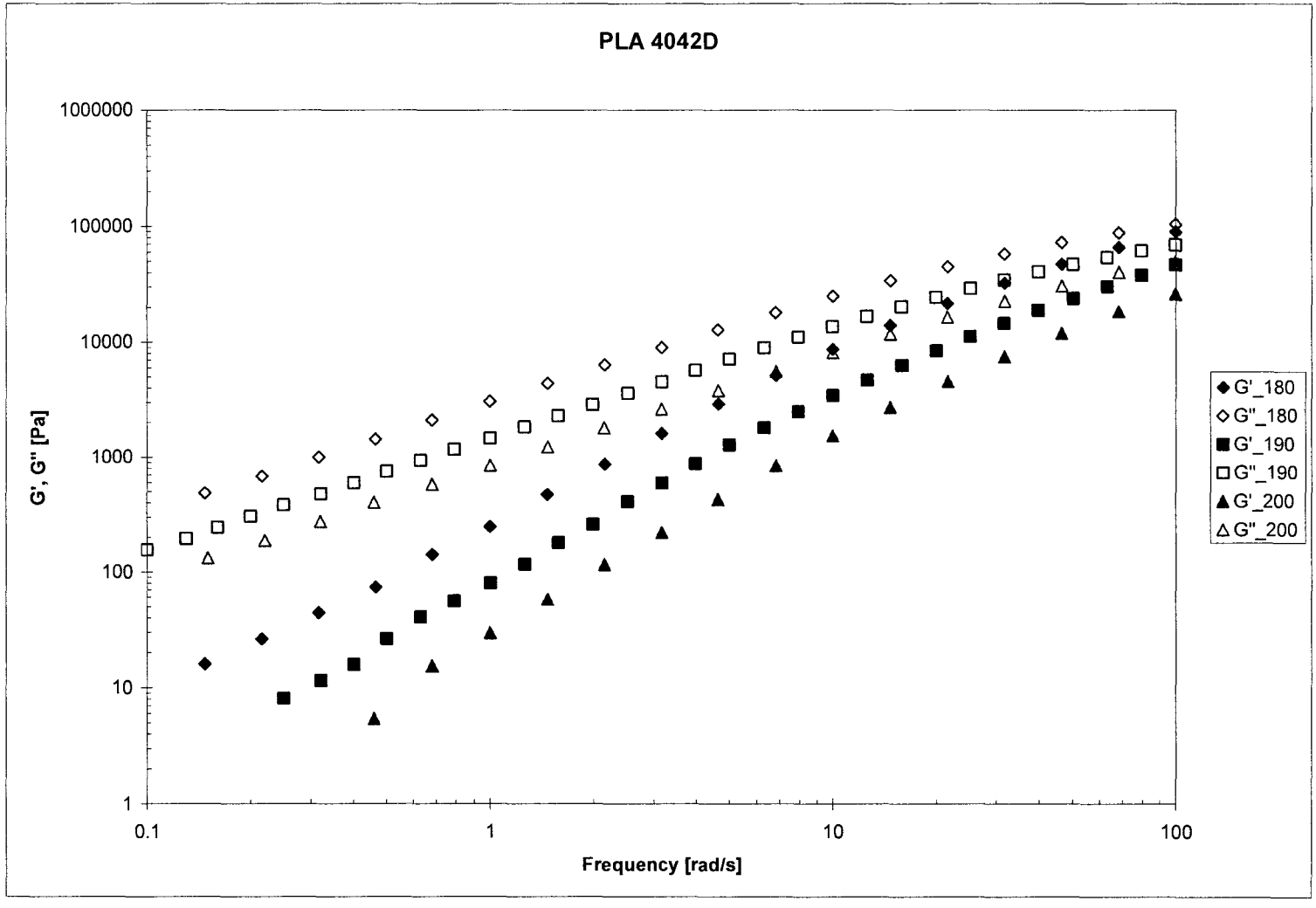

Figure 4.1.3. Curves of storage and loss moduli for PLA 4042D at 180°C, 190°C, and 200°C. Solid symbols represent loss modulus data (G").

4.1.3 Normal Stress Differences of PLA 4042D

Viscoelastic nature of polymer melts manifests itself in another interesting phenomenon – generation of anisotropic normal stresses in simple shear flow. In our case, when the melt is sheared between the parallel disks of the rheometer, a normal force is generated, trying to separate them. This normal force is explained with the tendency of the stretched polymer chains to revert to their equilibrium coiled conformations (Tadmor and Gogos, 2006). Since such normal force is not observed for Newtonian fluids, it can be considered as a measure of the elasticity of the polymer melt. It is customary in polymer rheology to describe this viscoelastic property of polymer liquids with the "first and second normal stress differences" (Dealy and Wissbrun, 1990). The parallel plate rheometer gives the normal stress difference N_1-N_2. The second normal stress difference N_2 can be calculated if N_1 values are known, but usually $N_2 = -0.1N_1$ to $- 0.2N_1$ (Tadmor and Gogos, 2006; Macosko, 1994). In capillary flows the first normal stress difference is also related to another important viscoelastic phenomenon – the extrudate swell (Vlachopoulos, 1981; Tadmor and Gogos, 2006).

Based on data from steady shear experiments in the parallel plate rheometer, the normal stresses were calculated according to the equations (3.4) and (3.7) listed in Chapter 3:

It is also known that for commodity plastics at low shear rates and frequencies (i.e. $\dot{\gamma} \leq 1\ s^{-1}$, $\omega \leq 1$ rad/s) $N_1 = 2G'$, i.e. the curves $N_1(\dot{\gamma})$ and $2G'(\omega)$ overlap (Macosko, 1994). Plots of the difference N_1-N_2 (i.e. first normal stress difference minus the second normal stress difference) as a function of shear rate and 2G' as a function of angular frequency of PLA 4042D at temperatures 180°C, 190°C, and 200°C are presented on figure 4.1.4. Since N_2 is usually much smaller than N_1, we see that generally the assumption that $N_1 \approx 2G'$ is approximately correct at 180°C. However, larger deviations are seen at higher temperatures.

The parallel plate rheometer does not permit the measurement of N_1 and N_2 separately. It only gives the difference $N_1 - N_2$. Although we made the assumptions that

$N_1 >> N_2$, the above results suggest that this can be further investigated by using a cone and plate rheometer which gives N_1 directly and then N_2 can be determined from the present data of $N_1 - N_2$.

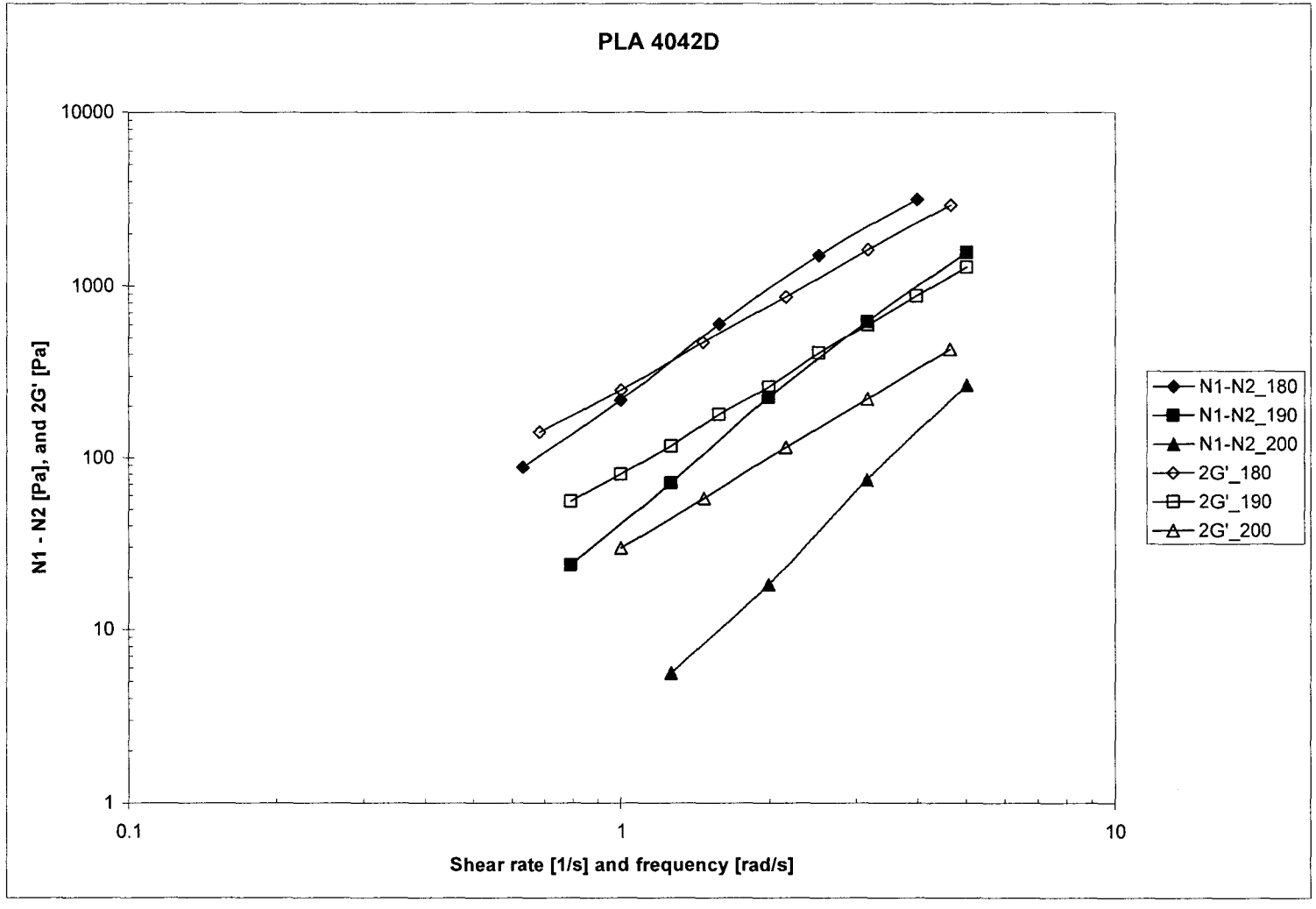

Figure 4.1.4. Normal stress difference and 2G' curves for PLA 4042D at 180°C, 190°C and 200°C. Open symbols represent 2G' values.

4.1.4 Extensional Viscosity of PLA 4042D

Measurements of extensional tensile viscosity are difficult even with sophisticated extensional rheometers. However, values of apparent elongational viscosity can be obtained from the entrance pressure drop data in capillary rheometer by the method of Cogswell. These values are close to the extensional viscosity data obtained by extensional rheometry within very narrow interval of extensional strain rates and they cannot be used for detailed characterisation of polymer melts or for design purposes. Nevertheless, extensional viscosity data obtained by entrance pressure drop can be used as a quick and inexpensive technique for comparing different polymers subjected to the same flow conditions (Dealy and Wissbrun, 1990). The apparent extensional rate of strain and the apparent extensional viscosity of PLA 4042D were calculated according to equations (3.14) and (3.15), which are found in Chapter 3.

Figure 4.1.5 shows the dependence of tensile extensional viscosity on extensional rate of strain, obtained by the Cogswell method for PLA 4042D. It is compared with shear viscosity data, which was obtained by combining the complex viscosity and shear viscosity curves. As expected the extensional viscosity is larger than the shear viscosity. The Trouton ratios η_e/η are approximately from 2.8 to 7.1 while for Newtonian fluids $\eta_e/\eta_0 = 3$ (as proven theoretically and confirmed by experiments (Macosko, 1994)). The values of Trouton ratios of PLA 4042D are much lower than the Trouton ratios of conventional polymers, which have been reported in the literature. For example, Binding *et al.* (1998) reported that η_e/η of 4 commercial polymers: HDPE, LDPE, PP, and PS , ranged from 15 to 35, from 23 to 50, from 17 to 60, and from 20 to 100, respectively.

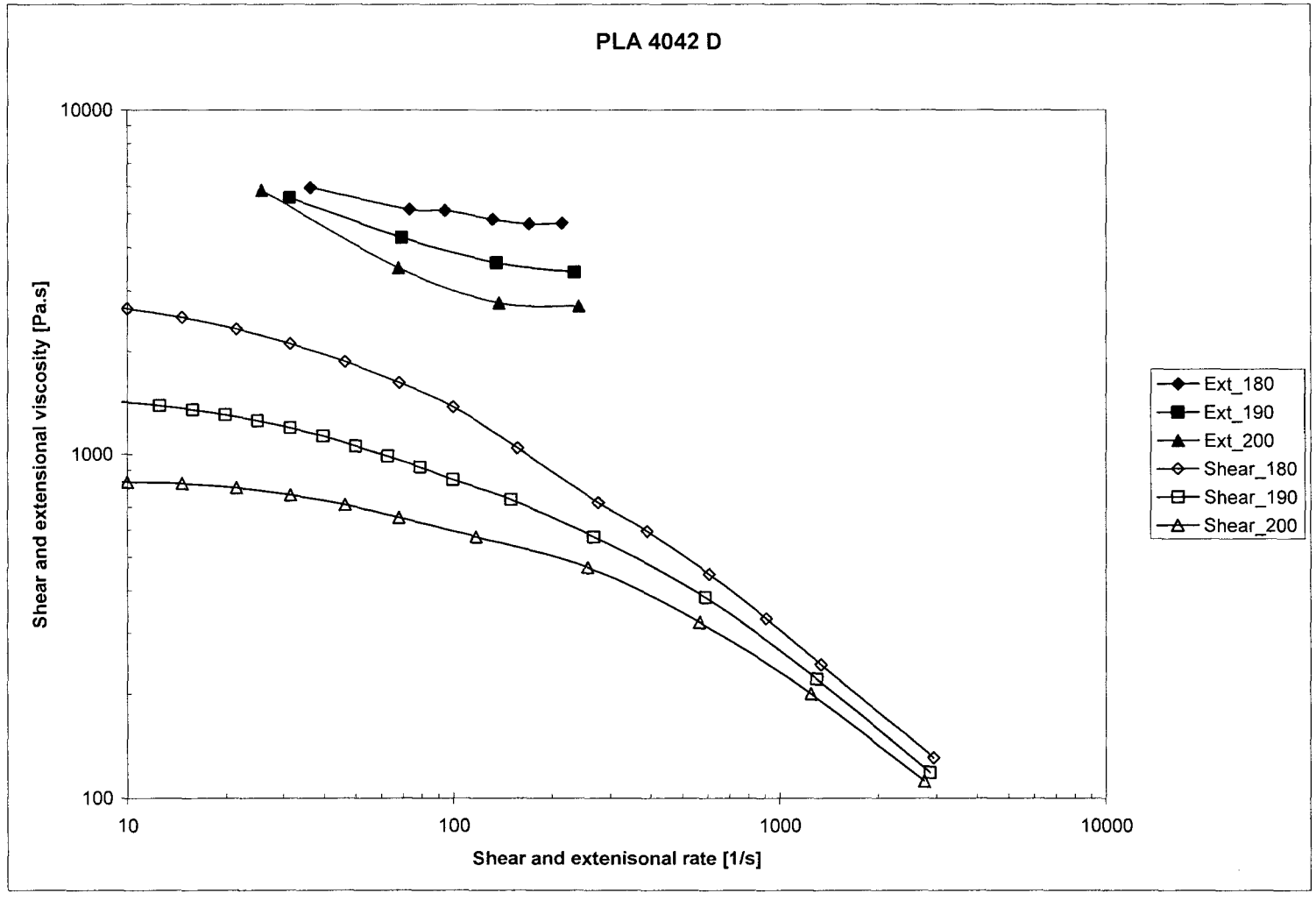

Figure 4.1.5. Extensional viscosity and shear viscosity curves for PLA 4042D at 180, 190, and 200°C

4.1.5 Wall Slip of PLA 4042D

Results from the wall slip study are presented in this subsection. Figure 4.1.6 presents the stress curves of PLA 4042D. The measurements were taken at 180°C in stainless steel dies with aspect ratio L/D = 16 and diameters 1 mm, 1.5 mm and 2 mm.

This plot shows that the flow curves of PLA 4042D obtained with different diameter dies do not collapse to a single curve, which is an evidence of slippage at the die wall (Hatzikiriakos and Dealy, 1992; Dealy and Wissbrun, 1990). The wall slip is small at low shear rates and it increases with the melt throughput increase. From the plot is obvious that PLA 4042D exhibits notable slippage even at low shear rates.

An attempt was made to quantify the wall slip exhibited by PLA 4042D by using the Mooney technique outlined in Chapter 3. It was found that large variation in the slip velocity V_s values exist at shear stresses ranging from 0.1 to 0.4 MPa. In addition, the deviation from linearity of the plots of apparent shear rate versus 1/D was larger than that of other polymers exhibiting slip (e.g. HDPE) (Ramamurthy, 1986; Denn, 2001). This is apparently die to the experimental difficulties as explained in Chapter 3.

It is evident that PLA slips at the die wall. On the other hand, to our knowledge, there are no reports in the open literature about wall slip of biodegradable polymers including PLA. It might be suggested that more sensitive methods than the Mooney technique be used for quantifying the wall slip of PLA. Gap-dependant wall slip measurements using rotational or planar parallel plate rheometers might produce more accurate and repeatable results (Archer, 2005). Once the wall slip of PLA is satisfactory quantified, further studies might be conducted to determine whether the underlying mechanism is failure at polymer-polymer interface or at polymer/wall interface.

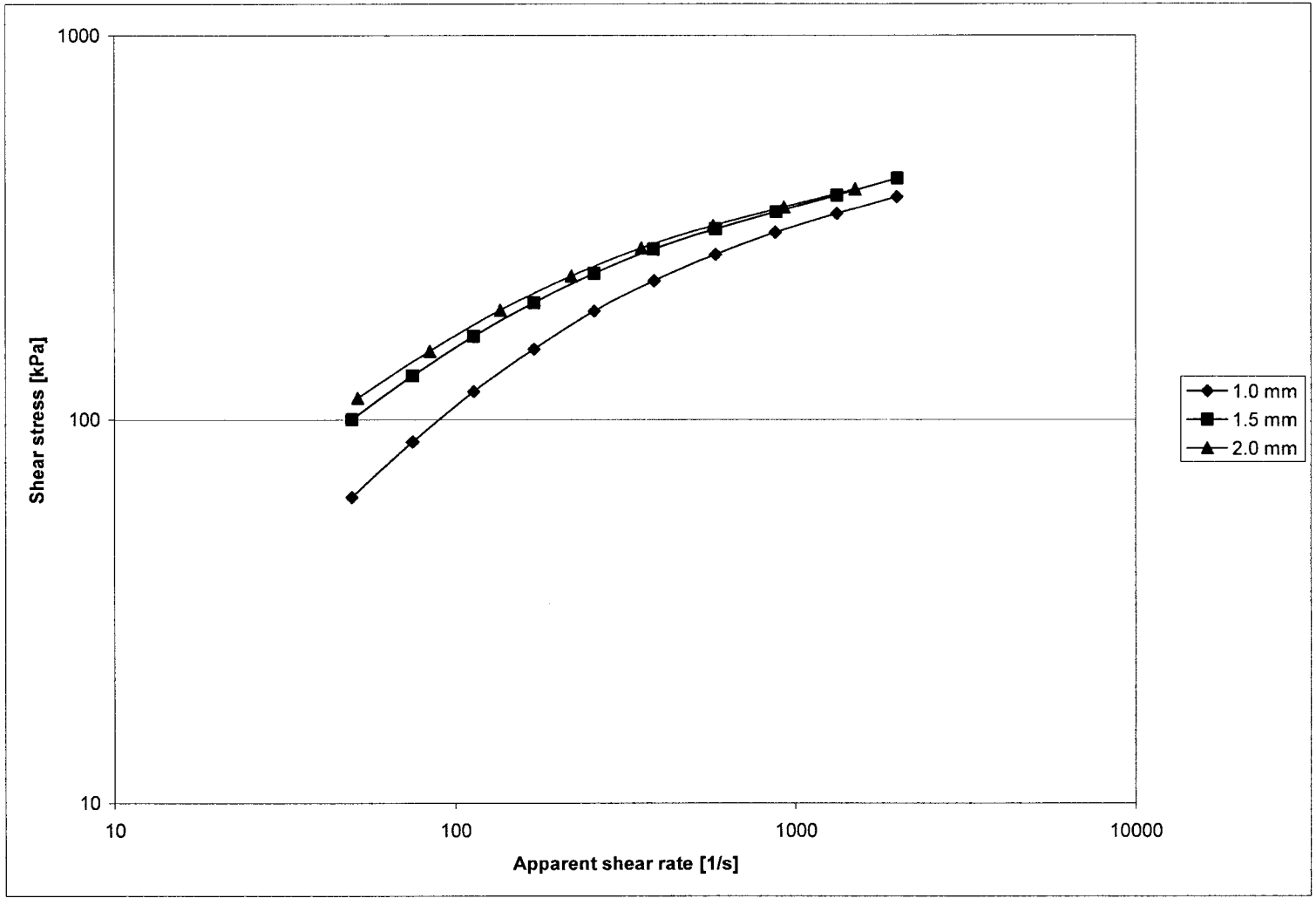

Figure 4.1.6. Flow curves for PLA 4042D at 180°C in different diameter dies with L/D = 16

4.1.6 Sharkskin and Gross Melt Fracture Phenomena in Flow of PLA 4042D

The onsets of flow instabilities and their location on the flow curve of PLA 4042D are schematically shown on figure 4.1.7.

Figure 4.1.8 shows the development of extrusion instabilities in capillary flow of PLA 4042 D. It was observed that at temperature 180°C PLA 4042D exhibits both sharkskin and gross melt fracture. For PLA 4042D sharkskin started at apparent shear rate of 160 s^{-1} and wall shear stresses of 180 kPa. Gross melt fracture for PLA 4042D appeared at shear rates of 1030s^{-1} and apparent shear stress of 360 kPa. For PLA the evolution of the flow instabilities with the increase of melt throughput was from smooth extrudate through sharkskin, more severe sharkskin, and finally, gross melt fracture. Although PLA has linear molecular structure (Auras, 2004) it did not exhibit the typical for linear polymers stick-spurt flow instability, which is characterised by a unstable flow with large pressure and shear stress fluctuations and by alternating smooth and distorted extrudate regions. The stick-spurt or stick-slip instability has not been observed with long-chain branched polymers such as LDPE (Georgiou, 2005). However, it has been observed with linear polymers with narrow molecular weight distribution, e.g., LLDPE, HDPE, PB and PDMS (Georgiou, 2005; Agassant *et al.*, 2006).

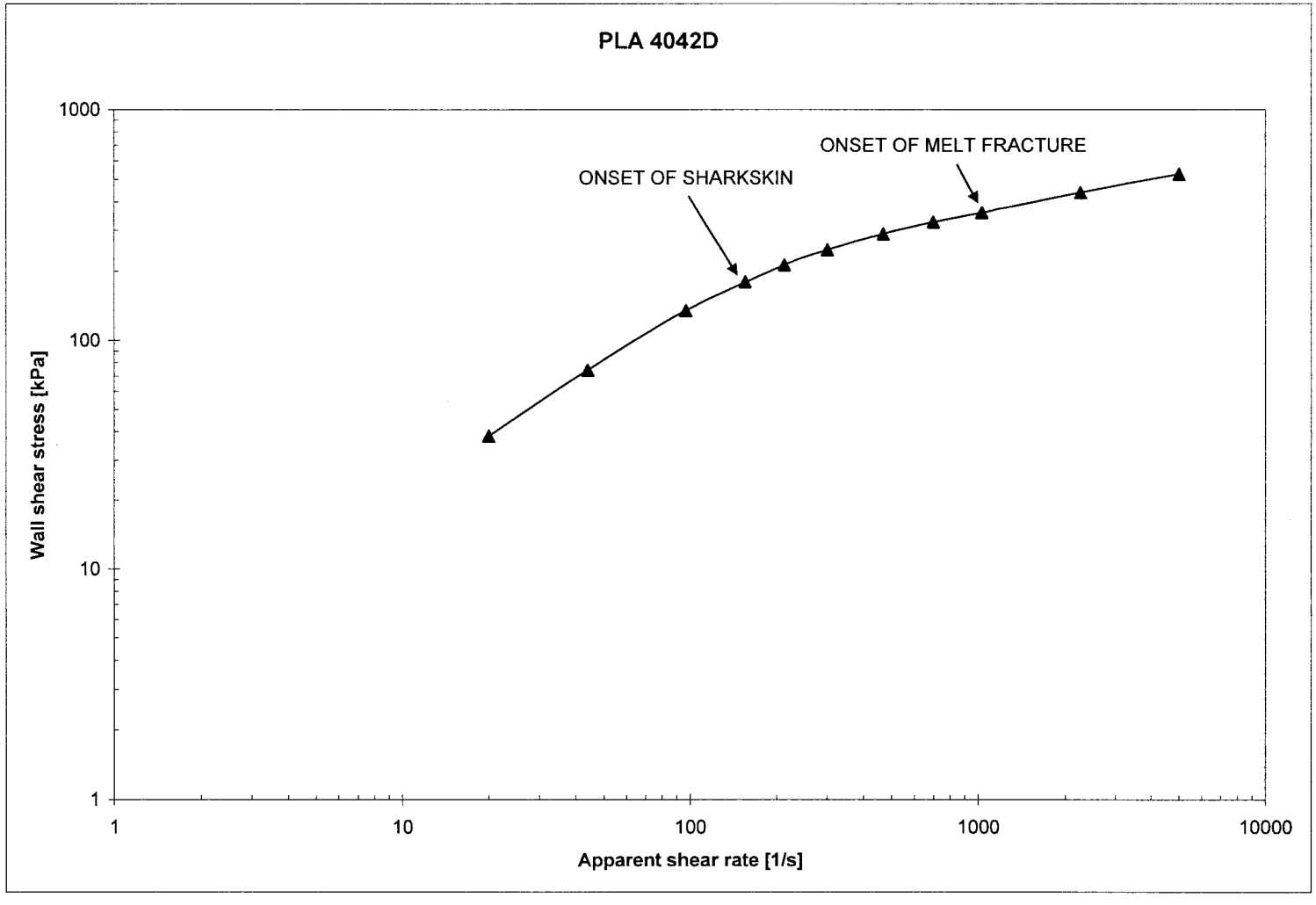

Figure 4.1.7. Flow curve and onsets of extrudate instabilities for PLA 4042D at 180°C in stainless steel die with D = 1mm and L/D = 16.

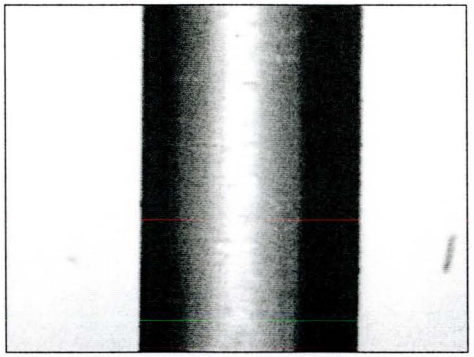

(a) smooth extrudate

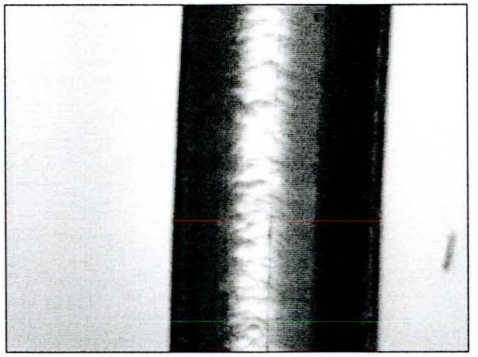

(b) start of sharkskin

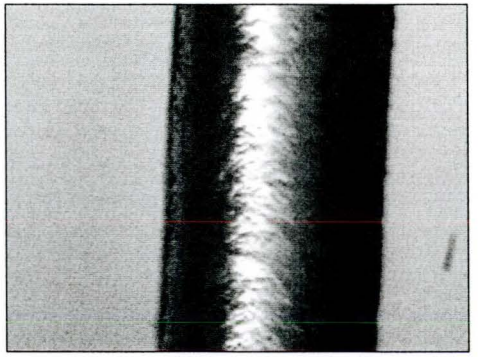

(c) more severe sharkskin

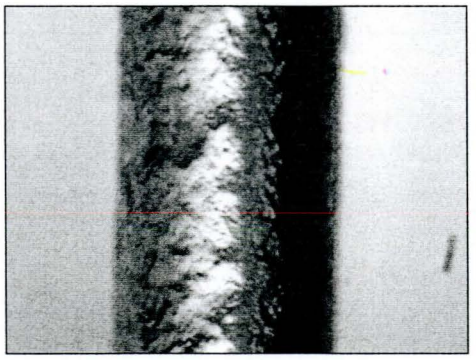

(d) very severe sharkskin

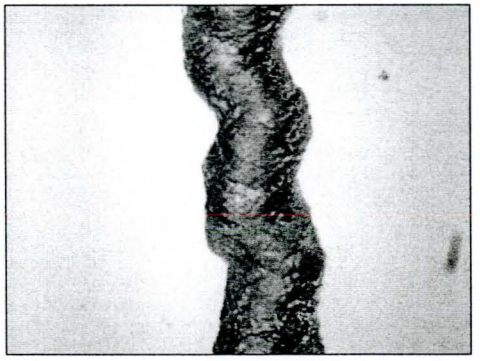

(e) gross melt fracture

Figure 4.1.8. Evolution of extrudate instabilities for PLA 4042D in die with diameter 1mm and L/D = 16 at 180°C. The corresponding values of apparent shear rates and wall shear stresses are: (a) 100 s^{-1}, 155 kPa; (b) 200 s^{-1}, 225 kPa; (c) 400 s^{-1}, 290 kPa; (d) 600 s^{-1}, 326 kPa; (e) 2500 s^{-1}, 350 kPa

4.1.7 Extrudate swell of PLA 4042D

Phenomenon of polymer swell after exiting from a die is very important in industrial processing, especially for technologies as film blowing, film casting, profile extrusion and fiber spinning. It is believed to be mainly caused by stress release at die exit and memory of entrance for short dies. (Vlachopoulos, 2005). Therefore die swell might be considered as an indication of polymer melt elasticity for single phase systems. In capillary geometry, the extrudate is axisymmetric and its swell is given by the ratio:

$$B = D/D_o, \qquad (4.4)$$

where D is the diameter of the extrudate and D_o is the die diameter.

Measurements of extrudate swell ratio of PLA 4042D were performed after extrusion through a stainless steel die of diameter 2mm and of aspect ratio 16 at temperature 180°C and cooling into air at room temperature. The results are summarized in Table 4.1.3. The swell ratio increased with the increase of shear rate. PLA 4042 D had die swell in the interval of 1.09 to 1.23. Typical swell value for Newtonian fluids is 1.13. However, for polymer liquids it usually reaches 2 or even 3 (Dealy and Wissbrun, 1990). The measured swell of PLA 4042D is rather small.

Table 4.1.2 Extrudate swell for PLA 4042D in die with D = 2mm and L/D = 16, at T = 180°C

Apparent shear rate 1/s	Swell Ratio D/D_0
50	1.086
100	1.1315
136	1.1655
150	1.17
200	1.193
300	1.225

4.2 Rheological Characterisation of PLA 7000D

This section presents results obtained by using a parallel plate and a capillary rheometer for resin PLA 7000D. These include results for loss and storage moduli, first normal stresses and elongational viscosity. Results from tests for wall slip, extrudate swell, sharkskin and melt fracture of PLA 7000D are also presented and discussed.

4.2.1 Shear Viscosity of PLA 7000D

Figures 4.2.1 and 4.2.2 explore the validity of the experimental Cox-Merz rule (Cox and Merz, 1958) at low and high circular frequencies and shear rates. Figure 4.2.1 shows results at low frequencies and shear rates. It is obvious that for temperature 190°C the Cox-Merz rule holds very well. At 180°C and 200°C some minor deviations from the Cox-Merz rule are observed.

Figure 4.2.2 presents results from complex viscosity measurements done in parallel plate rheometer operated in oscillatory mode together with shear viscosity, which was measured in capillary rheometer at high shear rates. It is seen from Figure 4.2.2 that at all temperatures the Cox-Merz rule holds for PLA 7000D.

From the above discussion it can be concluded that although there are some discrepancies between results from the different experimental methods, the Cox-Merz rule holds for PLA 7000D. The discrepancies could be explained with the differences and the limitations of the experimental techniques used as mentioned earlier in Chapter 3.

It can be seen from Figures 4.2.1 and 4.2.2 that shear viscosity of PLA 7000D is sensitive to both temperature and shear rates. Fitting to Cross model equations was employed to quantify the dependence of viscosity on shear rate and on temperature. Figure 4.2.2 shows the viscosity curves of PLA 7000D at three different temperatures. The lines represent viscosity values which are predicted by a fitted to the experimental

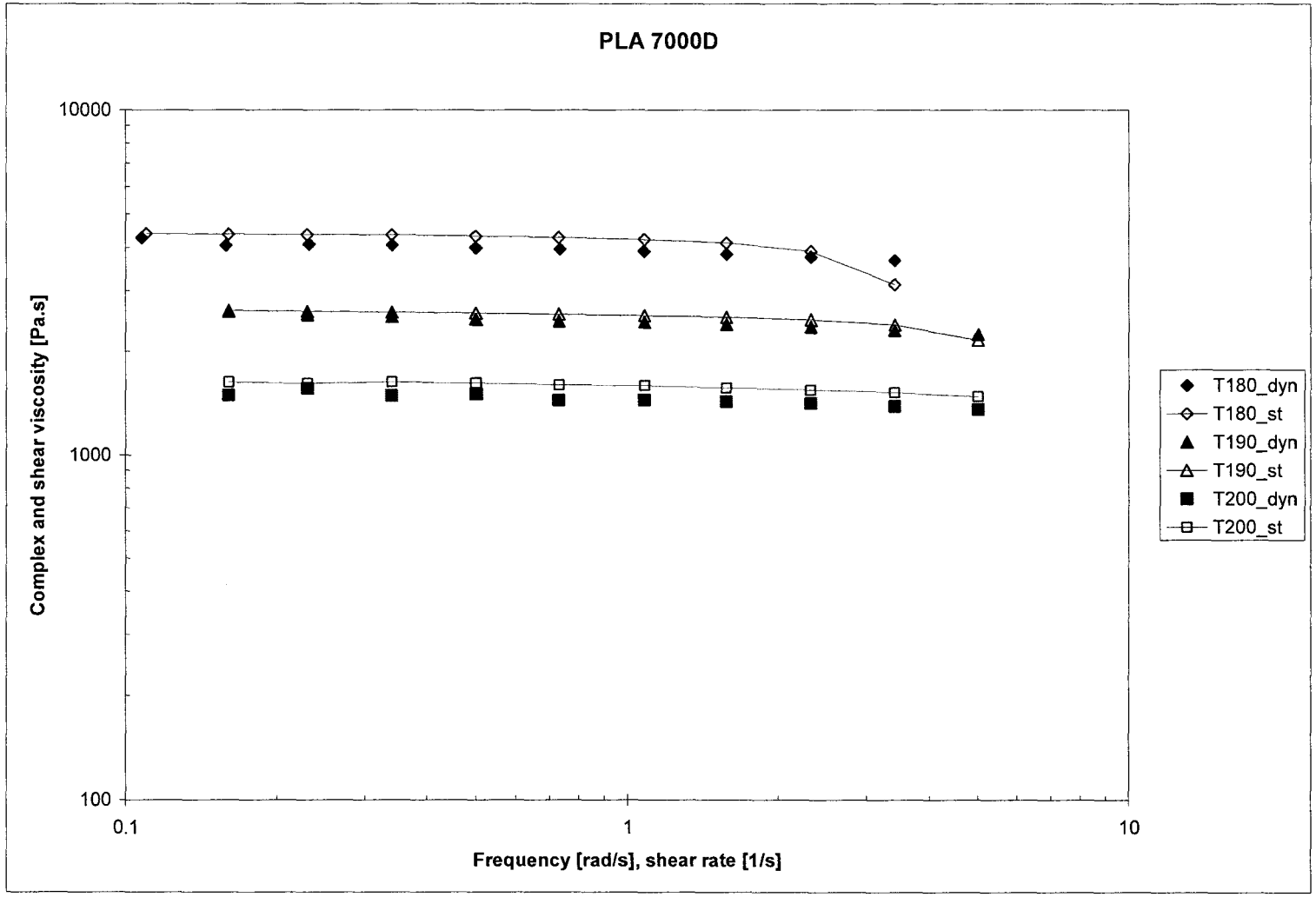

Figure 4.2.1. Complex and shear viscosity curves for PLA 7000D obtained in parallel plate rheometer at 180°C,190°C , and 200°C. Open symbols represent steady shear data. ("dyn" refers to dynamic and "st" to steady state measurements).

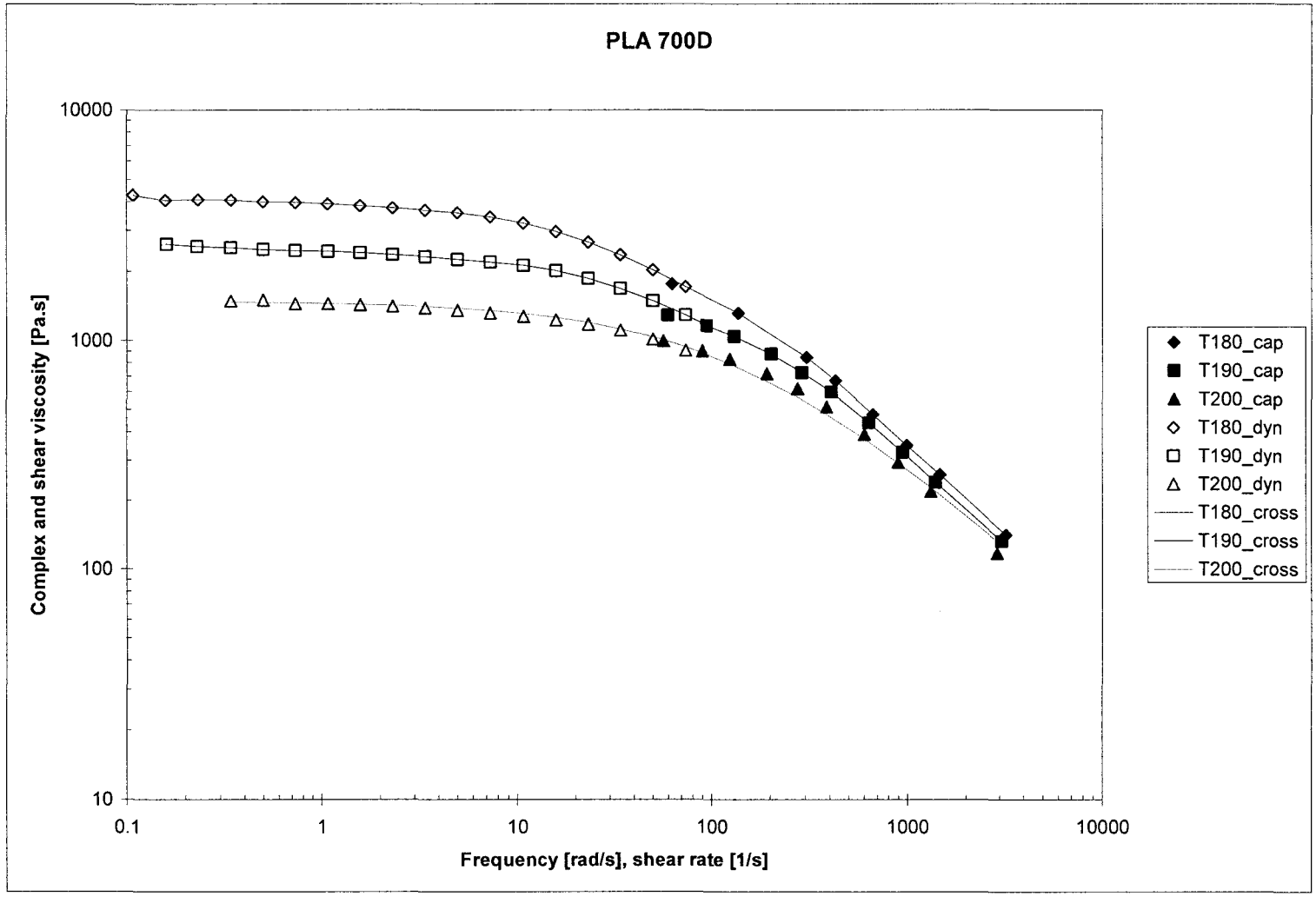

Figure 4.2.2. Complex and shear viscosity curves for PLA 7000D obtained correspondingly in parallel plate and capillary rheometers at 180, 190, and 200°C. Solid symbols represent capillary data. Lines represent Cross model fitted values.

data Cross model. It was observed that PLA 7000D exhibits typical pseudoplastic behaviour. At low shear rates this PLA resin has a well defined Newtonian region and at higher shear rates its shear viscosity declines rapidly. It is seen from Figure 4.2.2 that the Cross model fits the experimental data well.

The temperature coefficient *b* for the Cross model has been calculated as explained above in section 4.1. The results of the temperature sensitivity and shear rate dependence are summarized in Table 4.2.1.

Table 4.2.1 Cross model parameters: zero shear viscosity η_0, relaxation time λ, power-law exponent **n**, and temperature coefficient **b** for PLA 7000D, $T_{ref} = 180^{\circ}C$:

Polymer	T [°C]	Zero shear viscosity η_0 [Pa.s]	Relaxation time λ [s]	Power-law exponent *n*	Temperature coeff. *b* [$^{O}C^{-1}$]
PLA 7000D	180	4220	0.022	0.22	n.a.
	190	2630	0.013	0.22	0.05
	200	1485	0.007	0.22	0.05

The above presented results show that viscosity of PLA 7000 D is less sensitive to temperature variations than PLA 4042D. In comparison with some conventional polymers, PLA 7000D has temperature sensitivity (b = 0.05), which is similar to that of polystyrene (PS), but is bigger than polyethylenes (b = 0.01-0.03) (Vlachopoulos and Wagner, 2001).

4.2.2 Storage and Loss Moduli of PLA 7000D

Figure 4.2.3 shows the G' and G" curves of PLA 7000D at temperatures 180°C, 190°C, and 200°C. It can be seen that at all temperatures the storage modulus curve lies below the loss modulus curve (i.e. G" >> G'). Hence, for the temperature range 180°C –

200°C PLA 7000D exhibits liquid type viscoelastic behaviour The slope of the storage modulus curve on the log-log graph changes from 1.65 for 180°C, through 1.73 for 190°C, to 1.99 for 200°C. This behaviour shows the diminishing elastic contribution of the polymer chain entanglements with the temperature increase. The slopes of the loss modulus for 180°C, 190°C, and 200°C are correspondingly 0.96, 0.96, and 0.97.

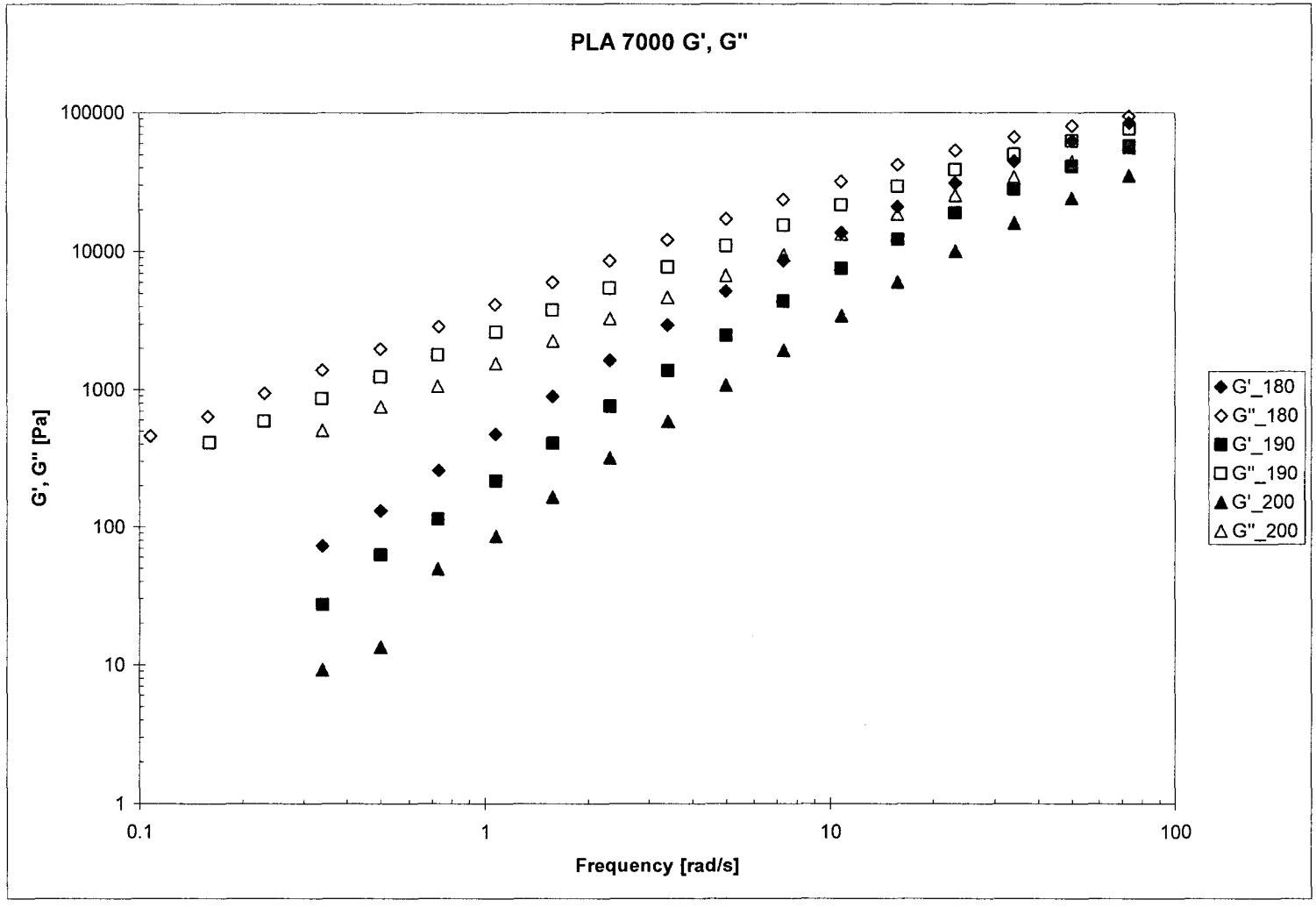

Figure 4.2.3. Curves of storage and loss moduli for PLA 7000D at 180°C, 190°C, and 200°C. Solid symbols represent loss modulus data (G").

4.2.3 Normal Stress Differences of PLA 7000D

Plots of the difference N_1-N_2 (i.e. first normal stress difference minus the secondary stress difference) as a function of shear rate and 2G' as a function of angular frequency of PLA 7000D at temperatures 180°C, 190°C, and 200°C are presented on figure 4.2.4. If we assume that N_2 is negligible, this plot shows that for this PLA resin there is a deviation from the assumption $N_1 \approx 2G'$ at low shear rates and frequencies for all temperatures. Like with PLA 4042D, these results suggest that this behaviour might be further investigated by using a cone and plate rheometer which gives N_1 directly and then N_2 can be determined from the present data of $N_1 - N_2$.

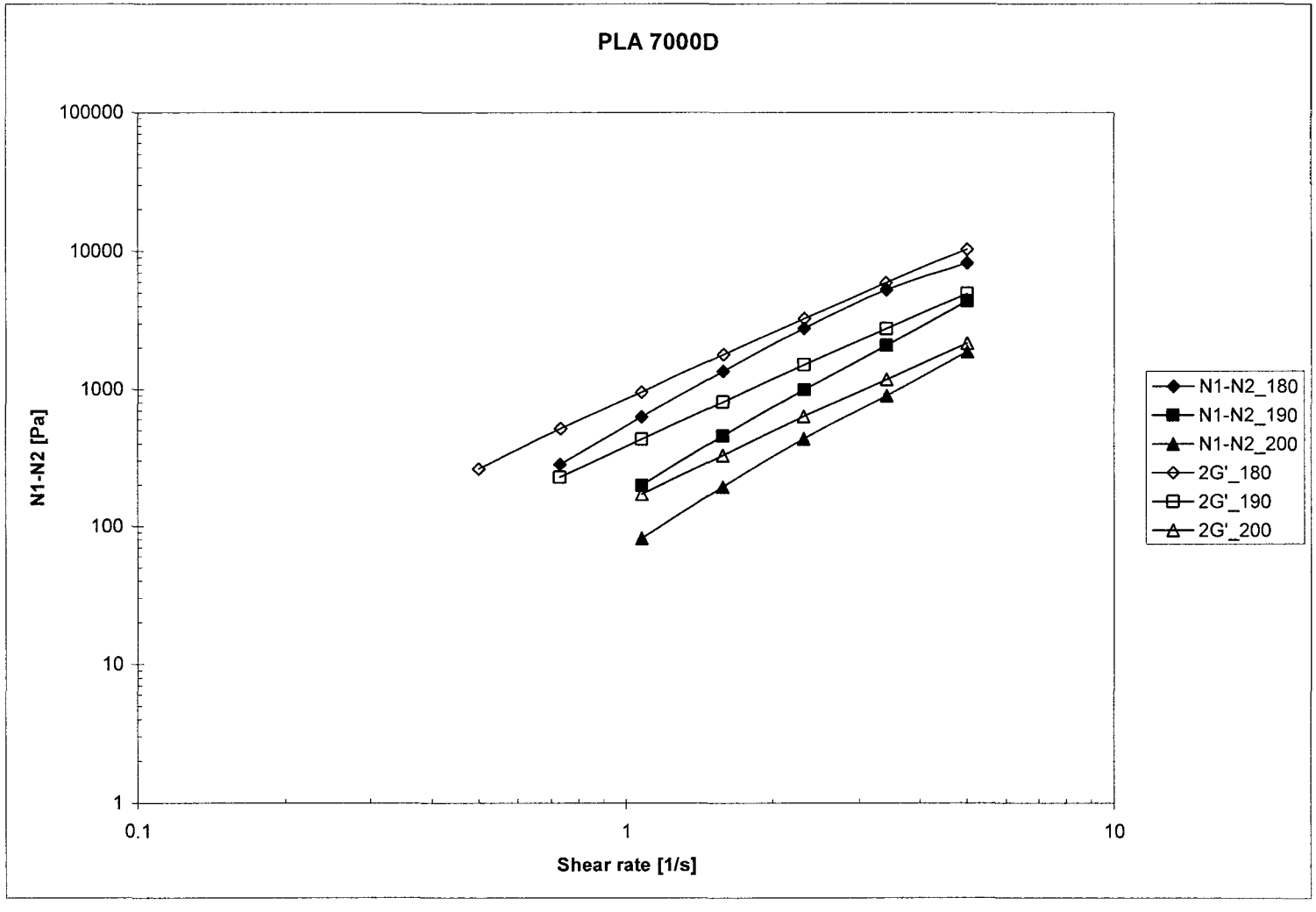

Figure 4.2.4. Normal stress difference and 2G' curves for PLA 7000D at 180°C, 190°C and 200°C. Open symbols represent 2G' values.

4.2.4 Extensional Viscosity of PLA 7000D

Figure 4.2.5 shows the dependence of tensile extensional viscosity on extensional rate of strain, obtained by the Cogswell method for PLA 7000D. It is compared with shear viscosity data, which was obtained by combining the complex viscosity and shear viscosity curves. Again, the values of the extensional viscosity are larger then those of the shear viscosity. For PLA 7000D the Trouton ratios η_e/η are approximately from 2.1 to 3.7, which are very close to the η_e/η ratio for Newotonian fluids at near zero rates of deformation. The PLA 7000D results differ largely from both the theory and the experimental data obtained with other polymers. For example, at high rates the Trouton ratio of branched LDPE can reach 200 – 300 (Vlachopoulos, 2005). For linear HDPE, the η_e/η are ranging from 10 to 35 (Vlachopoulos, 2005; Binding *et al.*, 1998).

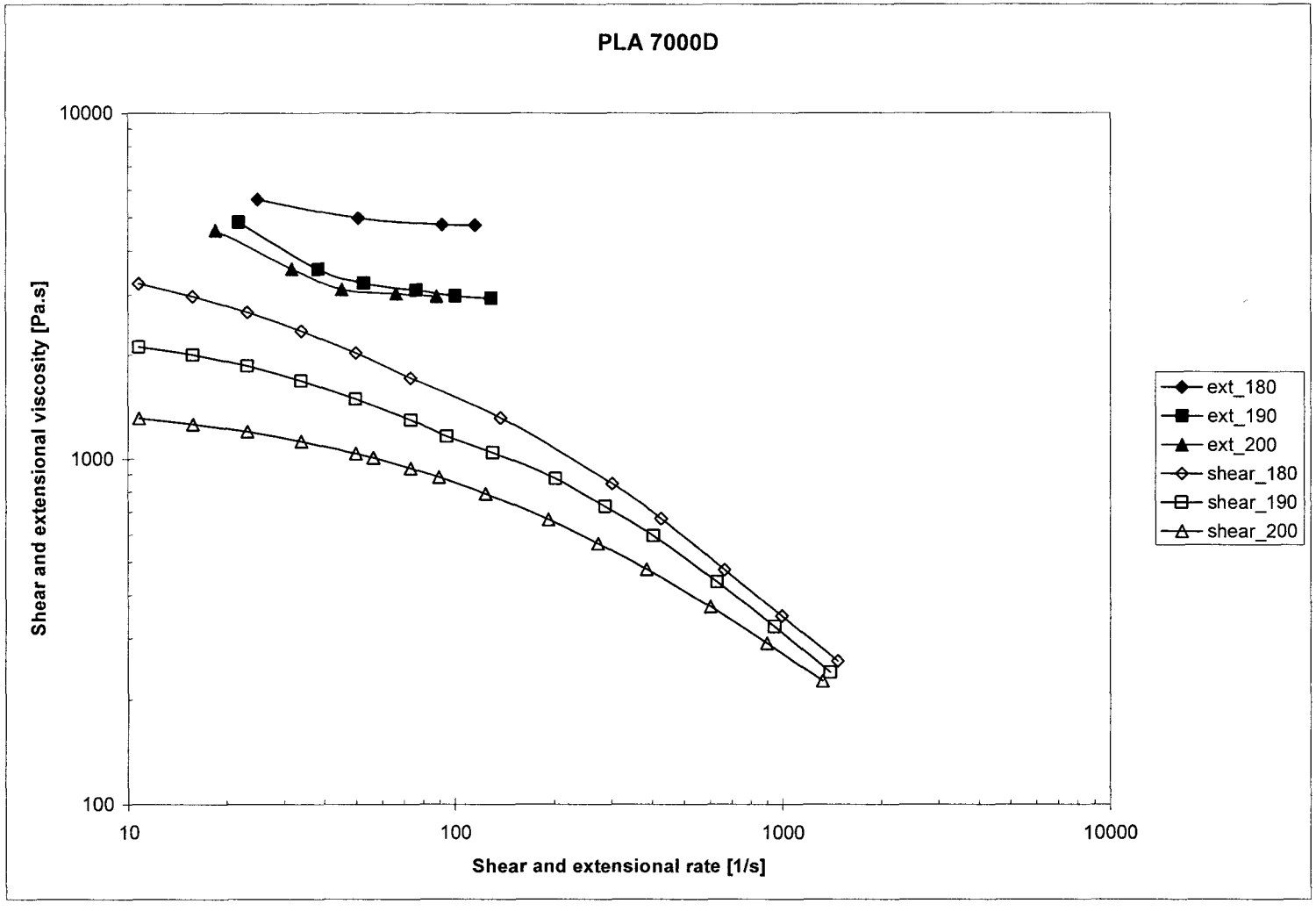

Figure 4.2.5. Extensional viscosity and shear viscosity curves for PLA 7000D at 180, 190, and 200°C. Open symbols represent shear viscosity data.

4.2.5 Wall Slip of PLA 7000D

Results from the wall slip study are presented in this subsection. Figure 4.2.6 presents the stress curves of PLA 7000D. The measurements were taken at 180°C in stainless steel dies with aspect ratio L/D = 16 and diameters 1 mm, 1.5 mm and 2 mm.

From this plot is obvious that since the flow curves of the PLA 7000D obtained with different diameter dies do not collapse onto a single curve, there is some slippage at the die wall (Hatzikiriakos and Dealy, 1992; Dealy and Wissbrun, 1990).

As discussed in the previous section, the attempt to determine the slip velocities of PLA7000D by using the Mooney technique did not bring satisfactory results. Obviously, more sensitive methods for quantifying V_s have to be used.

Further studies are needed to determine if the underlying mechanism is cohesive failure at polymer-polymer interface or adhesive failure at polymer/wall interface.

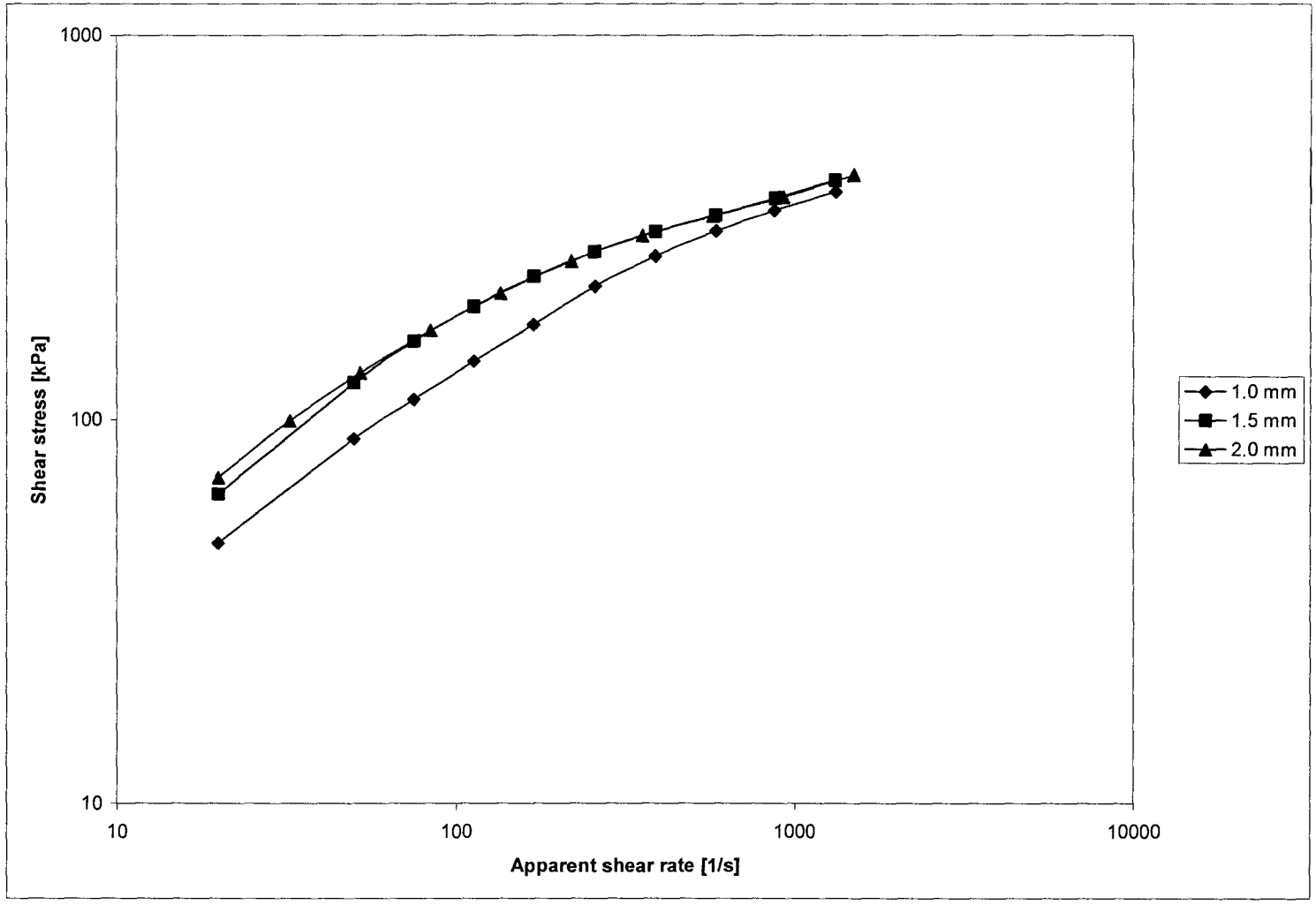

Figure 4.2.6. Flow curves for PLA 7000D at 180°C in different diameter dies with L/D = 16

4.2.6 Sharkskin and Gross Melt Fracture Phenomena in Flow of PLA 7000D

The onsets of flow instabilities and their location on the flow curve of PLA 7000D are schematically shown on figure 4.2.7.

Figure 4.2.8 shows the development of extrusion instabilities in capillary flow of PLA 7000 D. It was observed that PLA 7000D exhibits both sharkskin and gross melt fracture. For PLA 7000D sharkskin started at apparent shear rate of 75 s^{-1} and wall shear stresses of 140 kPa which is exactly the most frequently quoted value for the onset of sharkskin for HDPE and LLDPE. Gross melt fracture for PLA 7000D appeared at shear rates of 1200 s^{-1} and apparent shear stress of 400 kPa. This value of critical shear stress for onset of gross melt fracture of PLA 7000D is also often reported for LLDPE and HDPE. (Tadmor and Gogos, 2006; Dealy and Kim, 2005). Like PLA 4042D, PLA 7000D did not exhibit stick-spurt. Nevertheless, we can state that with regard to sharkskin and gross melt fracture, this grade of PLA behaves like other linear polymers such as linear low density polyethylene (LLDPE).

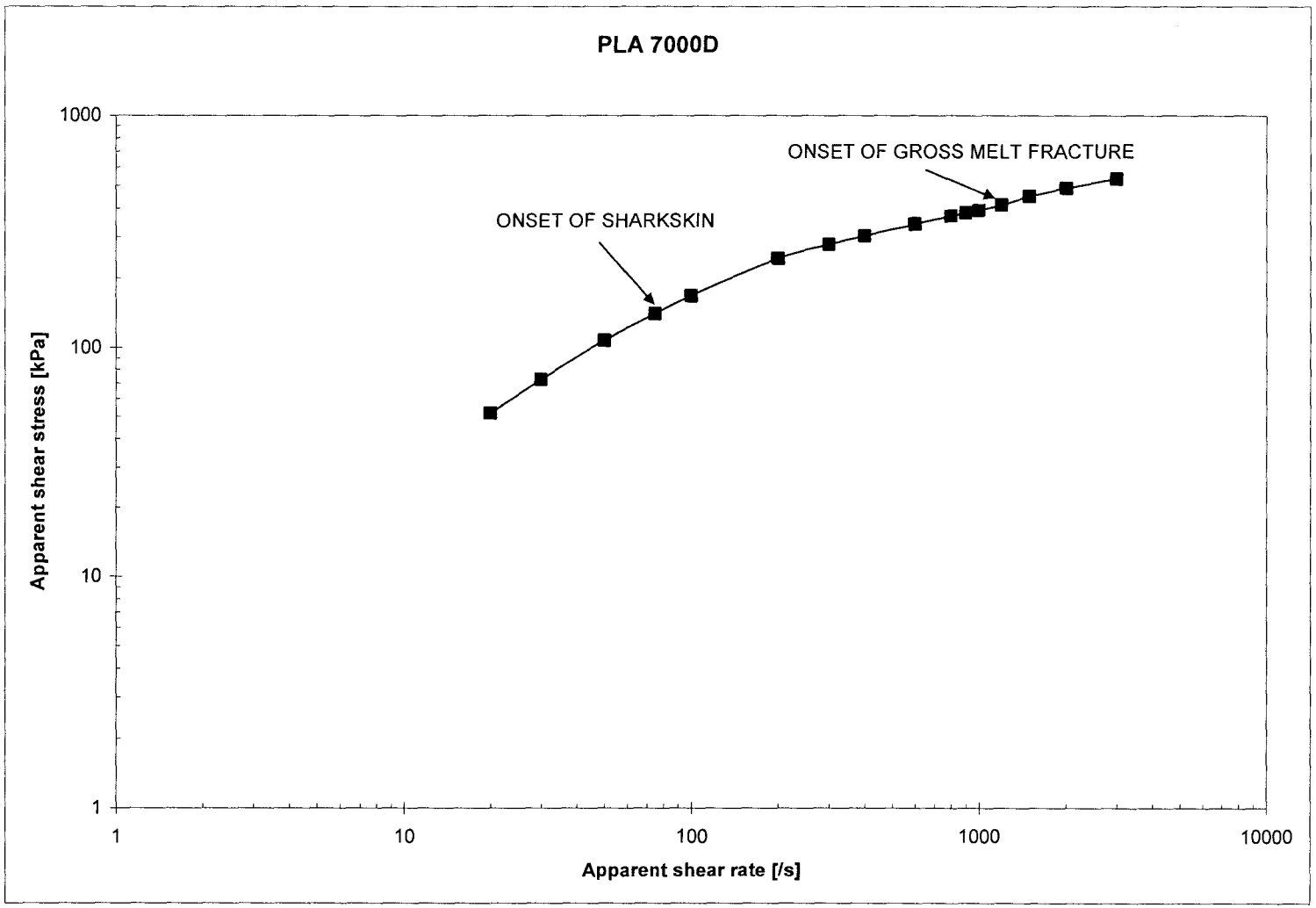

Figure 4.2.7. Flow curve and onsets of extrudate instabilities for PLA 7000D at 180°C in stainless steel die with D = 1mm and L/D = 16.

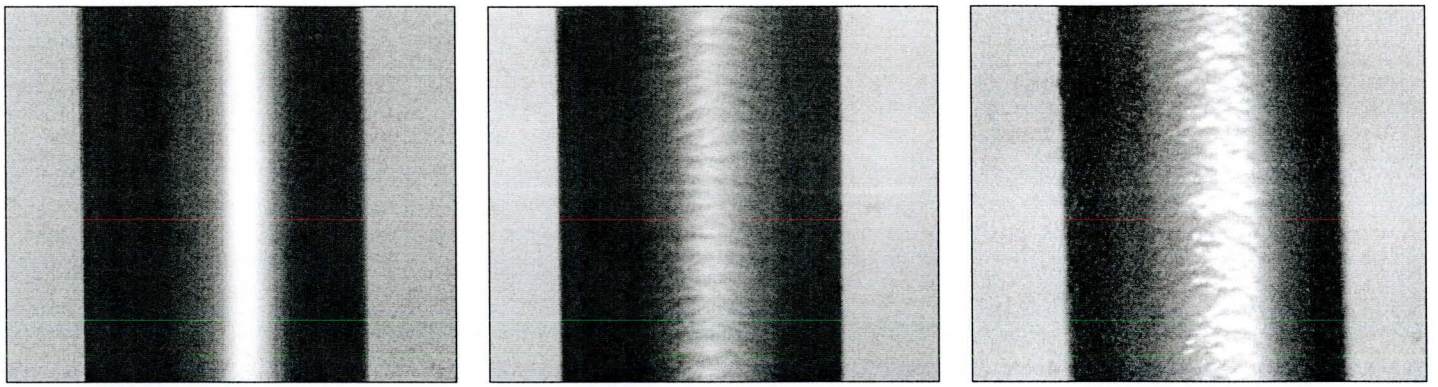

(a) smooth extrudate (b) start of sharkskin (c) more severe sharkskin

(d) very severe sharkskin (e) gross melt fracture

Figure 4.2.8. Evolution of extrudate instabilities for PLA 7000D in die with diameter 1mm and L/D = 16 at 180°C. The corresponding values of apparent shear rates and wall shear stresses are: (a) 50 s^{-1}, 110 kPa; (b) 100 s^{-1}, 170 kPa; (c) 600 s^{-1}, 280 kPa; (d) 1000 s^{-1}, 390 kPa; (e) 2000 s^{-1}, 490 kPa.

4.2.7 Extrudate Swell of PLA 7000D

Measurements of extrudate swell ratio of PLA 7000 D were performed after extrusion through a stainless steel die of diameter 2mm and of aspect ratio 16 at temperature 180°C and cooling into air at room temperature. The results are summarized in Table 4.2.3. The swell ratio increased with the increase of shear rate. PLA 7000 D had die swell in the interval of 1.18 to 1.29. Although the measured swell of PLA 7000D is bigger than the swell of PLA 4042D, it is small, compare to most conventional plastics. However, its values are approximately the same as of the rigid PVC, which is reported to have D/D0 from 1.27 to 1.3 at temperature 180°C (Huneault *et al.*, 1990)

Table 4.2.2 Extrudate swell for PLA 7000D in die with D = 2mm and L/D = 16, at T = 180°C

Apparent shear rate 1/s	Swell Ratio D/D_0
50	1.178
100	1.2
136	1.233
150	1.249
200	1.265
300	1.278

4.3 Rheological Characterisation of Ecoflex F BX 7011

This section presents results obtained using a parallel plate and a capillary rheometer for the biodegradable copolyester Ecoflex F BX 7011. These include results for loss and storage moduli, normal stresses and elongational viscosity. Results from tests for wall slip, extrudate swell, sharkskin and melt fracture of the aliphatic-aromatic copolyester are also presented and discussed.

4.3.1 Shear Viscosity of Ecoflex F BX 7011

Figures 4.3.1 and 4.3.2 explore the validity of the experimental Cox-Merz rule at low and high circular frequencies and shear rates. Figure 4.3.1 shows results at low frequencies and shear rates. It is obvious that for temperature 190°C the Cox-Merz rule holds very well. At 180°C and at 200°C some deviation from the Cox-Merz rule is observed.

Figure 4.3.2 presents results from complex viscosity measurements done in parallel plate rheometer operated in oscillatory mode together with shear viscosity, which was measured in capillary rheometer at high shear rates. It is seen from Figure 4.3.2 that at all temperatures the Cox-Merz rule holds for Ecoflex F BX 7011.

From the above it can be generally concluded that although there are some discrepancies between results from the different experimental methods, the Cox-Merz rule holds for Ecoflex F BX 7011. The discrepancies could be explained with the differences and the limitations of the experimental techniques, which were mentioned in Chapter 3.

From Figure 4.3.2 is obvious that the shear viscosity of Ecoflex F BX 7011 is sensitive to temperature and it exhibits moderate shear-thinning. Fitting to Cross model equations was employed to quantify the dependence of viscosity on shear rate and on temperature.

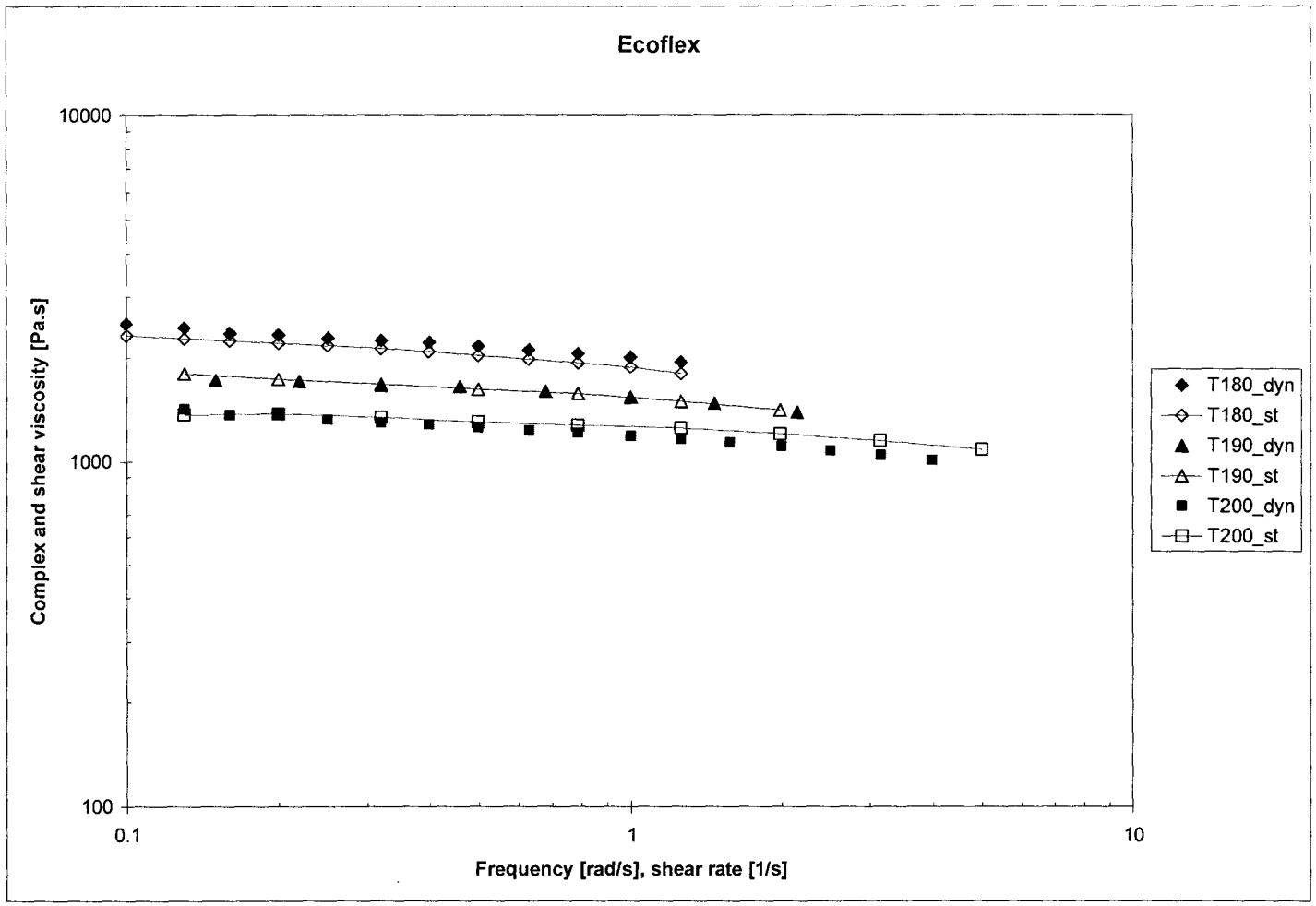

Figure 4.3.1. Complex and shear viscosity curves for Ecoflex F BX 7011 obtained in parallel plate rheometer at 180°C,190°C , and 200°C. Open symbols represent steady shear data. ("dyn" refers to dynamic and "st" to steady state measurements)

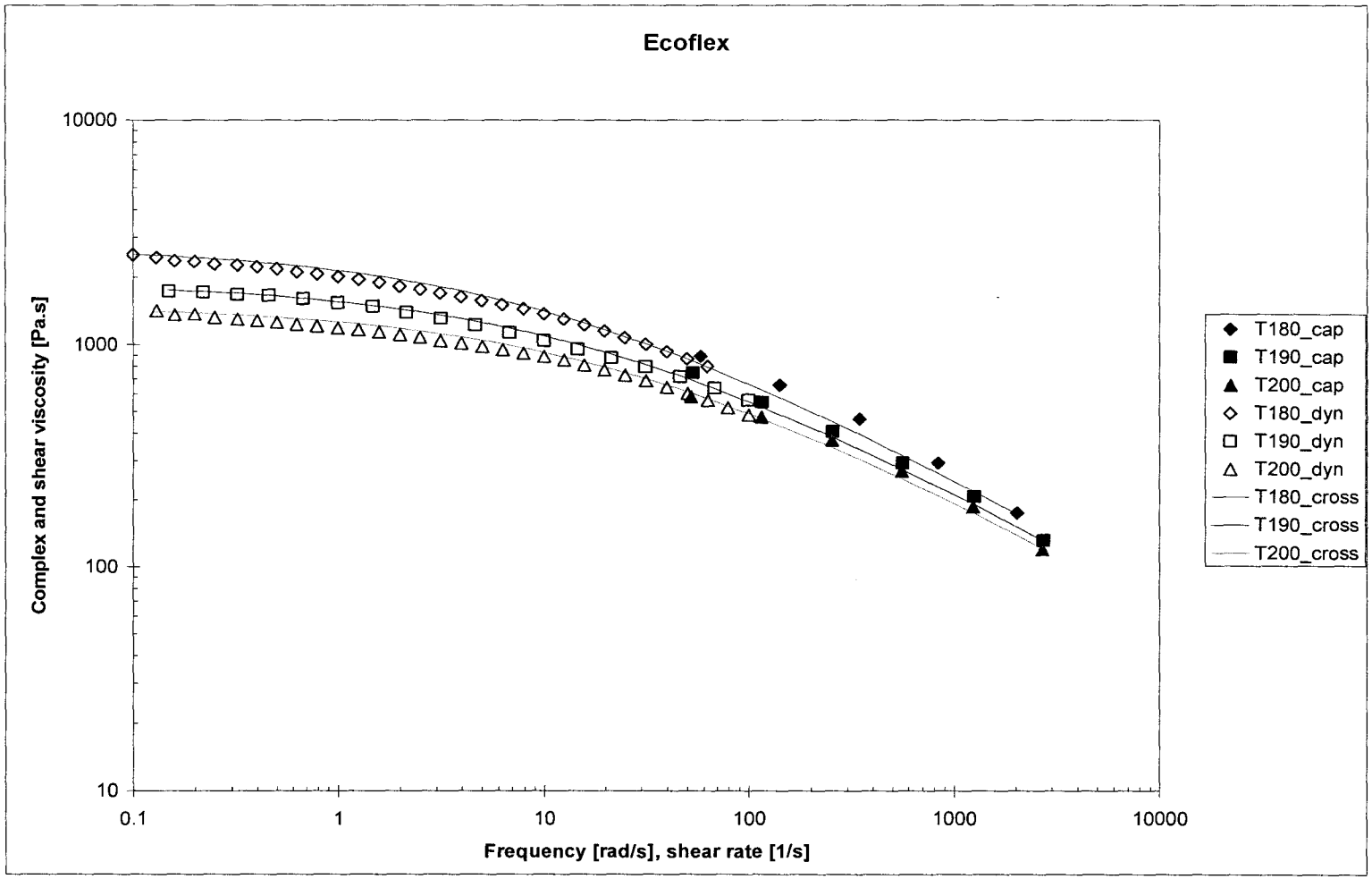

Figure 4.3.2. Complex and shear viscosity curves for Ecoflex F BX 7011 obtained correspondingly in parallel plate and capillary rheometers at 180, 190, and 200°C. Solid symbols represent capillary data. Lines represent Cross model fitted values.

Figure 4.3.2 shows the viscosity curves of Ecoflex F BX 7011 at three different temperatures. The lines represent viscosity values which are obtained by fitting Cross model to the experimental data. It was observed that Ecoflex exhibits pseudoplastic behaviour and does not have a well defined Newtonian region at low frequencies. Figure 4.3.2 also shows that the Cross model provides a good fit for the experimental data.

The temperature coefficient *b* for the Cross model has been calculated as explained above in section 4.1. The results of the temperature sensitivity and shear rate dependence are summarized in Table 4.3.1

Table 4.3.1 Cross model parameters: zero shear viscosity η_0, relaxation time λ, power-law exponent **n**, and temperature coefficient **b** for Ecoflex F BX 7011, $T_{ref} = 180^{\circ}C$:

Polymer	T [°C]	Zero shear viscosity η_0 [Pa.s]	Relaxation time λ [s]	Power-law exponent *n*	Temperature coeff. *b* [$^{O}C^{-1}$]
Ecoflex F	180	2750	0.09	0.48	n.a.
	190	1900	0.055	0.48	0.033
	200	1500	0.04	0.48	0.033

The above presented results show that viscosity of Ecoflex F BX 7011 is less sensitive to temperature variations than both PLA resins. In comparison with some conventional polymers, Ecoflex has temperature sensitivity similar to low density polyethylene (LDPE), for which $b = 0.03$. (Vlachopoulos and Wagner, 2001).

4.3.2 Storage and Loss Moduli of Ecoflex

Figure 4.3.3 shows the G' and G" curves of Ecoflex at temperatures 180°C, 190°C, and 200°C. It can be seen that at all temperatures the storage modulus curve lies below the loss modulus curve (i.e. G" >> G'). Hence, for the temperature range 180°C – 200°C Ecoflex F BX 7011 behaves as elastic liquid. The slope of the storage modulus curve on

the log-log graph changes from 1.32 for 180°C, through 1.34 for 190°C, to 1.46 for 200°C. This slope change shows the diminishing elastic contribution of the polymer chain entanglements with the temperature increase. The slopes of the loss modulus for 180°C, 190°C, and 200°C are correspondingly 0.87, 0.88, and 0.91

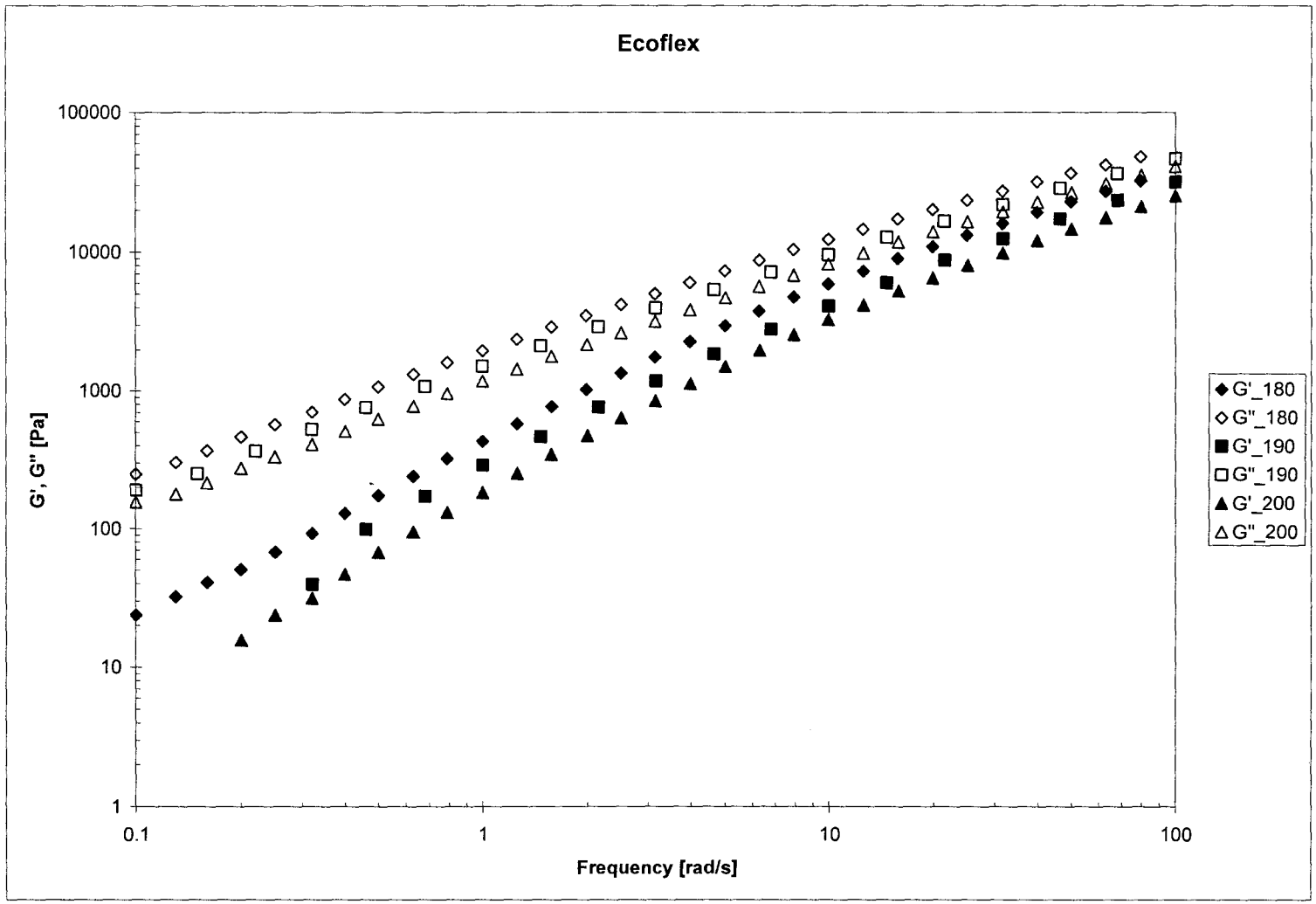

Figure 4.3.3. Curves of storage and loss moduli for Ecoflex F BX 7011 at 180°C, 190°C, and 200°C. Solid symbols represent loss modulus data (G").

4.3.3 Normal Stress Differences of Ecoflex

Plots of the difference N_1-N_2 (i.e. first normal stress difference minus the secondary stress difference) as a function of shear rate and 2G' as a function of angular frequency of Ecoflex F BX 7011 at temperatures 180, 190°C, and 200°C are presented on Figure 4.3.4. From this plot we can see that for 180°C the assumption $N_1 \approx 2G'$ at low shear rates and frequencies is approximately valid (especially if we consider the contribution of $N_2 = -0.1N_1$). For higher temperatures, though, larger deviations are seen. In similarity with both PLA resins, these results suggest that this behaviour might be further investigated by using a cone and plate rheometer which gives N_1 directly and then N_2 can be determined from the present data of $N_1 - N_2$

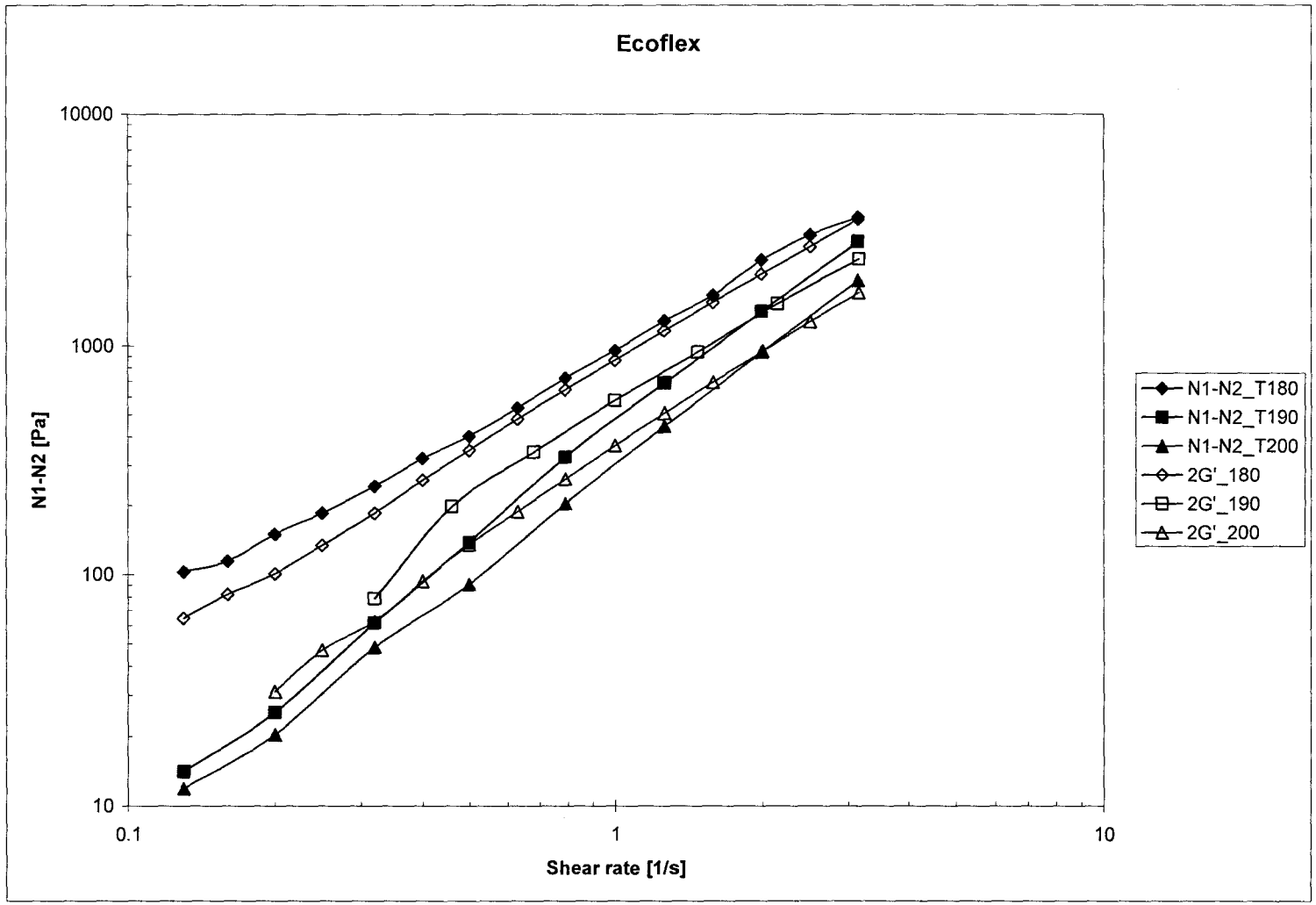

Figure 4.3.4. Normal stress difference and 2G' curves for Ecoflex F BX 7011 at 180°C, 190°C and 200°C. Open symbols represent 2G' values.

4.3.4 Extensional Viscosity of Ecoflex

Figure 4.3.5 shows the dependence of tensile extensional viscosity on extensional rate of strain, obtained by the Cogswell method for Ecoflex F BX 7011. It is compared with shear viscosity data, which was obtained by combining the complex viscosity and shear viscosity curves. From this figure we can see that the extensional viscosity of Ecoflex is larger than its shear viscosity. The values of the Trouton ratios η_e/η range approximately from 6.9 to 12.5. While these values are larger than the Newtonian fluids' η_e/η_0 ratio of 3, they are close to the η_e/η values of linear HDPE, which are ranging from 10 to 35 (Vlachopoulos, 2005, Binding *et al.*, 1998).

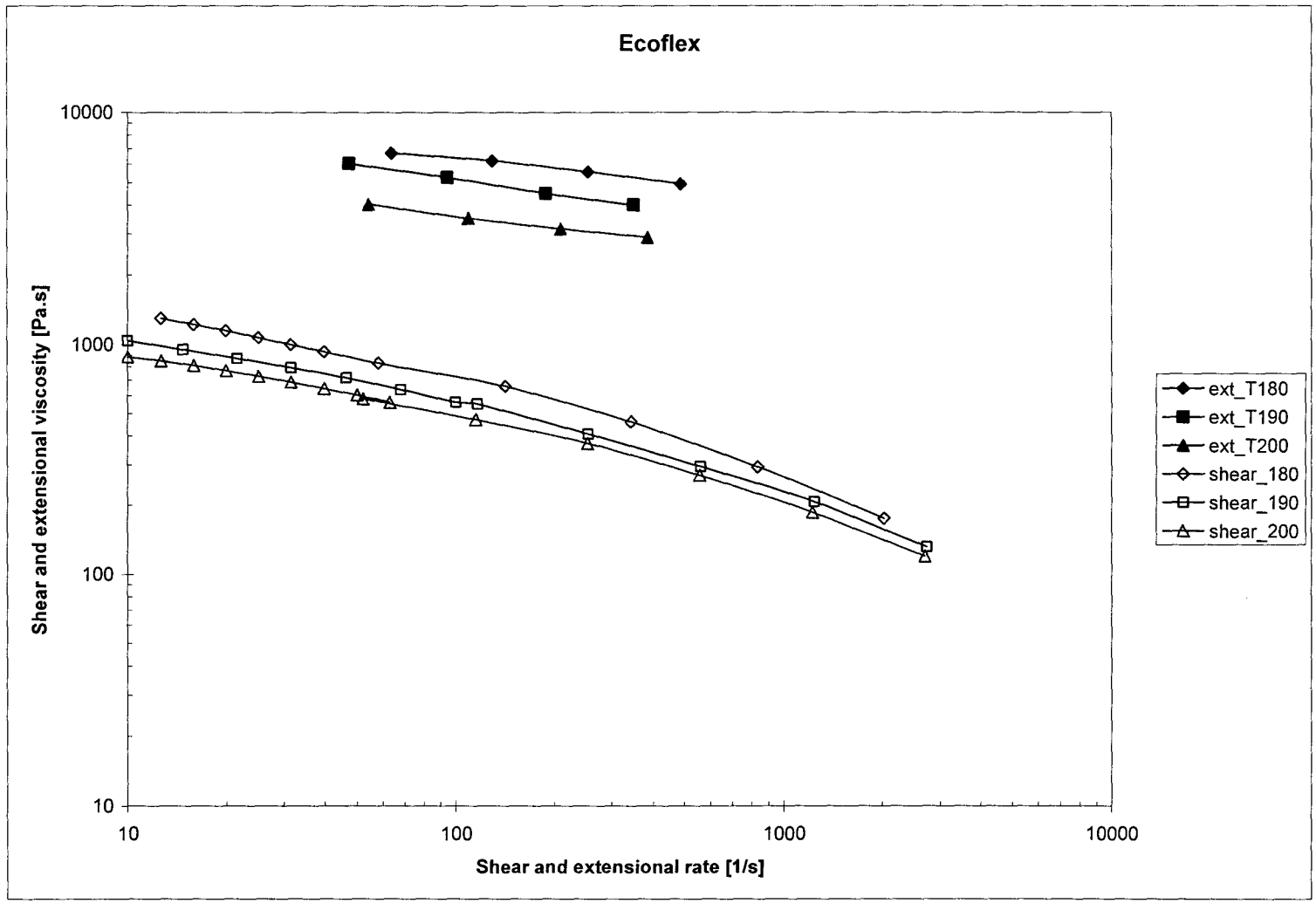

Figure 4.3.5. Extensional viscosity and shear viscosity curves for Ecoflex F BX 7011 at 180, 190, and 200°C. Open symbols represent shear viscosity data.

4.3.5 Wall Slip of Ecoflex

Results from the wall slip study are presented in this subsection. Figure 4.3.6 presents the stress curves of Ecoflex F BX 7011. The measurements were taken at 180°C in stainless steel dies with aspect ratio L/D = 16 and diameters 1 mm, 1.5 mm and 2 mm.

From this we see that the curves almost collapse as they should if there was no slip. However, the differences are small and they may be due to some degradation or other source of variance associated with this difficult to extrude material. We conclude that if there is indeed slip, it is probably small. As suggested above in section 4.1, gap-dependant wall slip measurements using rotational or planar parallel plate rheometers might be used for quantifying the slip velocity of Ecoflex instead of the Mooney method. It might be also desirable to conduct further studies to determine the underlying mechanism of wall slip of Ecoflex.

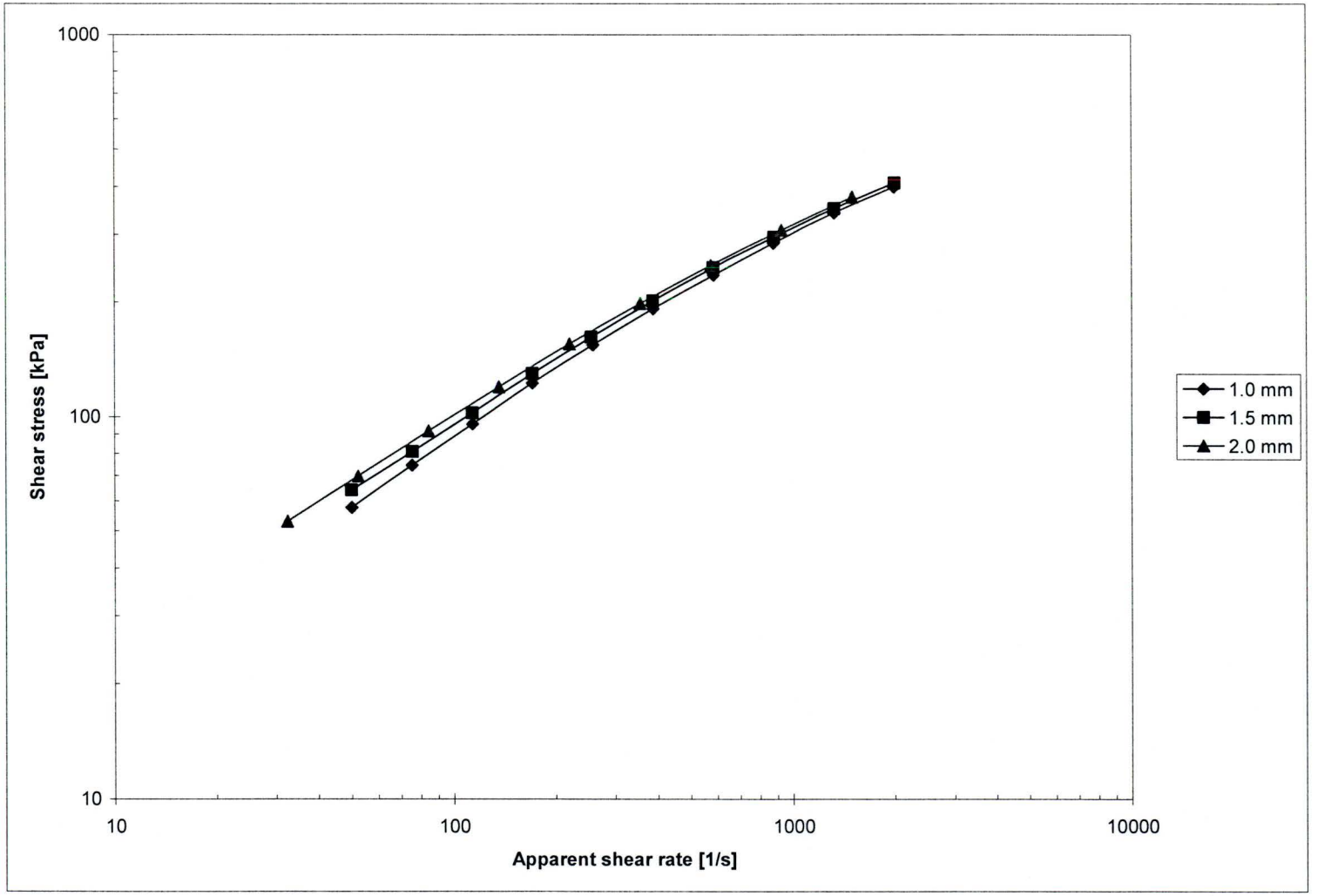

Figure 4.3.6. Flow curves for Ecoflex F BX 7011 at 180°C in different diameter dies with L/D = 16

4.3.6 Sharkskin and Gross Melt Fracture Phenomena in Flow of Ecoflex

The onsets of flow instabilities and their location on the flow curve of Ecoflex F BX 7011 are schematically shown on figure 4.3.7.

Figure 4.3.8 shows the development of extrusion instabilities in capillary flow of Ecoflex F BX 7011. While extruding Ecoflex at temperature 180 °C and shear rates from 20-5000 s^{-1} no instabilities were observed. In order to study its behaviour, Ecoflex was extruded through the same die as PLA at temperature 160°C. It was observed that the Ecoflex extrudate was smooth from low shear stresses to a certain critical shear stress 580 kPa (shear rate 3500 s^{-1}) when it became completely distorted. This behaviour showed that Ecoflex did not exhibit the sharkskin phenomenon but only had gross melt fracture, which is similar to the behaviour of low density polyethylene (LDPE) (Baird and Collias, 1998) or polystyrene (Agassant *et al.*,2006). Extrudates of Ecoflex are shown on Figure 4.3.8.

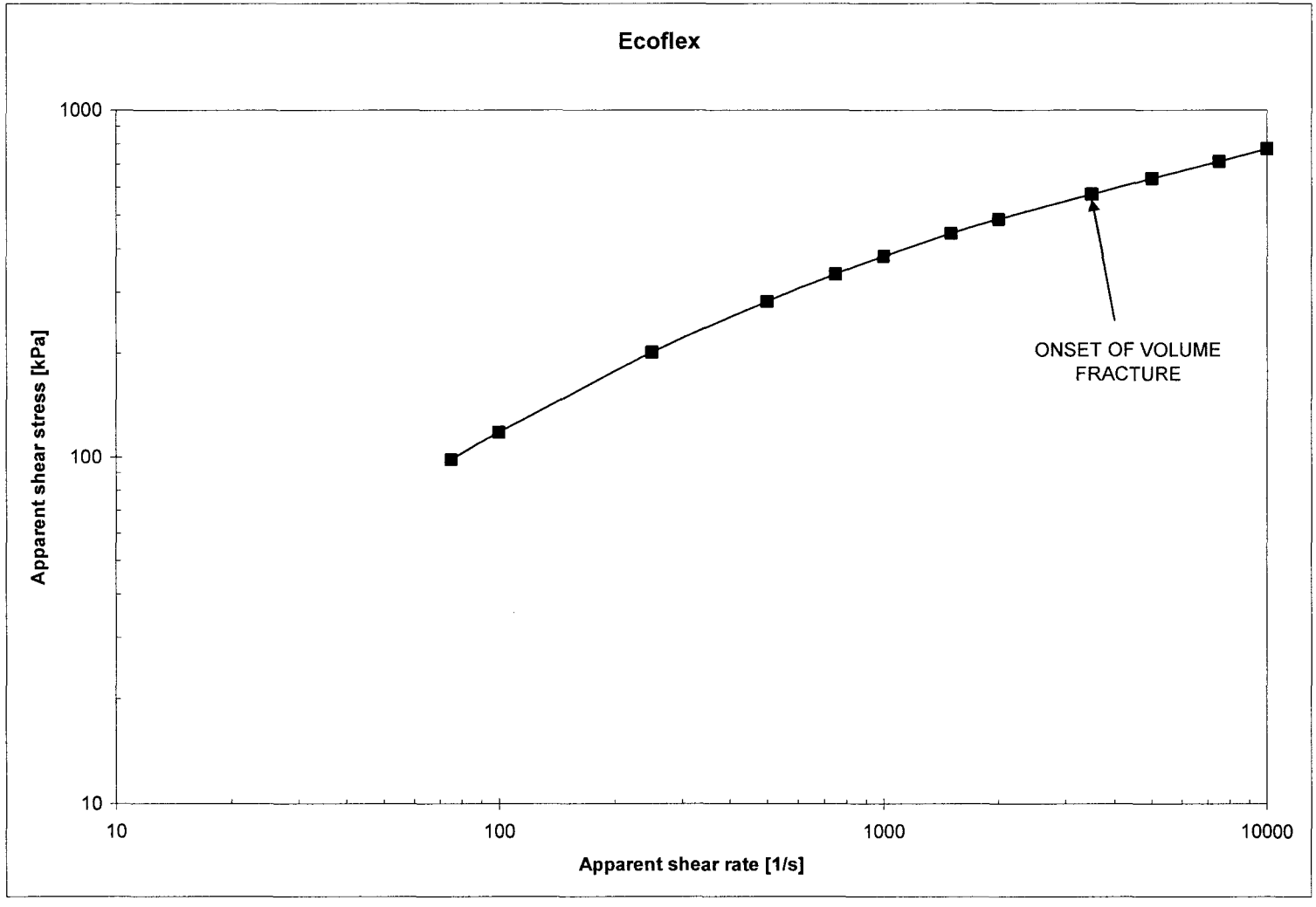

Figure 4.3.7. Flow curve and onsets of extrudate instabilities for Ecoflex F BX 7011 at 160°C in stainless steel die with D = 1 mm and L/D = 16.

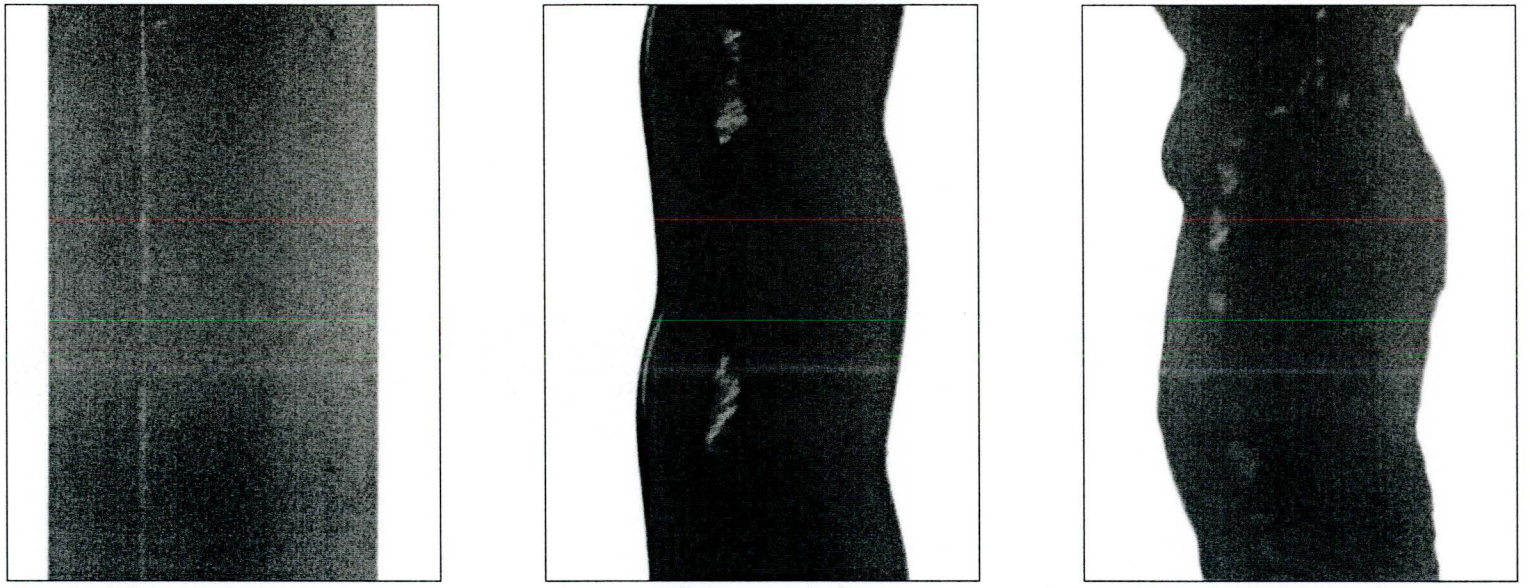

(a) smooth extrudate (b) start of gross melt fracture (c) helical gross melt fracture

Figure 4.3.8. Evolution of extrudate instabilities for Ecoflex F BX 7011 in die with diameter 1mm and L/D = 16 at 160°C. The corresponding values of apparent shear rates and wall shear stresses are: (a) 3000 s^{-1}, 540 kPa; (b) 5000 s^{-1}, 636 kPa; (c) 7000 s^{-1}, 713 kPa.

4.3.7 Extrudate Swell of Ecoflex

Measurements of extrudate swell ratio of Ecoflex F BX 7011D were performed after extrusion through a stainless steel die of diameter 2mm and of aspect ratio 16 at temperature 180°C and cooling into air at room temperature. The results are summarized in Table 4.3.2. The swell ratio increased with the increase of shear rate. Ecoflex F BX 7011 had die swell in the interval of 1.23 to 1.34. Although the measured swell of Ecoflex F BX 7011 is bigger than the die swell of both grades PLA, it is small in comparison with most conventional plastics, except rigid PVC, which is reported to have swell ratio from 1.27 to 1.3 at 180°C (Huneault *et al.*, 1990).

Table 4.3.2 Extrudate swell for Ecoflex F BX 7011 in die with D = 2mm and L/D = 16, at T = 180°C

Apparent shear rate 1/s	Swell Ratio D/D_0
50	1.227
100	1.292
136	1.299
150	1.313
200	1.328
300	1.34

4.4 Rheological Characterisation of PLA/Ecoflex Blends

Blends of PLA 7000 D and Ecoflex F BX 7011 were studied to determine the effect of blending on the processability of PLA. The blends were with PLA content 90 wt% and 10 wt%. For simplicity, these blends are referred to as P90E10 and P10E90, respectively.

This section presents results from viscosity measurements in parallel plate and capillary rheometers for the biodegradable polymer blends. Results for storage modulus and results from tests for sharkskin and melt fracture of the PLA/Ecoflex blends are also presented and discussed.

4.4.1 Shear Viscosity of PLA/Ecoflex Blends

First, the effect of mixing conditions on rheological properties of both biodegradable polyesters was investigated. On Figure 4.4.1 Viscosity curves of PLA and Ecoflex resins after processing for 10 minutes at 190°C in a Haake internal mixer together with viscosity curves of the neat polymers are presented. The complex viscosity measurements were done in parallel plate rheometer operated in oscillatory mode. Shear viscosity was measured in capillary rheometer at high shear rates. All the measurements were taken at 190°C. It can be seen that there is a significant drop in viscosity (up to 50%) as a result of the mixing procedure in Haake. For PLA the extent of Newtonian region and the shear-thinning behaviour remained the same. In the case of Ecoflex after processing in Haake, we observe a wider Newtonian region and less expressed shear-thinning in comparison with the neat resin. This could be attributed not only to a reduction of chain lengths but also to a lower degree of branching. It is also obvious from Fig. 4.4.1 that the Cox-Merz rule, $\eta^*(\omega) = \eta(\dot{\gamma})$ applies not only to the neat resins but

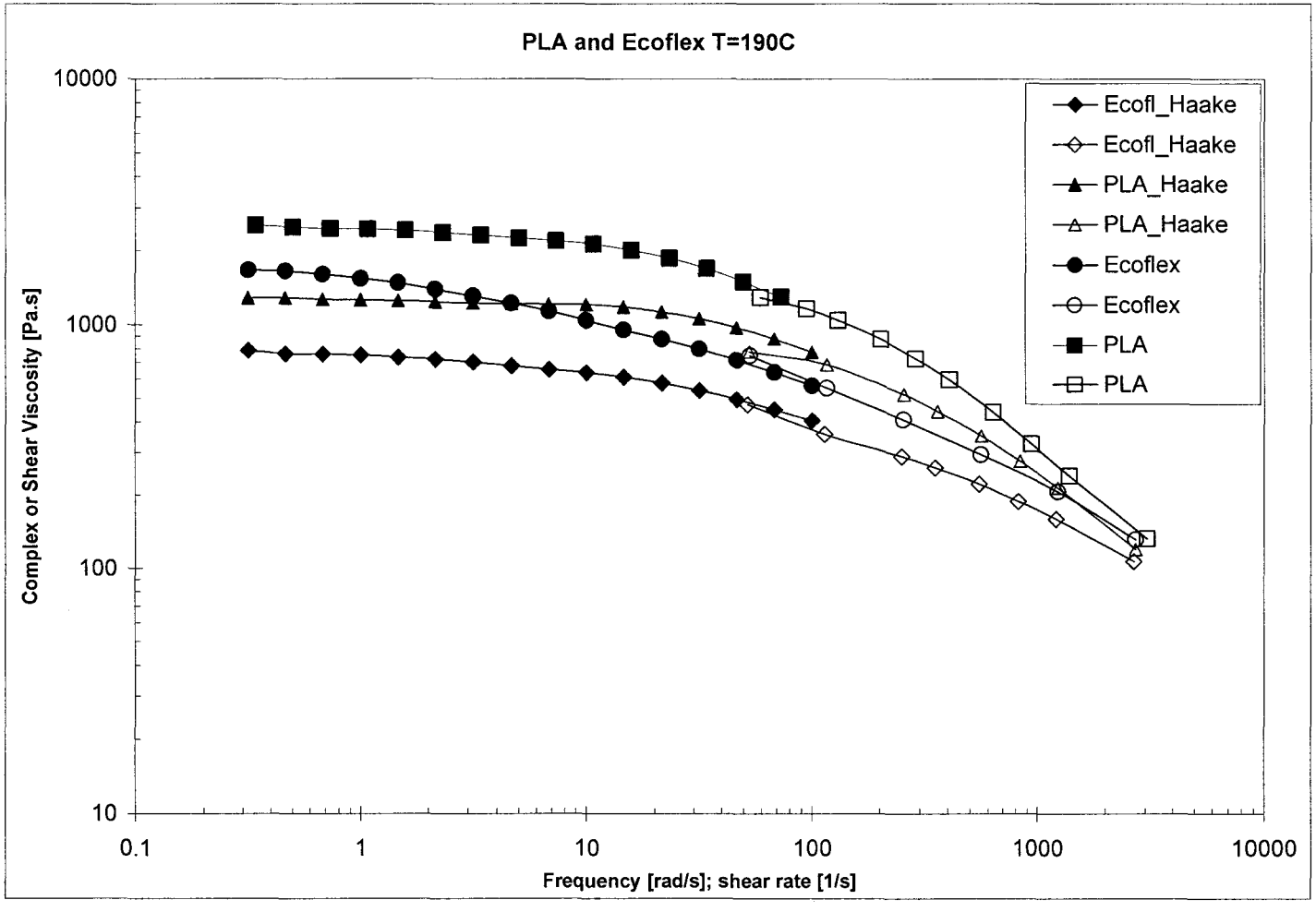

Figure 4.4.1. Complex and shear viscosity curves, obtained correspondingly in parallel plate and capillary rheometers at 190°C for PLA 7000 D and Ecoflex F BX 7011 before and after mixing in Haake mixer at T=190°C. Open symbols represent capillary data.

also to both polymers after being subjected to the Haake mixing cycle. The same behaviour was observed at temperature 180°C.

Figure 4.4.2 presents results from dynamic and steady viscosity measurements in parallel plate rheometer for PLA 7000 and Ecoflex resins, which were subjected to mixing in Haake. This figure shows that at temperature 190°C and at low frequencies and shear rates the Cox-Merz rule is valid. In similarity with the neat resins discussed in sections 4.2 and 4.3, a minor deviation from the Cox-Merz rule was observed at 180°C.

From the above it can be concluded that both resins degrade during a mixing process. Yet their morphology remains rheologically stable (i.e. it either does not change or changes in a well defined manner), because the validity of Cox-Merz rule proves that the rheological behaviour of the melts remains unaffected by the flow geometry or strain field.

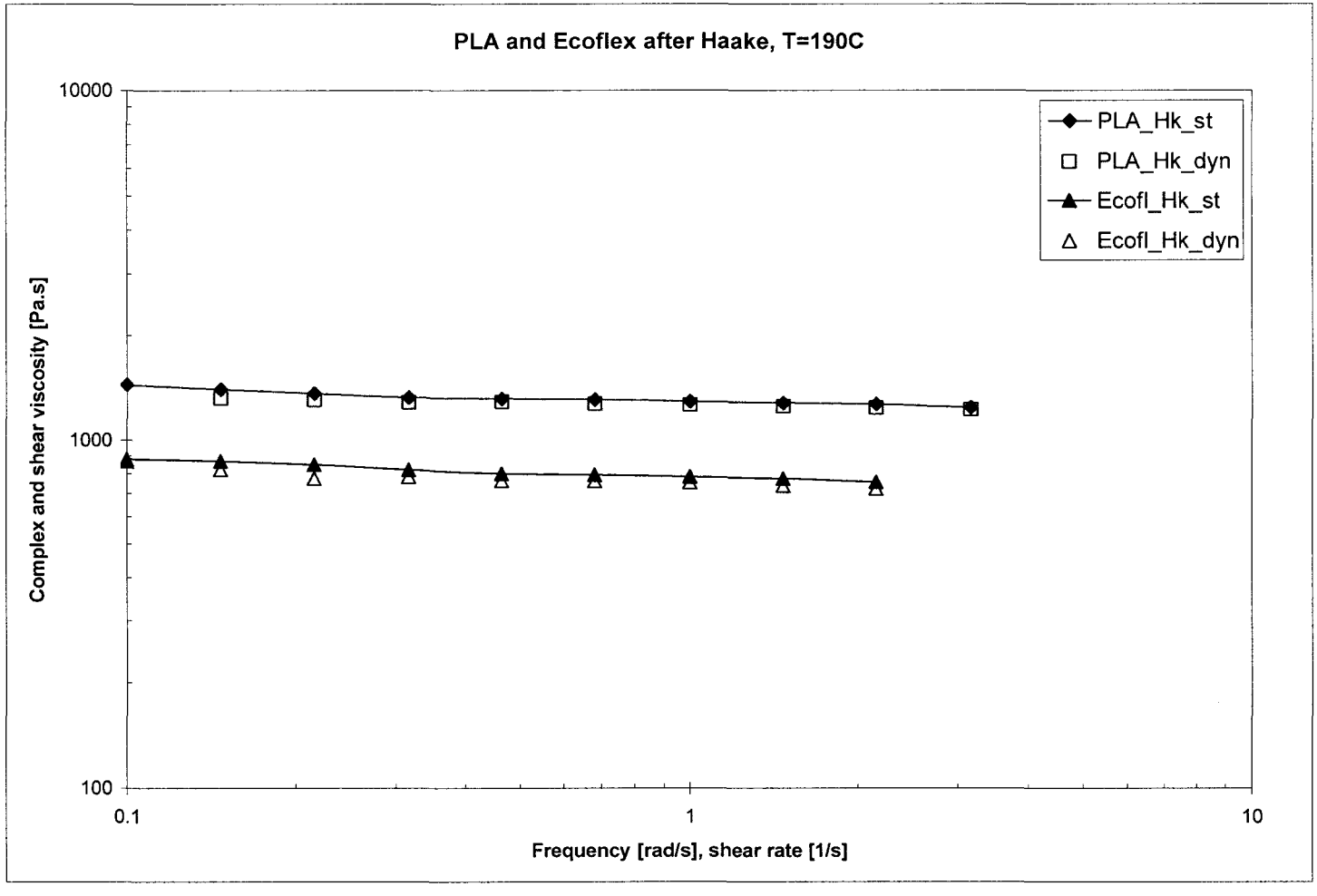

Figure 4.4.2 Complex and shear viscosity curves obtained in parallel plate rheometer at 190°C for PLA 7000D and Ecoflex F BX 7011, subjected to Haake mixing. Solid symbols represent steady shear data. ("dyn" refers to dynamic and "st" to steady state measurements)

Figures 4.4.3 and 4.4.4 show complex and steady shear viscosity results from parallel plate rheometer for blends P90E10 and P10E90 (i.e. PLA content 90 and 10 wt%, respectively). We can see that although the viscosity behaviour of the blends in steady shear and oscillatory flow is similar, there is notable deviation from the Cox-Merz rule - up to 20% difference is observed in the case of P10E90 (Figure 4.4.4).

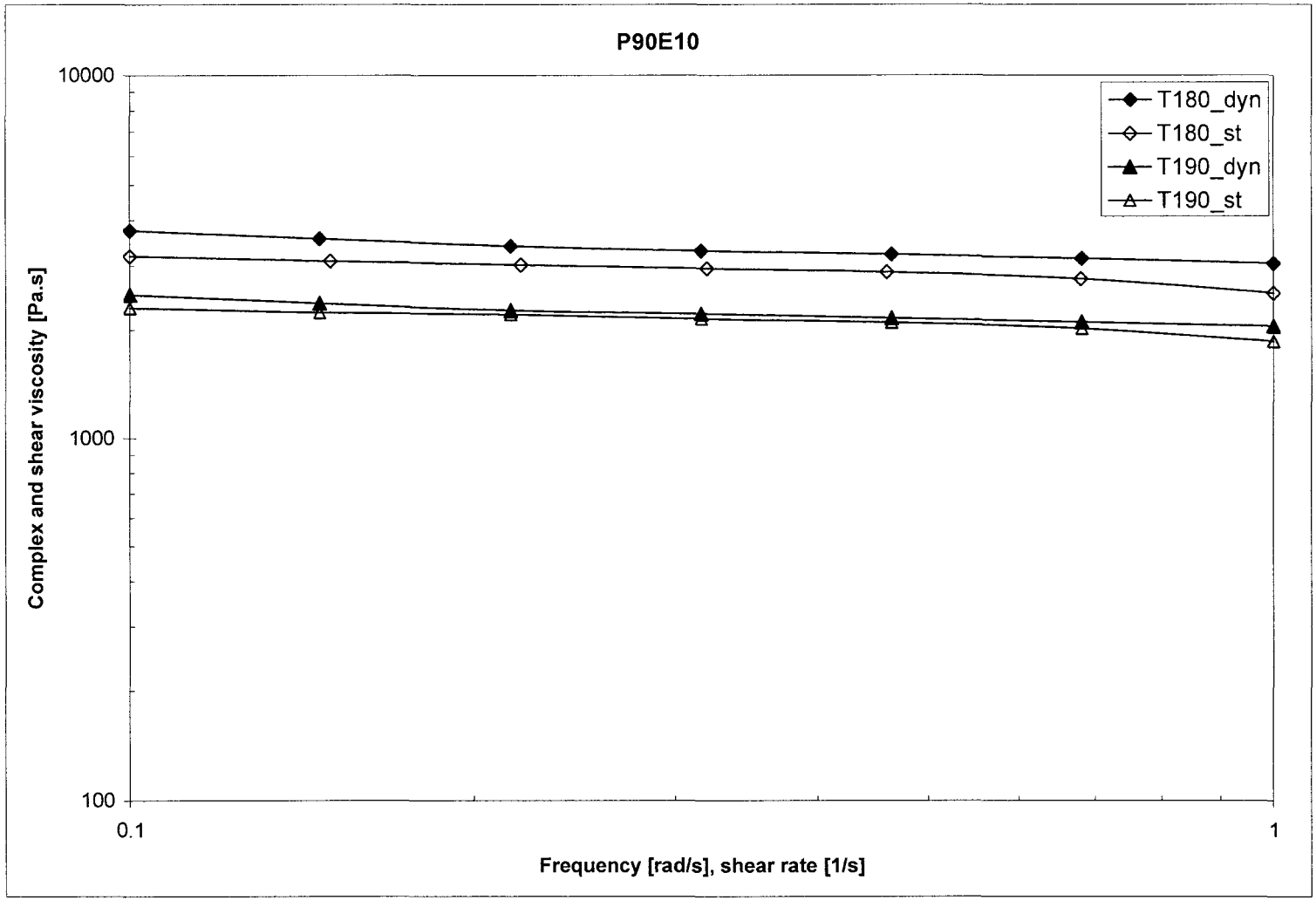

Figure 4.4.3. Complex and shear viscosity curves of blend 90% PLA/10% Ecoflex obtained in parallel plate rheometer at 180 and 190°C. Open symbols represent steady shear data. ("dyn" refers to dynamic and "st" to steady state measurements)

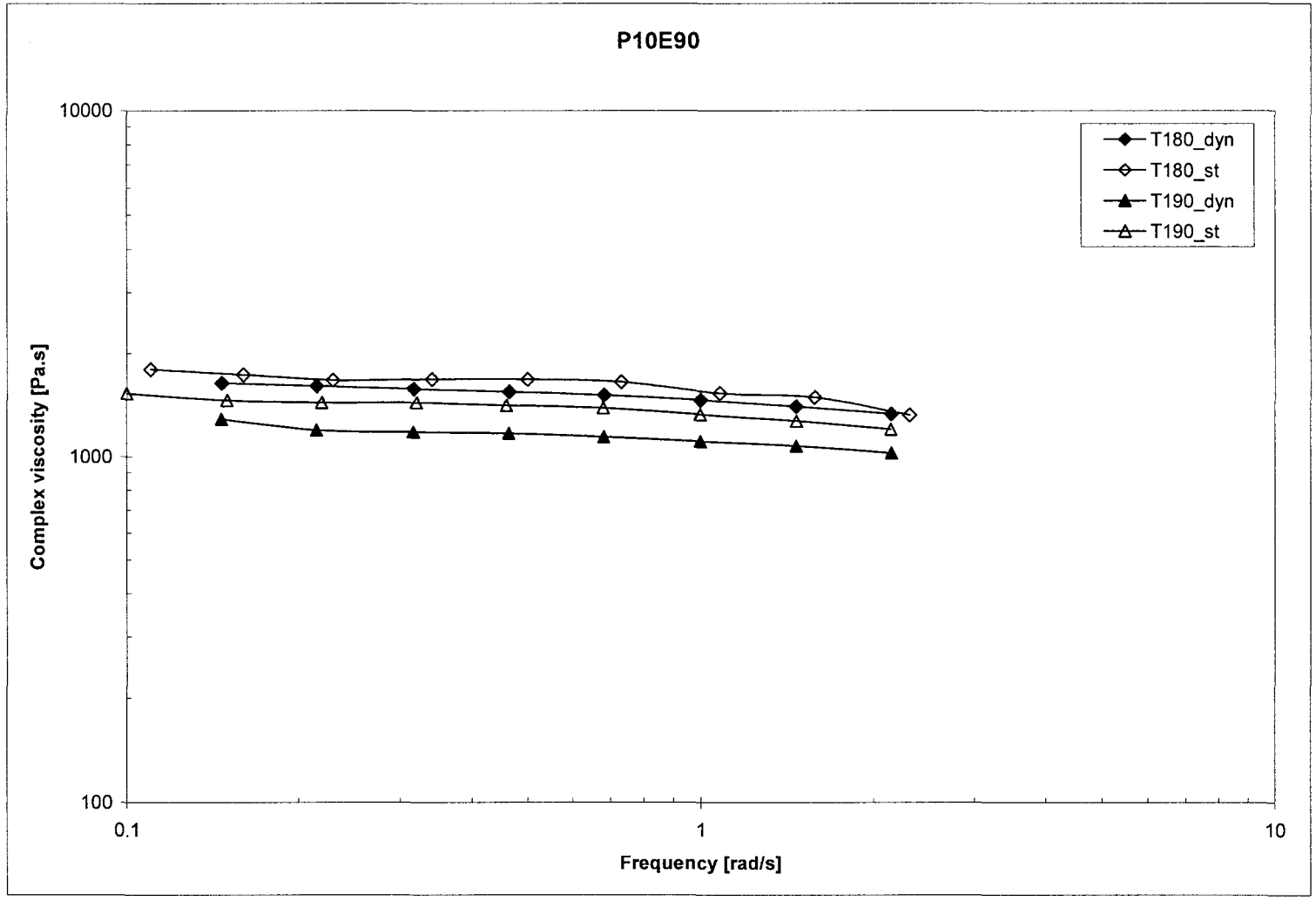

Figure 4.4.4. Complex and shear viscosity curves of blend 10% PLA/ 90% Ecoflex obtained in parallel plate rheometer at 180 and 190°C. Open symbols represent steady shear data. ("dyn" refers to dynamic and "st" to steady state measurements)

However, Figures 4.4.5 and 4.4.6 demonstrate that Cox-Merz rule does not hold for PLA/Ecoflex blends. Complex viscosity results from parallel plate rheometer and shear viscosity from capillary rheometer measured at 180 and 190°C for blends P90E10 and P10E90 are shown on Figure 4.4.5 and 4.4.6, respectively. From these plots is obvious that the viscosity measured by the capillary rheometer is 30-50% lower than that measured by parallel plate rheometer in dynamic mode. It can be also seen that the Cox-Merz rule is not valid for both blends and that the deviation from this rule is larger for the blend with 90% PLA content. Such a deviation from the Cox-Merz rule can be expected, because PLA and Ecoflex form immiscible blends (Jiang *et al.*, 2006). It is well known that the morphology of immiscible blends strongly depends on the imposed deformation (Utracki and Kamal, 2002). In capillary rheometer, the melt is subjected to both shear and extension, while in parallel plates it is subjected only to shear. In addition, for blend P90E10, the geometry of capillary (i.e. sudden contraction) might have lead to accumulation of the less viscous dispersed phase (Ecoflex) at the die entrance and thus to have contributed to the observed large viscosity drop of this blend.

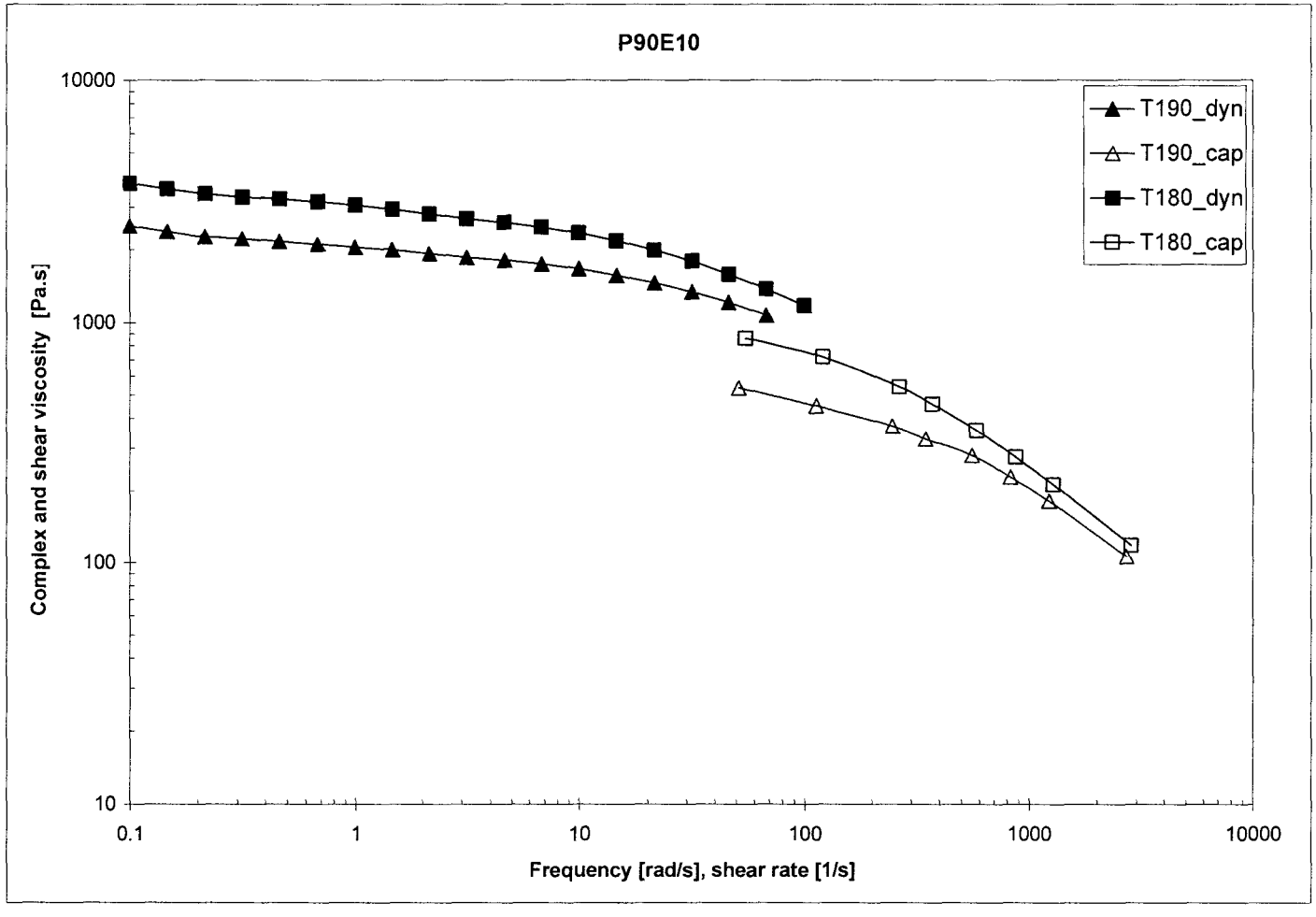

Figure 4.4.5. Complex and shear viscosity curves, obtained correspondingly in parallel plate and capillary rheometers at 180 and 190°C for .blend 90% PLA/ 10% Ecoflex. Open symbols represent capillary data. ("dyn" refers to dynamic and "st" to steady state measurements)

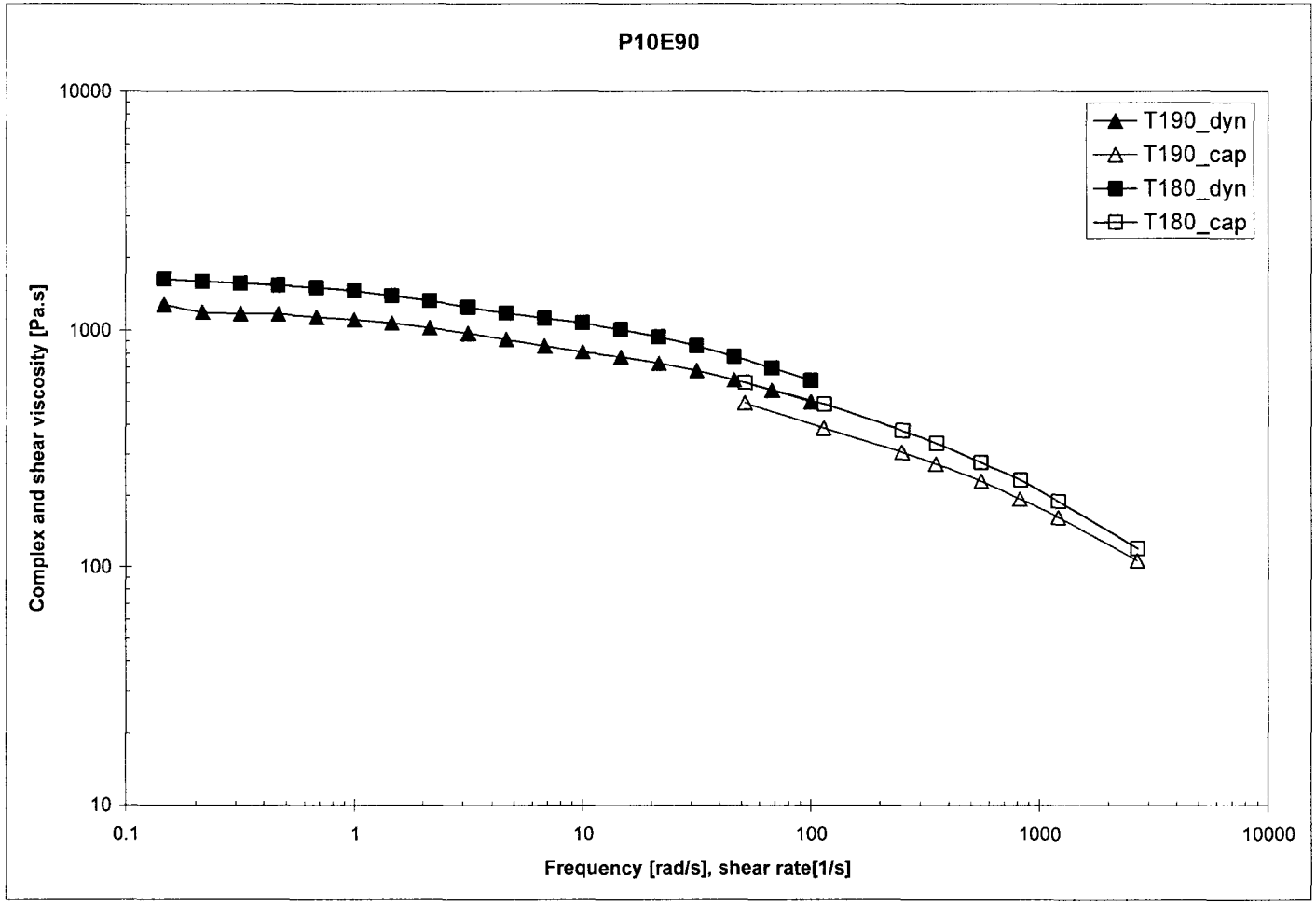

Figure 4.4.6. Complex and shear viscosity curves, obtained correspondingly in parallel plate and capillary rheometers at 180 and 190°C for .blend 10% PLA/ 90% Ecoflex. Open symbols represent capillary data. ("dyn" refers to dynamic and "st" to steady state measurements)

4.4.2 Storage Moduli of PLA/Ecoflex Blends

On Figure 4.4.7 results are shown from measurements of dynamic storage modulus as a function of frequency at 180°C and 190°C for pure PLA, processed in the Haake mixer and PLA/Ecoflex blend with 90wt% PLA. Similar results were obtained for Ecoflex, which was subjected to mixing procedure in Haake and its blend with PLA (PLA content 10 wt%). It was observed that mixing of Ecoflex and PLA results in higher elasticity (i.e. G') of the blends. Also, from Figure 4.4.7 is obvious that as a result of blending, a change in the slope of G' curve – from 1.7 for PLA after Haake to 1.35 for the blend P90E10 occurs. These two observations might be explained with the formation of droplets of dispersed phase. It is also plausible that molecular interactions such as transesterification (Porter, 1999) contribute to this effect. These reactions might have been induced during the mixing process in Haake, where the processing temperature was maintained well above the crystalline melting point of the neat biodegradable polyesters.

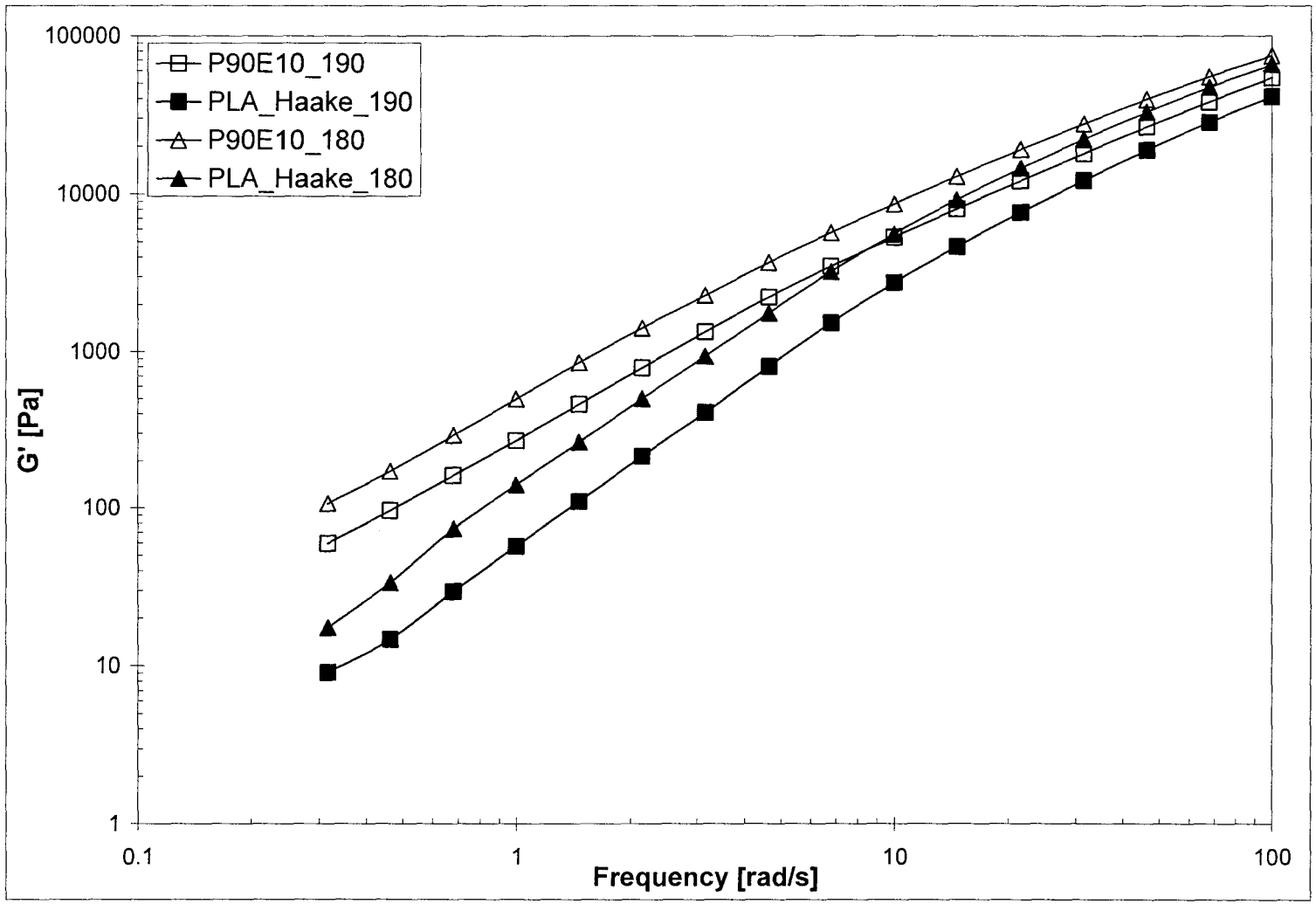

Figure 4.4.7 Storage modulus curves for PLA after mixing in Haake and blend P90E10 at 180°C and 190°C.

4.4.3 Sharkskin and Gross Melt Fracture Phenomena of PLA/Ecoflex blends

Since in industrial operations sharkskin is the first extrusion instability which limits the production rates, it is desirable to eliminate or at least postpone its onset. The effect of mixing conditions and the effect of blending PLA with Ecoflex on the onset of sharkskin and gross melt fracture are presented below.

It was found that mixing in Haake postpones the onset of sharkskin of PLA to higher shear rates and shear stresses in comparison with the neat resin. The onset of sharkskin of PLA after Haake occurred at shear rate of $1500s^{-1}$ and shear stress 340 kPa, which is 200 kPa higher than the onset of sharkskin for PLA 7000D. The onset of gross melt fracture for PLA after Haake occurred at higher shear rates than the neat PLA 7000D ($4000s^{-1}$ vs. $1200s^{-1}$). However, the critical shear stress for the onset of gross melt fracture of PLA after Haake was 400 kPa, which is the same as that of PLA 7000D.

Ecoflex after Haake exhibited only the gross melt fracture phenomenon. The onset of gross melt fracture for Ecoflex after Haake occurred at shear rate $6000s^{-1}$, which is almost twice as much as the critical shear rate of the neat Ecoflex – $3500s^{-1}$. The critical shear stress for onset of gross melt fracture of Ecoflex after Haake was 570 kPa, which is approximately the same as that of the neat Ecoflex – 580 kPa.

The onsets of flow instabilities and their location on the flow curves of blends P90E10 and P10E90 are schematically shown on Figures 4.4.8 and 4.4.9, respectively.

Blend P90E10 (i.e. 90 wt% PLA, 10 wt% Ecoflex) had both sharkskin and melt fracture. For this blend sharkskin was noticeable at apparent shear rate 480 $s^{-1}$and wall shear stress of 230 kPa, which is 90 kPa higher than the onset of sharkskin for PLA 7000D. However, as mentioned above, the onset of sharkskin of PLA after Haake occurred at critical shear stress 340 kPa and shear rate of 1500 s^{-1}. It could be then concluded that the observed increase in critical shear stress for the onset of sharkskin for blend P10E90 is probably due to some sort of lubricating effect as a result from the byproducts of resin degradation during blending in Haake and from the presence of Ecoflex. The onset of gross melt fracture of blend P90E10 was observed at shear rate 3400 s^{-1} and shear stress 400 kPa. It is obvious from the above observations that blending

with Ecoflex improved the processability of PLA. Figure 4.4.10 shows extrudates of blend P90E10, which were obtained at 180°C.

Blend P10E90 (i.e. 10 wt% PLA) also exhibited the two extrusion instabilities. In this case, the onset of sharkskin was observed at shear rate of 6750 s^{-1} and shear stresses of 640 kPa, which is 60 kPa higher than the onset of gross melt fracture of the neat Ecoflex. The gross melt fracture of blend P10E90 appeared at shear stress of 670 kPa and shear rate of 7600 s^{-1}, which are higher than these of Ecoflex after Haake. Extrudates of blend P10E90 at 160°C are presented on Figure 4.4.11.

From the above results it can be concluded that blending with Ecoflex provides some advantages for postponing the onset of sharkskin instability of PLA. On the other hand, blending with PLA seems to offer benefits in terms of delayed occurrence of gross melt fracture of Ecoflex.

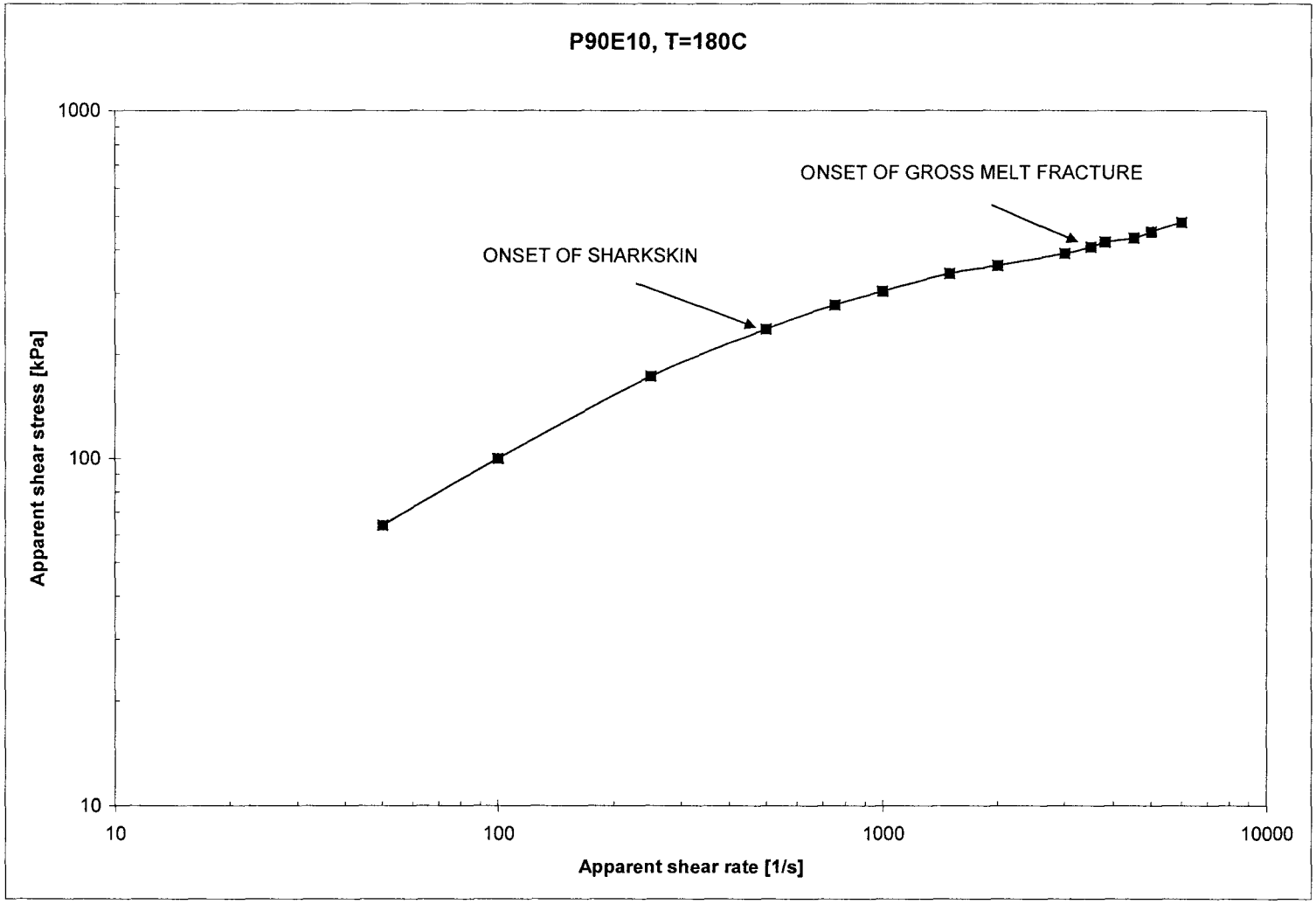

Figure 4.4.8. Flow curve and onsets of extrusion instabilities for blend P90E10 at 180°C in stainless steel die with D = 1 mm and L/D = 16

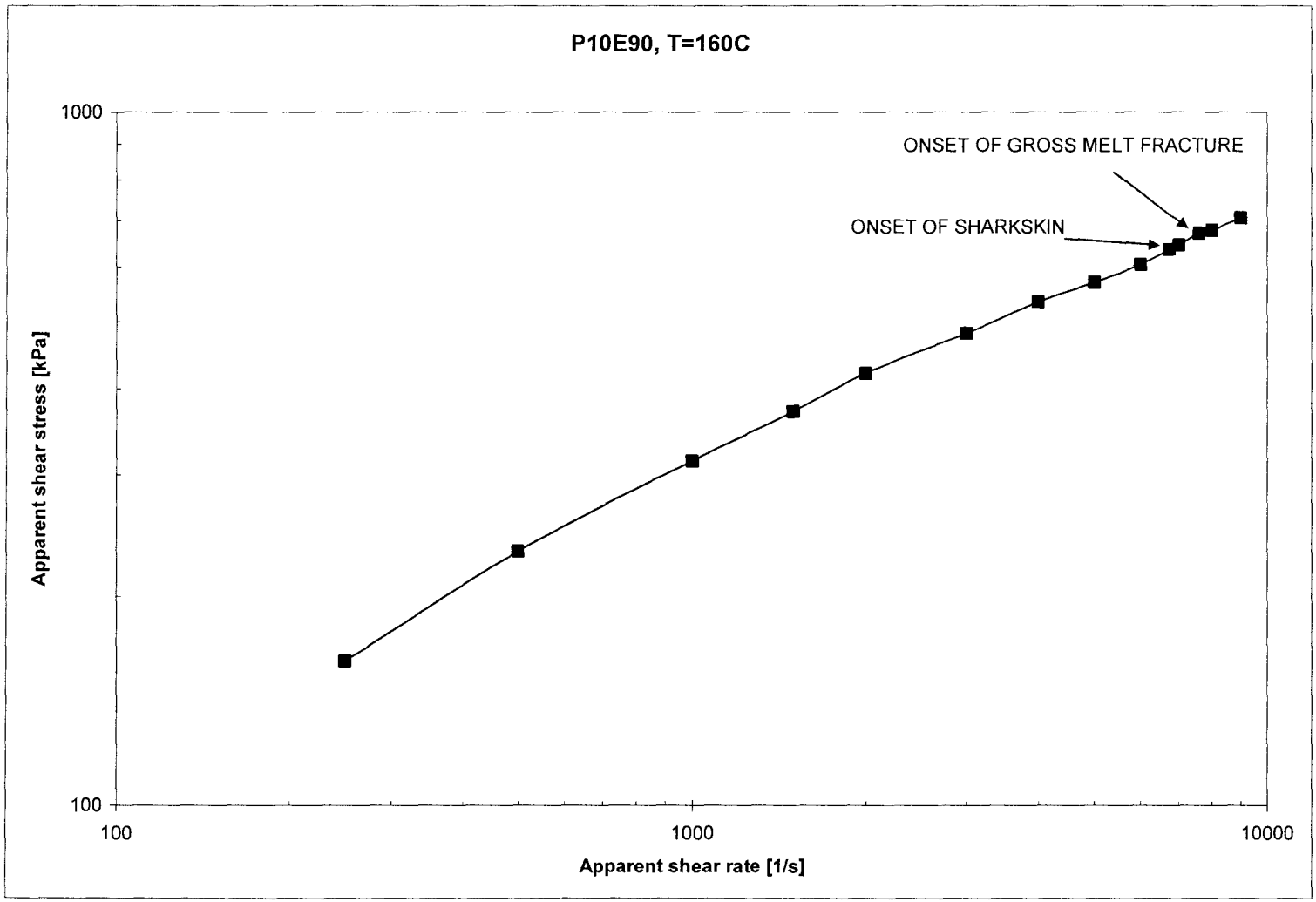

Figure 4.4.9. Flow curve and onsets of extrusion instabilities for blend P10E90 at 160°C in stainless steel die with D = 1 mm and L/D = 16

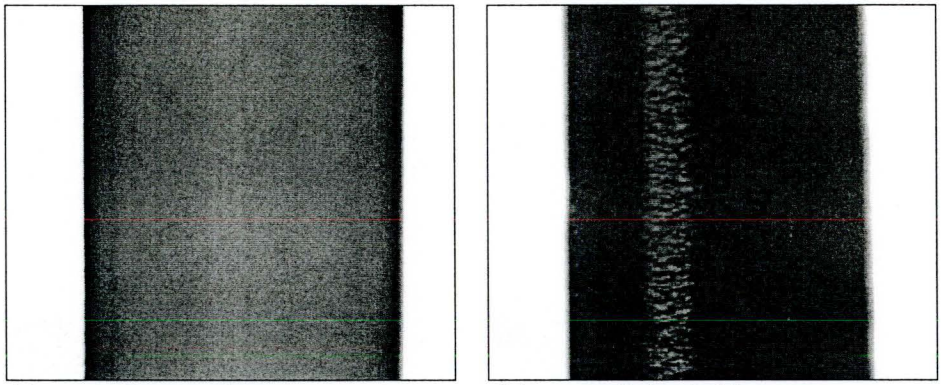

(a) smooth extrudate (b) start of sharkskin

(c) very severe sharkskin (d) gross melt fracture

Figure 4.4.10. Evolution of extrudate instabilities for blend P90E10 in die with diameter 1mm and L/D = 16 at 180°C. The corresponding values of apparent shear rates and wall shear stresses are: (a) 250 s^{-1}, 170 kPa; (b) 500 s^{-1}, 240 kPa; (c) 2000 s^{-1}, 350 kPa (d) 4500 s^{-1}, 430 kPa.

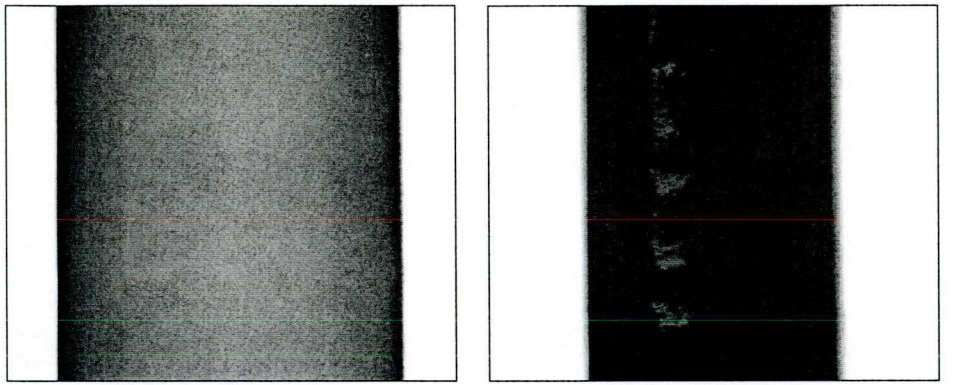

(a) smooth extrudate (b) start of sharkskin

(c) start of gross melt fracture (d) gross melt fracture

Figure 4.4.11. Evolution of extrudate instabilities for blend P10E90 in die with diameter 1mm and L/D = 16 at 160°C. The corresponding values of apparent shear rates and wall shear stresses are: (a) 6000s^{-1}, 0.6 MPa; (b) 7000 s^{-1}, 0.65 MPa; (c) 8000 s^{-1}, 0.68 MPa (d) 9000 s^{-1}, 0.7 MPa.

4.4.4 Morphology of PLA/Ecoflex Blends

Figure 4.4.11 shows SEM micrographs of extrudates of PLA/Ecoflex blends as well as of the neat PLA and Ecoflex, after being subjected to mixing procedure in Haake. The extrudates were obtained from a capillary die with D = 1mm, and L/D = 16, at 180°C. The extrudates of Ecoflex after Haake and of blend P10E90 were taken at shear rates 1000 s^{-1} and shear stress 0.24 – 0.25 MPa. Extrudates of PLA after Haake and of blend P90E10 were taken at shear rates of 700 s^{-1} and shear stress of 0.26 to 0.28 MPa. The specimen preparation is outlined in Chapter 3 of this thesis.

It can be seen from Figure 4.4.11 (b) and (c) that for both biodegradable blends the mixing procedure in Haake and the capillary flow in the rheometer were efficient in forming droplets of the dispersed phase with size of less than 1 μm. The small voids around some droplets of the dispersed phase on Figure 4.4.11 (b) and (c) confirm that PLA and Ecoflex form immiscible blends and that compatibilizer have to be used to reduce the interfacial tension and stabilize the morphology of the blends (Utracki, 2002).

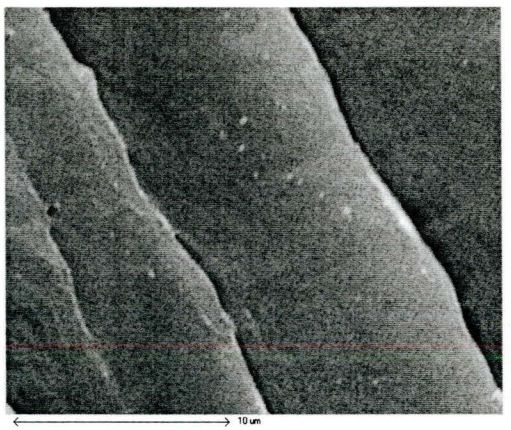

(a) Ecoflex after Haake

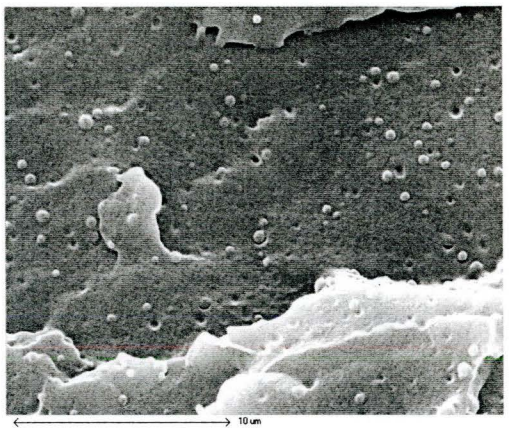

(b) P10E90

(c) P90E10

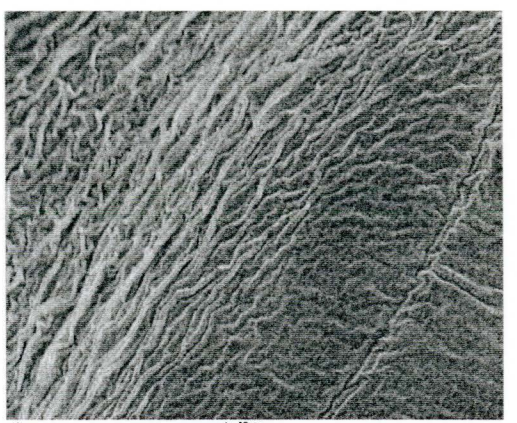

(d) PLA after Haake

Figure 4.4.12. SEM micrographs of extrudates of Ecoflex after Haake, blend P10E90, blend P90E10, and PLA after Haake. Extrudates were obtained from a die with diameter 1mm and L/D = 16 at 180°C and at shear stresses 0.24, 0.25, 0.26, and 0.28, correspondingly

CHAPTER 5

COMPARISONS

5.1 Introduction

The rheological properties of the polymers are the key factors which determine the efficiency of processing the polymer resins into useful items. Biodegradable polymers must provide sufficient cost and performance benefits both to the processor and to the customer in order to successfully penetrate into a market, which is presently dominated by thermoplastics such as polyethylenes, polypropylene, polystyrene and polyethylene terephthalate.

This section views from a broader perspective the results from the rheological studies presented in the previous subsections. First, the rheological behaviour of PLA is compared with that of Ecoflex. Second, these biodegradable polymers are compared with some conventional polymers on the basis of their rheological properties.

5.2 Comparison of PLA (4042D and 7000D) and Ecoflex F BX 7011

Figure 5.2.1 shows the Cross fitted viscosity curves of the three biodegradable resins. It can be seen that PLA 7000D has the highest zero shear viscosity. It is also obvious that both PLA grades have similar viscosity behaviour. The larger viscosity values of PLA 7000D are probably due to its higher molecular weight. We can also see from Figure 5.2.1 that at low shear rates, PLA viscosity behaviour is characterized with a large Newtonian region and their viscosity decreases more than that of Ecoflex at higher shear rates.

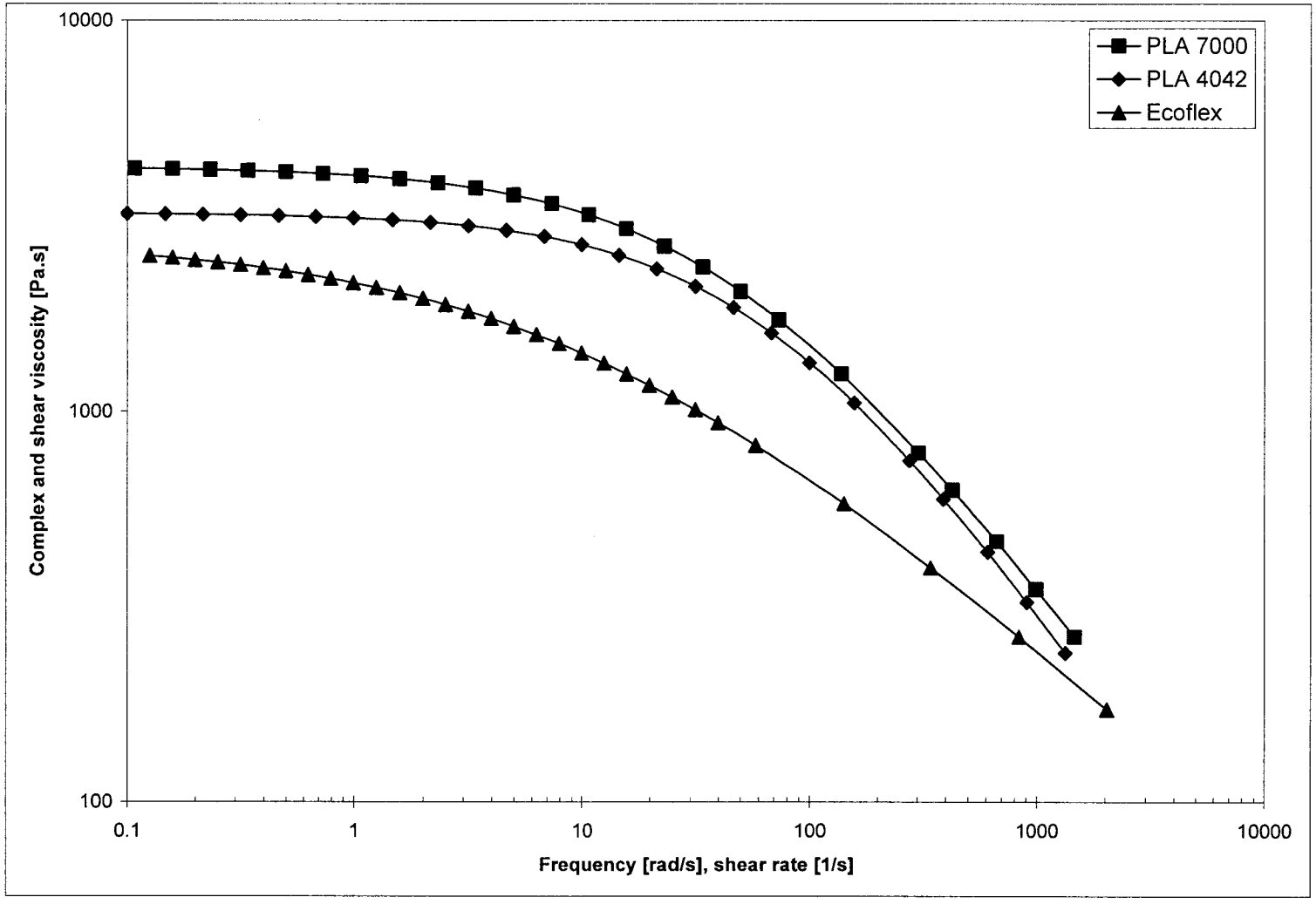

Figure 5.2.1 Fitted by Cross model viscosity curves of PLA 7000D, PLA 4042D, and Ecoflex F BX 7011 at 180°C.

Figure 5.2.2 presents results from storage and loss modulus measurements at 180°C for the neat biodegradable polyesters. Similar results (not presented in this subsection and available in the appendix) are obtained at temperatures 190 and 200°C. It is seen from Figure 5.2.2 that for all biodegradable polymers the storage modulus curves lie below the loss modulus curves, i.e. the melts behave as elastic liquids within the linear viscoelastic region. We also note that G' and G" curves of both PLA resins develop in a similar manner and are almost parallel, which shows that their molecular weight distribution is also similar. At low frequencies Ecoflex exhibits higher elasticity than PLA, which is indicated by larger values of G'.

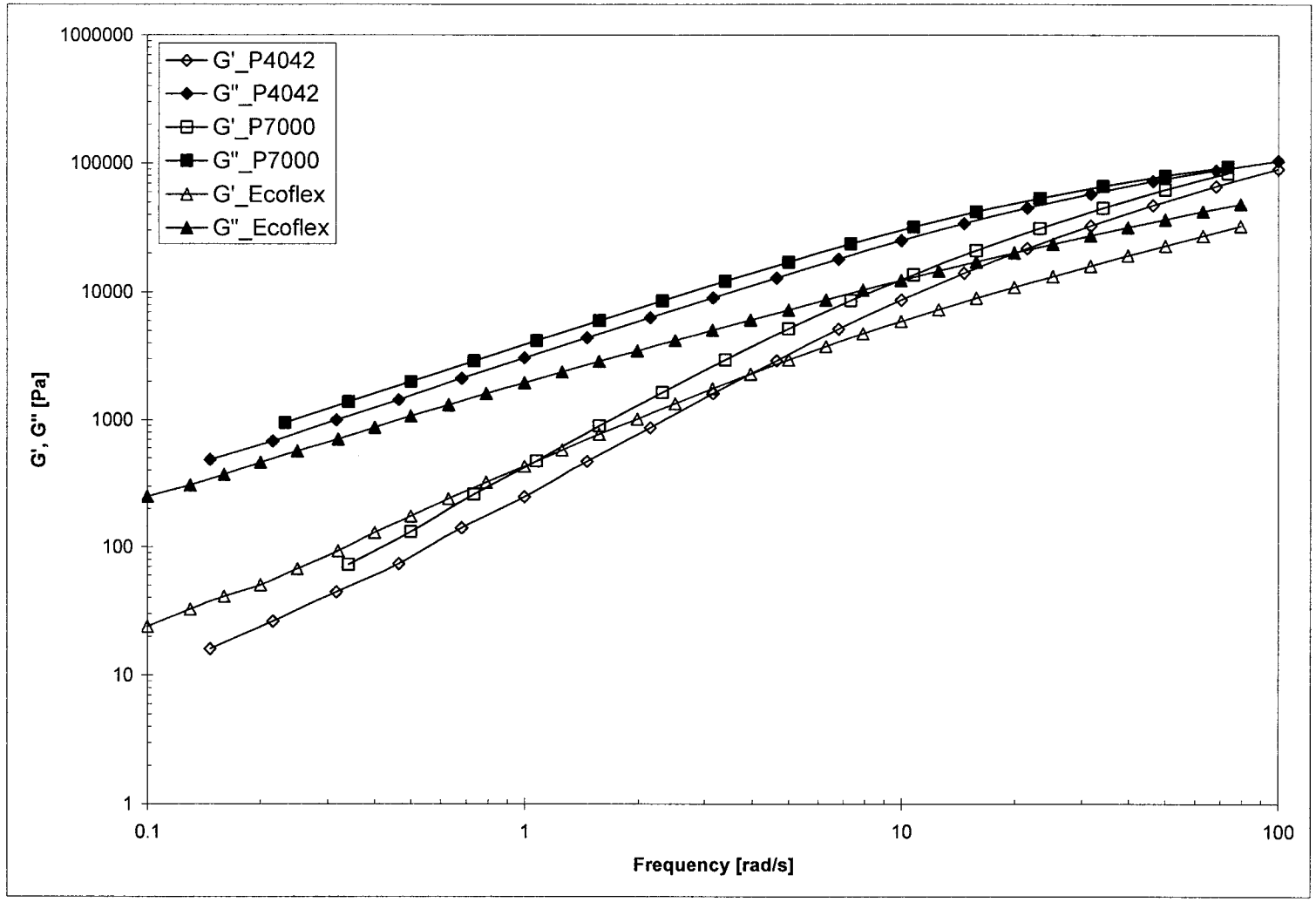

Figure 5.2.2 Storage (G') and loss modulus (G") curves of PLA 4042D, PLA 7000D, and Ecoflex F BX 7011, obtained in parallel plate rheometer at 180°C. Solid symbols represent loss modulus data.

Figure 5.2.3 illustrates the fact that Ecoflex has larger values of the normal stresses developed in simple shear than both grades PLA. It confirms the previous observation that it is more elastic than PLA. On the other hand, it can be seen that PLA 7000D is more elastic than PLA 4042D.

The elastic behaviour of our biodegradable polymers explains very well their extrudate swell. At shear rates ranging from 50 to 300s^{-1} the most elastic melt – Ecoflex, swells the most (23-34%). PLA 7000D is less elastic and it swells from 18 to 28%. PLA 4042D has the least amount of elasticity, and therefore swells only from 9 to 23%. However, as it will be discussed later, the melt elasticity of these biodegradable polymers is much smaller than the elasticity of some conventional plastics and this can cause lots of problems in processing technologies such as blown film, where high melt strength is a desirable property.

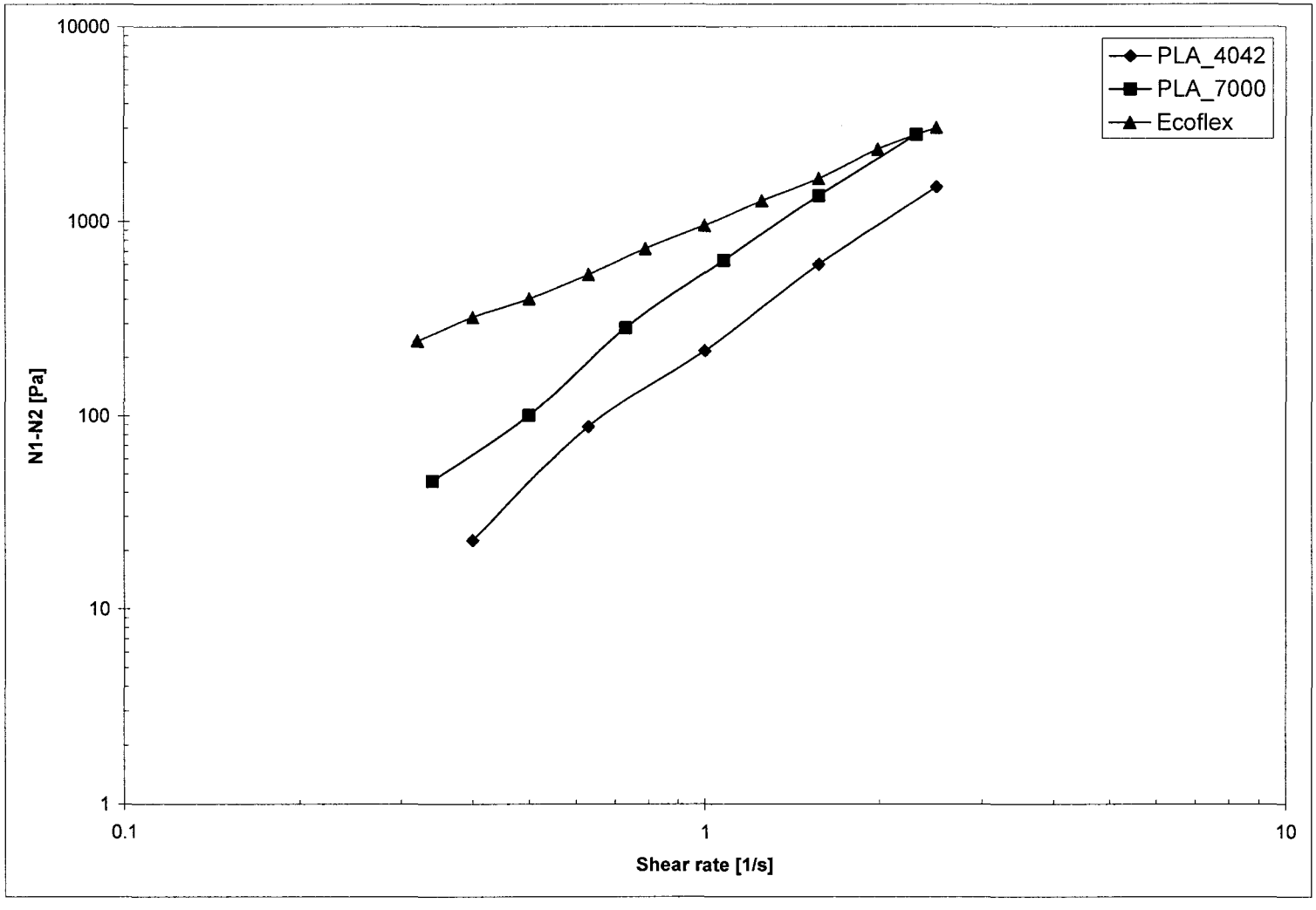

Figure 5.2.3 Normal stress difference curves of PLA 4042D, PLA 7000D, and Ecoflex F BX 7011, obtained in parallel plate rheometer at 180°C

The behaviour of polymer melts when subjected to extensional tensile deformation is one of the key factors for understanding the sharkskin phenomenon. Figure 5.2.4 shows the extensional viscosity curves of the PLA and Ecoflex resins at 180°C. It can be seen that Ecoflex has the highest elongational viscosity. In contrast to its behaviour in shear flow, PLA 7000D has lower extensional viscosity values than PLA 4042D.

Although Ecoflex has higher extensional viscosity than both PLA resins, the difference in their elongational flow behaviour is not large enough to explain the large difference between the polymers in view of their flow instabilities. However, when we compare the Trouton ratios (i.e. η_e/η) we observe a large difference. At 180°C, η_e/η of PLA 7000D range from 2.11 to 3.35 (the larger value is corresponding to high shear and extensional rates of strain). For PLA 4042D η_e/η vary from 2.83 to 5.88. For Ecoflex η_e/η values are much larger, ranging from 8.07 to 12.5. This demonstrates that in comparison with both polylactides, Ecoflex much more resists the tensile deformation than it resists the shear deformation. It might be conjectured that as a result of these properties of Ecoflex (which are due to its complex molecular structure), its extrudate must have very large throughput to reach the critical stress level for surface fracture in the short time frame of the extensional pulse immediately after exiting the die (Migler, 2005). The larger Trouton ratio could also explain why the onset of sharkskin for PLA 4042D occurs at larger shear stress than PLA 7000D (0.18 MPa vs. 0.14MPa). Wall slip of Ecoflex is less that that of PLA and this fact may also affect the sharkskin behaviour. These observations confirm that biodegradable polymers exhibit behaviour similar to that of conventional polymers and seem to prove the hypothesis of the critical role of extensional flow for the onset of sharkskin flow instabilities proposed by Cogswell (1977) and further developed by Migler (2002).

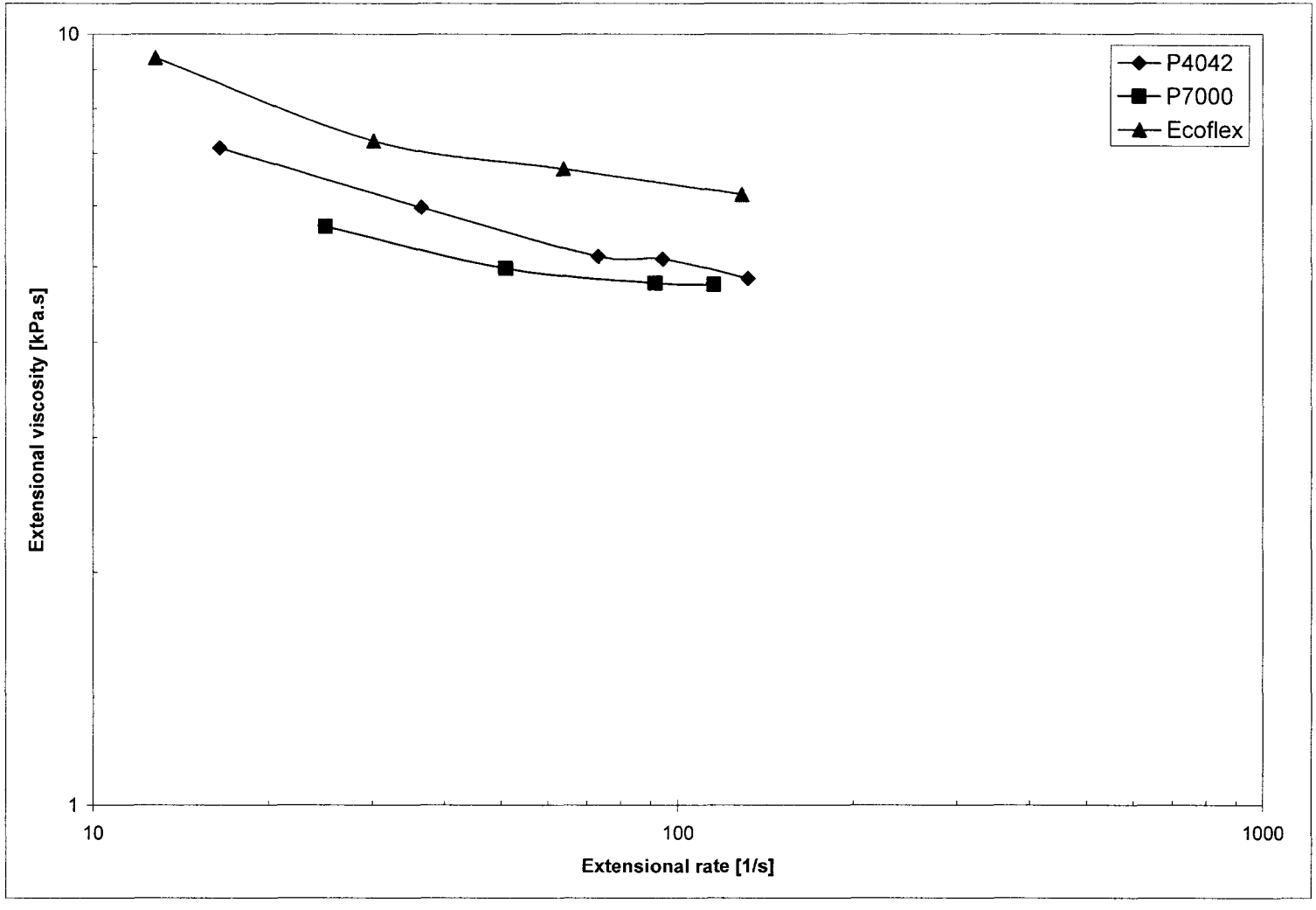

Figure 5.2.4 Extensional viscosity curves of PLA 4042D, PLA 7000D, and Ecoflex F BX 7011, obtained in a two bore capillary rheometer at 180°C.

As shown previously in Chapter 4, both PLA and Ecoflex exhibit slip at the die wall. Referring again to the previous paragraph, we see that the onsets of sharkskin for both PLA resins occur in a condition of slip. Extrusion instabilities, which were accompanied or preceded by wall slip, have been also observed with traditional thermoplastics such as linear low density polyethylene, high density polyethylene and branched low density polyethylene (Ramamurthy, 1986; Migler, 2002)

It can be concluded from the above discussions that the rheological behaviour of PLA and Ecoflex is very similar to that of LLDPE and LDPE, respectively, which is largely determined by the degree of branching, molecular weight and polydispersity of the resins.

5.3 Comparison of Biodegradable Polyesters with Conventional Plastics for Packaging Applications

5.3.1 Stability during Processing

The most important difference between biodegradable polymers and conventional thermoplastics is that biodegradable plastics degrade substantially during processing, while properties of conventional polymers do not change significantly.

For example, Zahavich (1995) and Zahavich *et al.* (1997) studied the effect of multiple passes through a single screw extruder on rheological properties of a blow molding grade high density polyethylene (HDPE). He observed insignificant reduction in viscosity of HDPE even after 8 extrusion passes. Viscosity curves of HDPE, subjected to zero to eight passes through a single screw extruder at 190°C and screw speed of 70 rpm are presented on Figure 5.3.1.

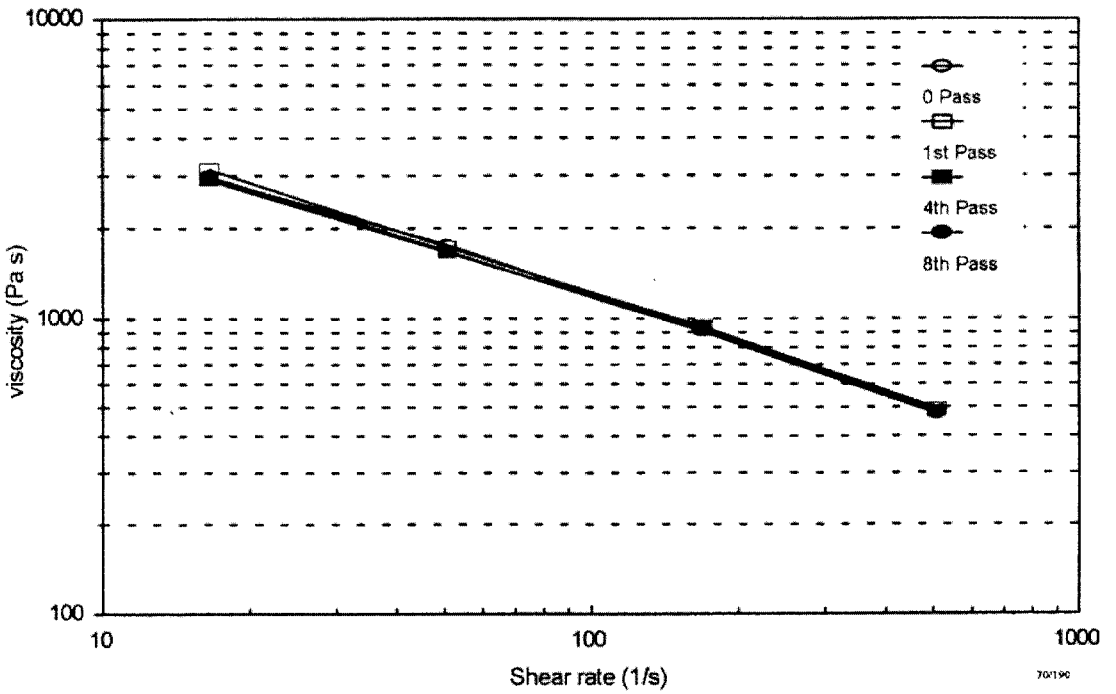

Figure 5.3.1 Viscosity curves of HDPE after up to eight extrusion passes at 190°C and 70 rpm. Adapted from Zahavich (1995)

However, we observed up to 50% reduction in viscosity of PLA 7000D after a single pass through Haake mixer. Our observations are in agreement with other reports found in the literature. Garlotta (2001) reported that there is 41% decrease in molecular weight of a general purpose PLA as a result of a pass through a twin screw extruder. Bigg (2005) observed as much as 55% molecular weight decrease due to thermal degradation when PLA was held for 30 min at 190°C. He also stated that this narrows the processing temperature window of PLA to up to 40°C, which is similar to that of PET. Migliaresi *et al.* (1991) reported molecular weight drop of 50% as a result of thermal degradation. They did not observe oxidation of PLA and attributed the molecular weight reduction to chain splitting and not to hydrolysis. It has also been reported that the degradation of PLA is not only a consequence of thermal degradation but also of some chemical degradation, which is induced by small amounts of residual monomer, catalyst, or

impurities and which contributes to the observed large molecular weight decrease (Garlotta, 2001).

As shown in Chapter 4, Ecoflex also degrades during processing. We observed up to 40% viscosity drop after the pass in Haake internal mixer. However, according to information from the manufacturer (BASF, 2005), Ecoflex has good thermal stability up to 230°C. We also did not observe any viscosity reduction or visual sign of degradation when conducting rheological experiments with Ecoflex for prolonged time to optimize the experimental conditions. It might be conjectured then, that the viscosity reduction we observed after Haake mixing, is due to mechanical and/or chemical degradation. To our knowledge there are no publications on degradation of Ecoflex during processing. Jiang *et al.* (2006) reported steady viscosity results for neat PLA 4032D and Ecoflex F BX 7011 resins and for their blends. Although the blends were prepared in twin screw extruder, the researchers did not discuss any degradation phenomena during processing.

Degradation of biodegradable polymers during extrusion is of utmost importance for choosing proper conditions for their processing. Degradation during polymer extrusion is a complex process, which is a combination of three specific degradation mechanisms – thermal, mechanical and chemical degradation (Rauwendaal, 1994) It might be suggested that further studies be conducted to determine the dominant type of degradation during processing. Such studies will provide basis for finding ways to reduce the large degradation which is presently observed. For example, eliminating access of ambient air by employing of nitrogen blanket, and /or adding antioxidants and other stabilizers could reduce the impact of the chemical degradation. On the other hand, optimizing of residence time and its distribution, of deformation rate and its distribution, and of stock temperature and its distribution inside the extruder will help to reduce the amount of thermal and mechanical degradation during processing of biodegradable polymers. Whatever the main source of degradation is, it is large, and it must be taken into consideration when choosing the processing technologies and their operating conditions. It imposes constraints not only on the processing operations but also on the

final product performance. As it might be expected, the degradation encountered during processing raises the manufacturing cost of biodegradable plastic packaging.

5.3.2 Comparisons of Rheological Properties

In this subsection, rheological properties of PLA and Ecoflex are compared with blown film grades of linear low density polyethylene (LLDPE) and low density polyethylene (LDPE). These polyethylenes were chosen, because film blowing is the most widely used technology for producing polyethylene films. Some of the properties of these commercial polyethylenes are listed in Table 5.3.1.

Table 5.3.1 Properties of commercial grades polyethylene

Resin	Producer	Melt Index g/10min	Density g/cm^3	T_m °C
Novapol LDPE LF-Y819-A	Nova Chemicals	0.75	0.919	110
LLDPE LL 1107x94	ExxonMobil	0.8	0.922	123

Figure 5.3.2 presents viscosity curves of PLA 7000D, Ecoflex F BX 7011, LDPE LF-Y819-A and LLDPE LL 1107x94. The measurements were conducted at 180°C in capillary rheometer with standard die (diameter 1mm and L/D = 16) and a "zero length" die for making the entrance corrections. It can be seen from the graph that PLA and LLDPE have very similar viscosity behaviour. According to information from BASF Ecoflex behaves like LDPE Lupolen 2420 F, which is a blown film grade LDPE, produced by BASF (BASF, 2005). Although the viscosity behaviour of Ecoflex is not very similar to LDPE-Y819-A, it is close enough for our purposes of qualitative comparisons.

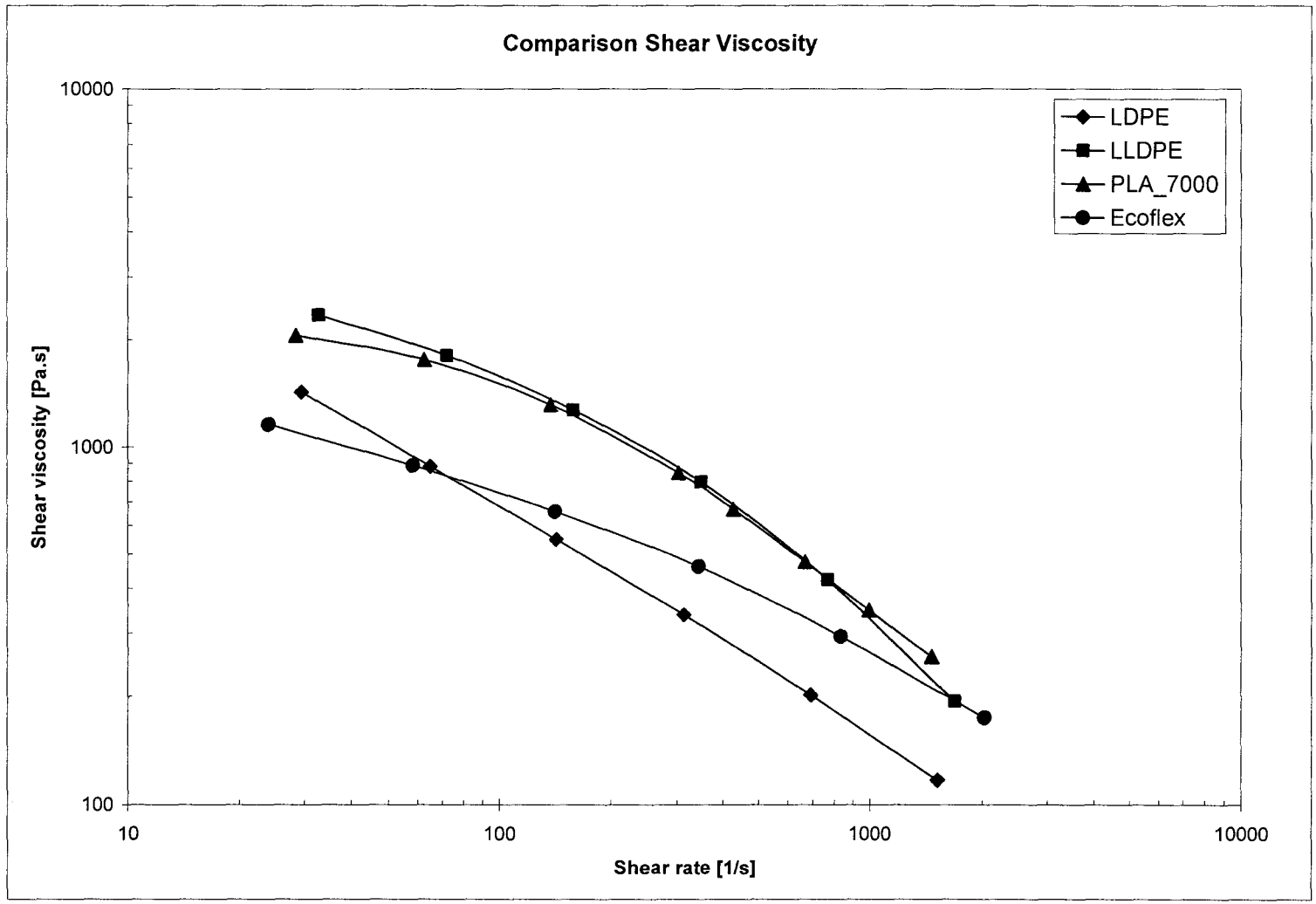

Figure 5.3.2 Viscosity curves of PLA 7000D, Ecoflex F BX 7011, LDPE LF-Y819-A and LLDPE LL 1107x94 obtained in a two bore capillary rheometer at 180°C

Figure 5.3.3 illustrates the well known fact that branched LDPE exhibits large extensional viscosity in comparison with LLDPE. From this figure can also be seen that both biodegradable polymers have slightly higher elongational viscosities than LLDPE. This means that in processing operations such as blown film extrusion, there might be problems with bubble stability due to the poor melt strength of biodegradable polymers. On the other hand, in similarity to LLDPE, the low values of elongational viscosities of PLA and Ecoflex could allow drawing down the melt to much thinner gages than LDPE.

As mentioned previously, PLA and Ecoflex exhibit much smaller extrudate swell than conventional plastics which can be an obstacle to their processing by blown film technology. Table 5.3.2 presents results from extrudate swell measurements conducted as outlined in Chapter 3 "Experimental Procedures" at apparent shear rates ranging from 50 to $300s^{-1}$.

Table 5.3.2 Extrudate swell for biodegradable and conventional polymers in die with D = 2mm and L/D = 16, at T = 180°C.

Polymer	Die Swell Ratio D/D_0
PLA 7000D	1.18 - 1.28
Ecoflex F BX 7011	1.23 – 1.34
LDPE LF-Y819-A	1.88 – 2.17
LLDPE LL 1107x94	1.27 – 1.52

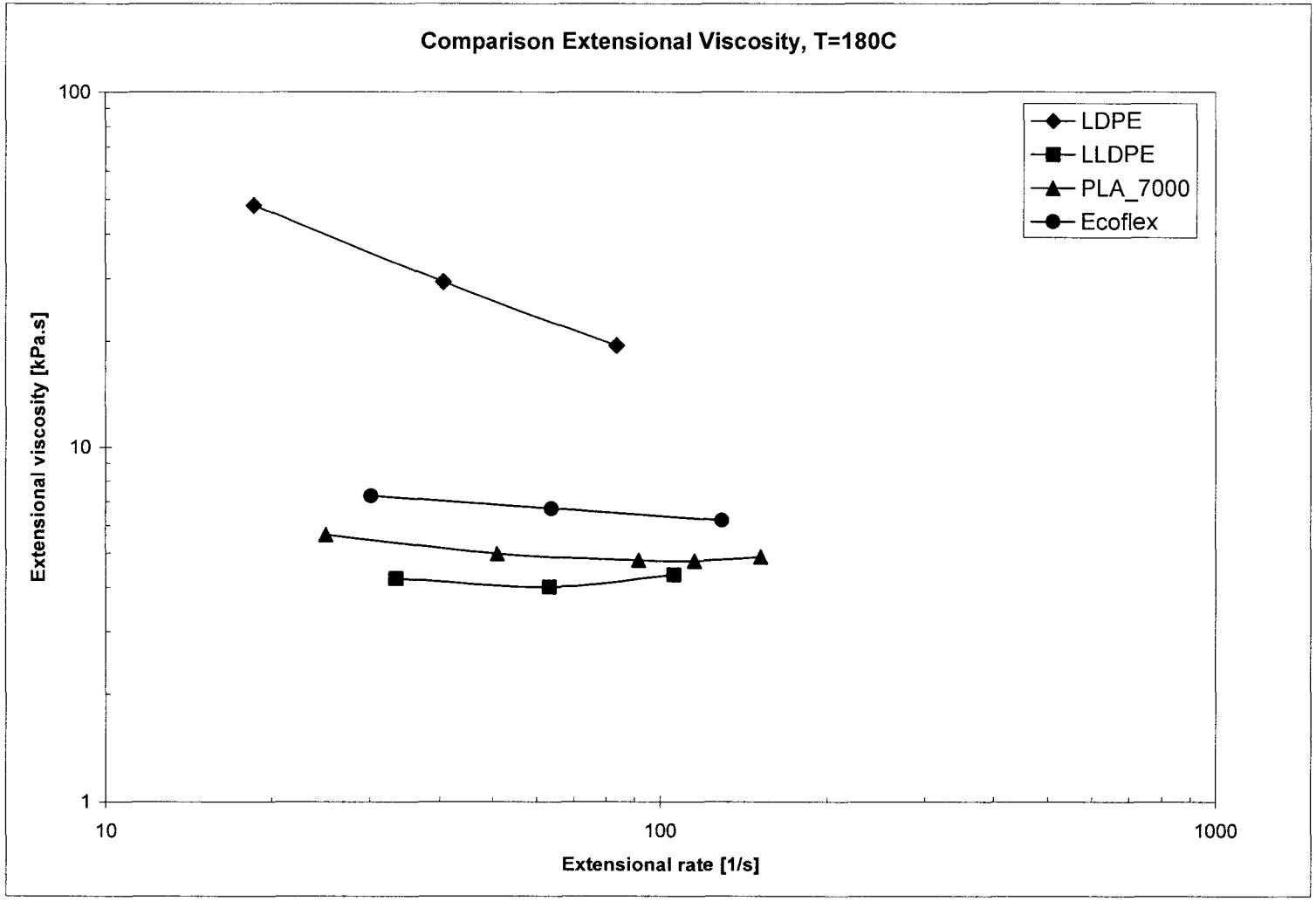

Figure 5.3.3 Extensional viscosity curves of PLA 7000D, Ecoflex F BX 7011, LDPE LF-Y819-A and LLDPE LL 1107x94, obtained in a two bore capillary rheometer at 180°C.

5.3.3 Comparisons of Extrusion Instabilities Phenomena

With regards to sharkskin and melt fracture, PLA and Ecoflex seem to behave like other conventional polymers for packaging applications. We did not study the sharkskin and gross melt fracture phenomena in the blown film grades LLDPE and LDPE, because there are hundreds of articles about extrusion instabilities of polyethylenes.

Although extensively investigated, the actual causes of sharkskin and gross melt fracture instabilities of conventional polymers are still a controversial topic (Migler, 2005). However, it is widely accepted that sharkskin is a die exit effect, which is caused by a localized stress concentration resulting in surface rupture, while gross melt fracture is considered to originate from severe flow destabilization at die entrance and other factors (Agassant *et al.*, 2006).

The most common values of the critical shear stress for the onset of sharkskin instability in conventional polymers are near 0.1 MPa. These shear stress values were observed with different polymers and in dies with various geometries. However, as pointed by Migler (2005), the critical shear stress value of 0.1 MPa might be considered as an order of magnitude value, because onset of sharkskin still depends on the aspect ratio of the die and the shape of the exit region (Migler, 2005). Another important factor for the onset or the severity of sharkskin is the molecular structure, especially the polymer polydispersity . Sharkskin phenomenon is usually observed in flows of narrow molecular weight linear polymers such as LLDPE and HDPE. Investigating sharkskin in LLDPE, Kazatchkov *et al.* (1999) observed that broad molecular weight resins had lower values of the elastic modulus at short times. On the other hand, one of the leading hypothesis for the onset of sharkskin states that the elastic behaviour at short times is a critical factor for stress build-up when the melt is subjected to sudden extensional pulse while exiting the die (Migler, 2005). Temperature manipulation in either direction is another method for reducing the severity of sharkskin or its onset (Migler, 2005). Obviously, all these factors, which influence the severity of sharkskin instability, could be clustered around their impact on the stress field in the die exit region.

The results of our study of flow instabilities of biodegradable polymers are compared with reported in the literature values for the onset of flow instabilities of some traditional plastics in Table 5.3.3. It can be concluded from Table 5.3.3 that PLA exhibit the characteristic for linear polyethylens instabilities. However, in similarity with LDPE, linear polypropylene (PP), PVC, polystyrene (PS), and polymethylmethacrylate (PMMA), PLA does not exhibit the stick-spurt phenomenon. It can be also seen that the values of the critical shear stress for the onset of sharkskin (0.14 – 0.18 MPa) and gross melt fracture (0.36-0.4 MPa) of PLA are very close to those values of LLDPE and HDPE.

Unlike sharkskin, which is characterized by a stable flow, gross melt fracture(GMF) regime is characterized by unstable flow. It is believed that it is caused by chaotic rupture of the melt as a response to the large tensile stresses which are generated at the sudden contraction of the die entrance (Dealy and Kim, 2005). It is known, that GMF onset depends on die geometry (die aspect ratio and convergence angle). It is reported that in single site polyethylenes, gross melt fracture depends on the molecular structure of the polymer (presence of long-chain branching and polydispersity index M_w/M_n) but does not depend on average molecular weight (Dealy and Kim, 2005). On the other hand, Vlachopoulos and Ladorikis (1971) and Vlachopoulos and Alam (1972) observed that the onset of GMF of polypropylene, polystyrene and HDPE did not depend on molecular weight distribution, but was inversely proportional to the weight average molecular weight M_w and increased with temperature increase.

It can be seen in Table 5.3.3 that Ecoflex does not exhibit sharkskin phenomenon like broad molecular weight polypropylene, polystyrene and LDPE. However, its gross melt fracture onset occurs at much higher shear stresses (0.58 MPa vs. 0.14 – 0.15 MPa). This desirable property is probably due to its lower elongational viscosity and the presence of processing aids in the Ecoflex masterbatch (BASF, 2005).

Table 5.3.3 Comparison of biodegradable polymers with conventional plastic materials on the base of extrudate swell, and critical shear stresses for the onset of sharkskin and gross melt fracture instabilities

Polymer	Die Swell, D/D_0	Critical Shear Stress for onset of Sharkskin, MPa	Critical Shear Stress for onset of Gross Melt Fracture, MPa
Polystyrene	1.2-1.8 (Baird and Collias, 1998) (Tadmor and Gogos, 2006)	not observed	0.13-0.14 MPa (Vlachopoulos and Ladorikis, 1971)
Polypropylene	1.2-2 (Baird and Collias, 1998)	not observed with typical resins 0.1 MPa (very narrow MWD) (Fujiyama and Inata, 2002)	0.15MPa (Fujiyama and Inata, 2002)
LLDPE	1.35-1.8 (Macosko, 1994)	0.1 MPa (0.3 MPa - stick-spurt) (Denn, 2001) 0.14 MPa (Ramamurthy, 1986)	0.4-0.42 (Tadmor and Gogos, 2006) 0.43 (Ramamurthy, 1986)
HDPE	1.75–2.2 (Baird and Collias, 1998) 1.2-1.6 (Ariawan et al., 2001)	0.15 MPa (Migler, 2005)	0.3-0.5 MPa (Dealy and Kim, 2005)
LDPE	1.88 – 2.17 (present work)	not observed (Dealy and Kim, 2005) (Baird and Collias, 1998) 0.12MPa (determined from change of slope of stress curve) (Ramamurthy, 1986)	0.13 MPa (Ramamurthy, 1986)
PLA	1.18-1.28 (present work)	0.14-0.18 MPa (present work)	0.36-0.4 MPa (present work)
Ecoflex	1.23-1.34 (present work)	not observed (present work)	0.58 MPa (present work)

CHAPTER 6
CONCLUSIONS AND RECOMMENDATIONS

6.1 Conclusions

A study of the rheological properties of three commercial biodegradable polymers is presented. Results of extrusion instabilities of biodegradable polymers are reported for the first time. The rheological experiments were conducted using a parallel plate and a capillary rheometer. Nonlinear regression was used to fit experimental viscosity data to a Cross model. The extensional rheological properties of the biodegradable plastics studied were calculated according to the Cogswell method. Optical microscopy was used to study the extrudate instabilities phenomena.

It was found that viscosity behaviour of PLA and Ecoflex is similar to that of conventional polyethylenes and that the Cox-Merz rule is obeyed within the temperature interval 180 - 200°C. It was observed that PLA has larger Newtonian region than Ecoflex and that viscosity curves of the three biodegradable polymers can be well fitted to the Cross model. Viscosity measurements at 180°C, 190°C, and 200°C revealed that PLA4042D is very sensitive to temperature like PMMA and rigid PVC. On the other hand, viscosity of PLA 7000D is slightly less sensitive to temperature changes and the values of its temperature coefficient are similar to polystyrene. Ecoflex has approximately the same temperature sensitivity as LDPE. Therefore, it might be expected that processing of PLA will be more difficult than that of Ecoflex.

The results from storage and loss modulus measurements showed that the three biodegradable polymers behave as elastic liquids within the frequency span of 0.1-100 rad/s.

It was observed that biodegradable polymer melts generated normal stress differences, which deviate from the typical behaviour of common plastics that $N_1 \approx 2G'$ at low shear rates and frequencies. Comparative plots of $N_1 - N_2$ showed that Ecoflex has larger elasticity than both grades PLA.

Measurements of the extrudate swell revealed that biodegradable polymers exhibit swell similar to rigid PVC, which is considerably lower than most conventional plastics for packaging applications. Ecoflex exhibited slightly larger swell than PLA, which is consistent with its larger normal stresses.

With regards to melt behaviour in extensional strain field, we observed that Ecoflex had higher extensional viscosity than both PLA resins. Values of the extensional viscosity of the biodegradable polymers were near those of a blown film grade of LLDPE, which are considerably lower than those of a branched LDPE. The industrial implication of this extensional behaviour is, that while easy down-gauging of biodegradable films might be possible, problems with bubble stability might be expected.

It was observed that biodegradable polymers slip at the die wall, which is a typical phenomenon in polymer liquids. However, the experimental results show that the Mooney method is not sensitive enough for quantifying the slip velocity of biodegradable polymer melts.

A study of the extrusion instabilities of biodegradable polymers is reported for the first time. It was observed that PLA exhibit both sharkskin and gross melt fracture. The values of the critical shear stress for the onset of sharkskin (0.14 – 0.18 MPa) and gross melt fracture (0.36-0.4 MPa) of PLA are very close to those values of LLDPE and HDPE, which are reported in the literature. However, unlike these linear polyethylenes, PLA does not exhibit stick-spurt instability. This is a phenomenological similarity with LDPE, PP, PVC, and PS.

It was also found that Ecoflex did not exhibit sharkskin phenomenon, in similarity with broad molecular weight polypropylene, polystyrene and LDPE. However, the onset of gross melt fracture of Ecoflex occurs at higher shear stresses (0.58 MPa) than those of conventional plastics, for which values of 0.13 – 0.5 MPa are reported.

Results of passing PLA and Ecoflex through an internal mixer show that significant degradation (expressed by a large shear viscosity drop) occurs during processing of biodegradable polymers.

Blending PLA and Ecoflex produced immiscible blends, for which Cox-Merz rule did not hold. It was observed that PLA/Ecoflex blends exhibit both sharkskin and gross melt fracture. It was found that blending with Ecoflex moved the onset of PLA sharkskin to higher value of wall shear rates and stresses, which was attributed to some sort of lubricating effect as a result from the byproducts of resin degradation during blending in Haake and from the presence of Ecoflex. On the other hand we found that the onset of sharkskin of PLA/Ecoflex blend with 10 wt% PLA occurred at higher shear stress than the onset of gross melt fracture of the neat Ecoflex. It was concluded that blending with Ecoflex provides some advantages for postponing the onset of sharkskin instability of PLA, and that blending with PLA seems to offer benefits in terms of delayed occurrence of flow instabilities of Ecoflex.

6.2 Recommendations

From the experience of this rheological study of biodegradable polymers, the following recommendations can be made:

1. A comprehensive study of mechanisms of degradation during extrusion of PLA and Ecoflex should be conducted in order to determine the dominant type of degradation during processing. This will provide basis for finding ways to reduce the large degradation which is presently observed.
2. Studies should be conducted, which investigate the effects of die material, die geometry, and die temperature on the onset of extrusion instabilities of biodegradable polymers. It might be appropriate to use nitrogen in order to reduce oxidation and hydrolysis during experiments.
3. The effect of various processing aids on rheology (especially on the onset of flow instabilities) and on final mechanical properties of biodegradable polymers should be studied
4. Gap-dependant wall slip measurements using rotational or planar parallel plate rheometers should be used for quantifying the slip velocity of biodegradable polymers.

5. Effect of compatibilizing PLA and Ecoflex blends should be studied in view of morphology, rheology (including flow instabilities), and final mechanical properties of the blends. It would be desirable for the blends to be prepared in a twin screw extruder under nitrogen blanket.

REFERENCES

Agassant, J.-F., D. Arda, C. Combeaud, A. Merten, H. Munstedt, M. Mackley, L. Robert, B. Vergnes, "Polymer Processing Extrusion Instabilities and Methods for Their Elimination or Minimisation", *Intern. Polym. Proc.*, **21(3)**, 239-255 (2006)

Anderson, K., M. Hillmyer, "The Influence of Block Copolymer Microstructure on the Toughness of Compatibilized Polylactide/Polyethylene blends", *Polymer* **45,** 8809–8823 (2004)

Anderson, K., S. Lim, and M. Hillmyer, " Toughening of Polylactide by Melt Blending with Linear Low-Density Polyethylene", *J.Appl.Polym. Sci.* **89**, 3757–3768 (2003)

Archer, L., "Wall Slip: Measurement and Modeling Issues" Chapter 3 in Hatzikiriakos, S. and K. Migler (Eds.), "Polymer Processing Instabilities: Control and Understanding", Marcel Dekker, Monticello, NY, USA (2005)

Ariawan, A., S. Hatzikiriakos, S. Goyal, and H. Hay, "Effects of Molecular Structure on the Rheology and Processability of Blow-Molding High Density Polyethylene Resins", *Adv.Polym.Tech.*, **20(1)**, 1-13 (2001)

ASTM D 638-03 "Standard Test Method for Tensile Properties of Plastics", ASTM International, West Conshohocken, PA, 2003

ASTM D 6866-05, "Standard Test Methods for Determining the Biobased Content of Natural Range Materials Using Radiocarbon and Isotope Ratio Mass Spectrometry Analysis", ASTM vol.**08.03**

Auras, R., B. Harte and S. Selke, "An Overview of Polylactides as Packaging Materials", *Macromol. Biosci.*, **4,** 835-864, (2004)

Baird, D. and D. Collias, "Polymer Processing: Principles and Design", John Wiley & Sons, Inc., New York, NY (1998)

BASF, "Product Information Ecoflex F BX 7011 – Version1", retrieved on 19/05/2005 from http://www.corporate.basf.com

BASF, "MSDS of Ecoflex F BX 7011", retrieved on 19/05/2005 from http://www.corporate.basf.com

Bhattacharya M., R. Reis, V. Correlo, and L. Boesel, "Material Properties of Biodegradable Polymers" Chapter 13 in R.Smith (Ed.) "Biodegradable Polymers for Industrial Applications", Woodhead Publishing Ltd., Cambridge, England (2005)

Binding, D., M. Couch, and K. Walters, "The Pressure Dependence of the Shear and Elongational Properties of Polymer Melts", *J.Non.-Newt. Fluid Mech.*, **79**, 137-155 (1998)

Bigg, D., "Polylactide Copolymers: Effect of Copolymer ratio and End Capping on Their Properties", *Adv.Polym.Tech.*, **24(2)**, 68-82 (2005)

Biresaw, G, and C. Carriere, "Interfacial Tension of Poly(lactic acid)/ Polystyrene Blends", *J. Polym. Sci., Part B: Polym.Phys.* **40**, 2248-2258 (2002)

Box, G. W. Hunter and J.S. Hunter, "Statistics for Experimenters", John Wiley & Sons, New York, NY (1978)

Braun, B., J. Dorgan, and D. Knauss, "Reactively Compatibilized Cellulosic Polylactide Composites", *J.Pol. and Env.*, **14(1)**, 49-58, (2006)

Buchholz, B. "Analysis and Characterization of Resorbable DL-lactide-Trimethylene Carbonate Copolyesters", *J. Mater. Sci.: Mater. Med.*, **4**, 381-388 (1993)

Chapleau, N. M. Huneault and H. Li, "Properties of Biaxially oriented PLA/Starch Blends", *BioPlastics 2006 International Conference*, Montreal, PQ, Sept. 2006

Chen, G., "Polyhydroxyalkanoates" Chapter 2 in R.Smith (Ed.) "Biodegradable Polymers for Industrial Applications", Woodhead Publishing Ltd., Cambridge, England (2005), p.32

Cogswell, F. "Converging Flow of Polymer Melts in Extrusion Dies", *Polym. Eng. Sci.* **12,** 64 (1972)

Cogswell, F. "Stretching Flow Instabilities at the Exits of Extrusion Dies", *J.Non-Newton.Fluid Mech.* **2,** 37-47 (1977)

Cooper-White, J., and M. Mackay, "Rheological Properties of Poly(lactides). Effect of Molecular Weight and Temperature on the Viscoelasticity of Poly(L-lactic acid)", *J.Pol.Sci., Part B: Polymer Physics*, **37**, 1803-1814 (1999)

Cox, W. and E. Merz, "Correlation of Dynamic and Steady Flow Viscosities", *J. Polym. Sci.* **28**, 619-622 (1958)

Dealy, J. and K. Wissbrun, "Melt Rheology and Its Role in Polymer Processing", Van Nostrand Reihnolds, New York (1990)

Dealy, J. and P. Saucier "Rheology in Plastics Quality Control". Hanser Gardner Publications, Inc., Cincinnati, OH (2000)

Dealy, J. and S. Kim, "Gross Melt Fracture in Extrusion" Chapter 7 in Hatzikiriakos, S. and K. Migler (Eds.), "Polymer Processing Instabilities: Control and Understanding", Marcel Dekker, Monticello, NY, USA (2005)

Dealy, J., "Elements of Rheology", Chapter 2 in Hatzikiriakos, S. and K. Migler (Eds.), "Polymer Processing Instabilities: Control and Understanding", Marcel Dekker, Monticello, NY, USA (2005)

Denn, M., "Extrusion Instabilities and Wall Slip", *Annu. Rev. Fluid Mech.*, **33,** 265-287 (2001)

Di, Y., S. Iannace, E. Di Maio and L. Nicolais, "Poly(lactic acid)/ Organoclay Nanocomposites: Thermal, Rheological Properties and Foam Processing", *J.Pol. Sci. Part B: Pol. Phys.* **43**, 689–698 (2005)

Dorgan, J., and J. Williams, "Melt Rheology of Poly(lactic acid): Entanglement and Chain Architecture Effects", *J.Rheol.* **43(5)**, 1141-1155 (1999)

Dorgan, J., J. Janzen, and M. Clayton, "Melt Rheology of Variable Content Poly(lactic acid)", *J.Rheol.*, **49(3)**, 607-619 (2005)

Dorgan, J; Lehermeier, H; Mang, M.: "Thermal and Rheological Properties of Commercial-Grade Poly(Lactic Acid)s, J. Pol. And Env., **8(1)**, 1-9, (2000)

Drumright, R., P. Gruber, and D. Henton, "Polylactic Acid Technology", *Adv.Mater.*, **12(23)**, 1841-1846, (2000)

Eickhoff, H. and G. Harrison, "The Rheology and Degradation of Renewable Resource Polymers", GPEC, Atlanta, GA, March 2006

Fang, Q, and M. Hanna, "Rheological Properties of Amorphous and Semicrystalline Polylactic Acid Polymers", *Ind. Crops and Prod.*, **10,** 47-53, (1999)

Fujiyama, M., and H. Inata, "Melt Fracture Behaviour of Polypropylene-Type Resins with Narrow Molecular Weight Distribution. I. Temperature Dependence", *J.Appl.Polym.Sci.*, **84**, 2111-2119 (2002)

Fukushima, K. and Yoshiharu Kimura, "Stereocomplexed Polylactides (Neo-PLA) as High-performance Bio-based Polymers: Their Formation, Properties, and Application, *Polym. Int.* **55,** 626-642 (2006)

Garlotta, D. "A Literature Review of Poly(Lactic Acid)", *J.Pol. and Env.*, **9(2)**, 63-84, (2001)

Georgiou, G., "Stick-Slip Instability" Chapter 6 in Hatzikiriakos, S. and K. Migler (Eds.), "Polymer Processing Instabilities: Control and Understanding", Marcel Dekker, Monticello, NY, USA (2005)

Grijpma, D., G. Zondervan, and A. Pennings "High Molecular Weight Copolymers of L-lactide and ε-caprolactone as Biodegradable Eastomeric Implant Materials", *J. Polym. Bull.*, **25**, 327-333 (1991)

Halley, P., Thermoplastic Starch Biodegradable Polymers", Chapter 6 in R.Smith (Ed.) "Biodegradable Polymers for Industrial Applications", Woodhead Publishing Ltd., Cambridge, England (2005), p. 140

Hatzikiriakos, S. and J.Dealey, "Wall slip of Molten High Density Polyethylenes. II. Capillary Rheometer Studies", *J.Rheol.* **36** (4), 703-741 (1992)

Hatzikiriakos, S. and K. Migler, "Overview of Processing Instabilities" Chapter 1 in Hatzikiriakos, S. and K. Migler (Eds.), "Polymer Processing Instabilities: Control and Understanding", Marcel Dekker, Monticello, NY, USA (2005)

Hatzikiriakos, S., "Boron Nitride Based Polymer Processing Aids", Chapter 9 in Hatzikiriakos, S. and K. Migler (Eds.), "Polymer Processing Instabilities: Control and Understanding", Marcel Dekker, Monticello, NY, USA (2005)

Heufel, D. "Ecoflex-Performance Enhancer for Renewables", ANTEC, Boston, MA, May 2005

Hiljanen-Vainio, M., T. Karjalainen, and J. Seppala, "Biodegradable Lactone Copolymers. I. Characterization and Mechanical Behaviour of ε-caprolactone and Lactide Copolymers", *J. Appl. Polym. Sci.*, **59**, 1281-1288 (1996)

Huda, M., L. Drzal, A. Mohanty, M. Misra, "Chopped Glass and Recycled Newspaper as Reinforcement Fibers in Injection Molded Poly(lactic acid) (PLA) Composites: A Comparative Study", *Compos. Sci. Tech.* **66,** 1813–1824 (2006)

Huneault, M and H. Li, "Interfacial Modification of PLA/Starch Blends", *BioPlastics 2006 International Conference*, Montreal, PQ, Sept. 2006

Huneault, M., P. Lafleur, and P. Carreau, "Extrudate Swell and Drawdown Effects on Extrudate Profile Dimensions and Shape", *Pol.Eng.Sci.*, **30 (23)**, 1554-1550 (1990)

ISO 1143, "Plastics – Determination of the Fluidity of Plastics Using Capillary and Slit-Die Rheometers"

Jiang, L., M. Wolcott, and J. Zhang, "Study of Biodegradable Polylactide/Poly(butylene adipate-*co*-terephthalate) Blends", *Biomacromolecules*, **7**, 199-207 (2006)

Joziasse, C., H. Grablowitz, and A. Pennings, "Star-shaped Poly[(trimethylene carbonate)-co-(e-caprolactone)] and Its Block Copolymers with Lactide/Glycolide.

Synthesis, Characterization, and Properties" *Macromol. Chem. Phys.* **201**, 107-112 (2000)

Kazatchkov, I., N. Bohnet, S. Goyal, and S. Hatzikiriakos, "Influence of Molecular Structure on the Rheological and Processing Behaviour of Polyethylene resins", *Polym.Eng.Sci.*, **39**, 804-815 (1999)

Kharchenko, S, K. Migler and S. Hatzikiriakos, "Conventional Polymer Processing Additives" Chapter 8 in Hatzikiriakos, S. and K. Migler (Eds.), "Polymer Processing Instabilities: Control and Understanding", Marcel Dekker, Monticello, NY, USA (2005)

Ki, H. and O. Ok Park, "Synthesis, Characterisation and Biodegradability of the Biodegradable Aliphatic-aromatic Random Copolyesters", *Polymer*, **42**, 1849-1861 (2001)

Kim, C., K. Cho, E. Choi, J. Park, "Effect of P(/LA- co-εCL) on the Compatibility and Crystallization Behaviour of PCL/PLLA Blends", *J.Appl.Polym. Sci.* **77**, 226-231 (2000)

Kolstad, J., "Crystallization Kinetics of Poly(L-lactide-co-*meso*-lactide)", *J.Appl.Pol.Sci*, **62**, 1079-1091, (1996)

Labrecque, L., R.Kumar, V.Dave, R. Cross, and S. McCarthy, "Citrate Esters as Plasticizers for Poly(lactic acid)", *J.Appl.Pol.Sci.* **66**, 1507-1513 (1997)

Larrazabal, H., A. Hrymak, and J. Vlachopoulos, "On the Relationship between the Work of Adhesion and the Critical Shear Stress for the Onset of Flow Instabilities", *Rheol. Acta*, **45**, 705-715 (2006)

Lee, C., E. Kim, and J. Yoon, "Reactive Blending of Poly(L-lactic acid) with Poly(ethylene-*co*-vinyl alcohol), *J.Appl.Polym. Sci.* **98**, 886–890 (2005)

Lehermeier, H. and J. Dorgan, "Melt Rheology of Poly(lactic acid): Consequences of Blending Chain Architectures", *Pol.Eng. and Sci.* **41(12)**, 2172-2184 (2001)

Lewitus, D., S. McCarthy, A. Ophir and S. Kenig, "The Effect of Nanoclays on the Properties of PLLA-Modified Polymers Part 1: Mechanical and Thermal Properties", *J Polym Environ* **14**, 171–177 (2006)

Ljungberg, N. and B. Wesslen, "The Effect of Plasticizers on the Dynamic Mechanical and Thermal Properties of Poly(lactic acid)", *J.Appl.Pol.Sci.* **86**, 1227-1234 (2002)

Lunt, J.; "Large-scale Production, Properties and Commercial Applications of Polylactic Acid Polymers" *Polymer Degradation and Stability* **59,** pp.145-152, (1998)

Ma, X., J. Yu and N. Wang, "Compatibility Characterization of Poly(lactic acid)/ Poly(propylene carbonate) Blends", *J. Polym. Sci., Part B: Polym. Phys.* **44**, 94-101 (2006)

Mackley, M., "Capillary Rheology", Chapter 1 in Collyer, A. and D. Clegg (Eds), "Rheological Measurement", Elsevier Applied Science Publishers LTD., Essex, England (1988)

Macosko, C., "Rheology: Principles, Measurements, and Applications", VCH Publishers, Inc., New York, NY (1994)

Martin, O. and L. Averous, "Poly(lactic acid): Plasticization and Properties of Biodegradable Multiphase Systems", *Polymer*, **42**, 6209-6219, (2001)

Migler, K., "Sharkskin Instability in Extrusion" Chapter 5 in Hatzikiriakos, S. and K. Migler (Eds.), "Polymer Processing Instabilities: Control and Understanding", Marcel Dekker, Monticello, NY, USA (2005)

Migler, K., Y. Son, F. Qiao, and K. Flynn, "Extensional Deformation, Cohesive Failure, and Boundary Conditions during Sharkskin Melt Fracture", *J.Rheol.*, **46**, 383-400 (2002)

Migliaresi, C., D. Cohn, A.De Lollis, and L. Fambri, "Dynamic Mechanical and Calorimetric Analysis of Compression Molded PLLA of Different Molecular Weights: Effect of Thermal Treatments", *J.Appl.Polym.Sci.*, **43**, 83-95 (1991)

Mohanty, A., M. Misra, and G. Hinrichsen, "Biofibres, Biodegradable Polymers and Biocomposites: An Overview", *Macromol.Mater.Eng*, **276/277,** 1-24, (2000)

Mooney, M., "Explicit Formulas for Slip and Fluidity", *Trans. Soc. Rheol.*, **2**, 210 (1931)

Muliawan, E, S. Hatzikiriakos, and M. Sentmanat, "Melt Fracture of Linear PE: A Crytical Study in Terms of Their Extensional Behaviour", *Intern.Polym.Proc.*, **20(1)**, 60-67 (2005)

Nakafuku, C. and M. Sakoda, "Melting and Crystallization of Poly(L-lactic acid) and Poly(ethylene oxide) Binary Mixture" *Polym. J.*, **25 (9)**, 909-917 (1993)

Nakafuku, C. and S. Takehisa, "Glass Transition and Mechanical Properties of PLLA and PDLLA-PGA Copolymer Blends", *J.Appl.Polym. Sci.* **93**, 2164–2173 (2004)

Nakayama, A.; Kawasaki, N.; Arvanitoyannis, I.; Iyoda, J.; Yamamoto, N. "Synthesis and Degradability of a Novel Aliphatic Polyester: Poly(b-methyl-d-valerolactone-co-L-lactide)" *Polymer*, **36 (6)**, 1295-1301 (1995)

Narayan, R., "Biobased and Biodegradable Materials: Rationale, Drivers, and Technology Exemplars", *BioPlastics 2006 International Conference*, Montreal, PQ, Sept. 2006

Noda, I., M. Satkowski, A. Dowrey, and C. Marcott, "Polymer Alloys of Nodax Copolymers and Poly(lactic acid)", *Macromol. Biosci.*, **4**, 269–275 (2004)

Okhita, T. and S. Lee, "Thermal Degradation and Biodegradability of Poly(lactic acid)/Corn Starch Composites", *J.Appl.Polym. Sci.* **100**, 3009-3017 (2006)

Oksman K., M. Skrifvars, J.-F. Selin, "Natural Fibres as Reinforcement in Polylactic Acid (PLA) Composites", *Compos. Sci. Tech.* **63,** 1317-1324 (2003)

Omura, M., T. Tsukegi,Y. Shirai, H. Nishida, and T. Endo, "Thermal Degradation Behaviour of Poly(Lactic Acid) in a Blend with Polyethylene", *Ind. Eng. Chem. Res.* **45**, 2949-2953 (2006)

Palade, L., H. Lehermeier, and J. Dorgan, "Melt Rheology of High L-content Poly(lactic acid)", *Macromolecules*, **34**, 1384-1390 (2001)

Park, J. and S. Im, "Phase Behaviour and Morphology in Blends of Poly(lactic aacid) and Poly(butylene succinate)", *J.Appl.Polym. Sci.* **86**, 647-655 (2002)

Petersson, L. and K. Oksman, "Biopolymer Based Nanocomposites: Comparing Layered Silicates and Microcrystalline Cellulose as Nanoreinforcement", *Comp.SciTech* **66**, 2187-2196 (2006)

Pillin, I., N. Montrelay, and Y. Grohens, "Thermo-mechanical Characterization of Plasticized PLA: Is the Miscibility the Only Significant Factor?", *Polymer* **47**, 4676-4682 (2006)

Porter, R.S. and L.-H. Wang, "Compatibility and Transesterification in Binary Polymer Blends", *Polymer*, **33(10)**, 2019 – 2031 (1992)

Pyda, M., R. Bopp, and B. Wundelich, "Heat Capacity of Poly(lactic acid)", *J.Chem. Thermodynamics,* **36,** 731-742 (2004)

Ramamurthy, A., "Wall Slip in Viscous Fluids and Influence of Materials of Construction", *J.Rheol.*, **30(2)**, 337-357 (1986)

Ramkumar, D. and M. Bhattacharya, "Steady Shear and Dynamic Properties of Biodegradable Polyesters", *Pol.Engand Sci.*, **38(9)**, 1426-1435, (1999)

Rauwendaal, C. "Polymer Extrusion", Hanser Gardner Publications, Inc,. Cincinnati, OH (1994)

Ray, S. and S. Bousmina, "Biodegradable Polymers and Their Layered Silicate Nanocomposites: In Greening the 21st Century Materials World", *Progress in Materials Science* **50**, 962–1079 (2005)

Ray, S., K. Yamada, M. Okamoto and K. Ueda, "New Polylactide-Layered Silicate Nanocomposites. 2. Concurrent Improvements of Material Properties, Biodegradability and Melt Rheology", *Polymer* **44**, 857-866 (2003)

Ren, Z., L. Dong, and Y. Yang, "Dynamic Mechanical and Thermal Properties of Plasticized Poly)lactic acid)", *J.Appl.Pol.Sci.* **101**, 1583-1590 (2006)

Satkowski, M; D. Melik; J. Autran, P. Green, I. Noda, and L. Schechtman," Physical and Processing Properties of Polyhydroxyalkanoate Copolymers", Chapter 9 in Doi, Y. and A.Steinbuchel, (Eds.), "Biopolymers", volume 3b, Wiley-VCH Verlag GmbH, Weinheim, Germany (2002), p.231

Scherzer, D. "Plastics from Renewable Resources", ANTEC, Boston, MA, May 2005

Sentmanat, M. and S. Hatzikiriakos, "Mechanism of Gross Melt Fracture Elimination in the Extrusion of Polyethylenes in the Presence of Boron Nitride", *Rheol. Acta*, **43**, 624-633 (2004)

Serizawa, S., K. Inoue, M. Iji, "Kenaf-Fiber-Reinforced Poly(lactic acid) Used for Electronic Products", *J.Appl.Polym. Sci.* **100,** 618–624 (2006)

Shanks R., A. Hodzic, D. Ridderhof, "Composites of Poly(lactic acid) with Flax Fibers Modified by Interstitial Polymerization", *J.Appl.Polym. Sci.* **101**, 3620–3629 (2006)

Sheth, M., R. Kumar, V. Dave, R. Gross, and S. McCarthy, "Biodegradable Polymer Blends of Poly (lactic acid) and Poly (ethylene glycol)", *J.Appl.Polym. Sci.* **66**, 1495–1505 (1997)

Sinclair, R. , "The Case for Polylactic Acid as a Commodity Packaging Plastic", *J. Macromol. Sci. Pure Appl. Chem.*, **A33(5)**, 587, (1996)

Smith, R. *Ed.*, "Biodegradable Polymers for Industrial Applications", Woodhead Publishing Ltd., Cambridge, England (2005)

Sodergard, A. and M. Stolt, "Properties of Lactic Acid Based Polymers and Their Correlation with Composition", *Prog.Polym.Sci.*, **27**, 1123-1163 (2002)

Son, Y. and K. Migler, "Cavitation of Polyethylene during Extrusion Processing Instabilities", *J. Polym. Sci: Part BL Polym. Phys.*, **40**, 2791-2799 (2002)

Steinbuchel, A., "Use of Biosynthetic, Biodegradable Thermoplastics and Elastomers from Renewable Resources: the Pros and Cons", *J.M.S.-Pure Appl. Chem.*, **A32(4)**, 653-660, (1995)

Storey, R. F.; Wiggins, J. S.; Puckett, A. D. "Hydrolyzable Poly(ester-urethane) Networks from L-lysine Diisocyanate and D,L-lactide/e-caprolactone Homo- and Copolyester Triols" *J. Polym. Sci., Part A: Polym. Chem.* **32 (12)**, 2345-2363 (1994)

Tadmor, Z. and C. Gogos, "Principles of Polymer Processing, 2nd Ed.", John Wiley & Sons, Inc., Hoboken, NJ (2006)

Tsuji, H. and I. Fukui, "Enhanced Thermal Stability of Poly(lactide)s in the Melt by Enantiomeric Polymer Blending", *Polymer*, **44**, 2891-2896 (2003)

Tsuji, H., "Poly(lactide) Stereocomplexes: Formation, Structure, Properties, Degradation, and Applications", *Macromol. Biosci.* **5**, 569-597 (2005)

Utracki, L and M. Kamal, "The Rheology of Polymer Alloys and Blends", Chapter 7 in L. Utracki (Ed.), "Polymer Blends Handbook", Kluwer Academic Publishers, Dordrecht, The Netherlands (2002)

Utracki, L., "Introduction to Polymer Blends", Chapter 1 in L. Utracki (Ed.), "Polymer Blends Handbook", Kluwer Academic Publishers, Dordrecht, The Netherlands (2002)

Vlachopoulos, J, "Extrudate Swell in Polymers", *Rev.Deform.Beh.Mater.*, **3**, 219-248 (1981)

Vlachopoulos, J. and J. Wagner, "The SPE Guide on Extrusion Technology and Troubleshooting", The Society of Plastic Engineers, Brookfield, CT (2001)

Vlachopoulos, J. and M. Alam, "Critical Stress and Recoverable Shear for Polymer Melt Fracture", *PolymEng.Sci.*, **12**, 184-192, (1972)

Vlachopoulos, J. and S Lidorikis, "Melt Fracture of Polystyrene", *Polym.Eng.Sci.*, **11**, 1-5 (1971)

Vlachopoulos, J., "Polymer Rheology – Course Notes", McMaster University, Hamilton, ON, (2005)

Wang, Y., M. Hillmyer, "Polyethylene-poly(L-lactide) Diblock Copolymers: Synthesis and Compatibilization of Poly(L-lactide)/Polyethylene Blends", *J. Polym. Sci., Part A: Polym. Chem.* **39 (16)**, 2755-2766 (2001)

Witt, U., T. Einig, M. Yamamoto, I. Kleeberg, W.-D. Deckwer, R.-J. Muller, "Biodegradation of Aliphatic-aromatic Copolyesters: Evaluation of the Final Biodegradability and Ecotoxicological Impact of Degradation Intermediates", *Chemosphere*, **44**, 289-299 (2001)

Witzke, D., " Introduction to Properties Engineering and Prospects of Polylactide Polymers", PhD Thesis, Michigan State University, East Lansing, MI 1997, p.389

Wu, C. and H. Liao, "A New Biodegradable Blends Prepared From Polylactide and Hyaluronic Acid", *Polymer* **46,** 10017–10026 (2005)

Yamamoto, M., U. Witt, G. Skupin, D. Beimborn, RJ. Muller, "Biodegradable Aliphatic-Aromatic Polyesters: Ecoflex®," Chapter 11 in Doi Y, A. Steinbuchel (Ed.) "Biopolymers", volume 4, Wiley-VCH Verlag GmbH, Weinheim, Germany (2002), p.299

Yamane, H., K. Sasai, M. Takano, and M. Takashi, "Poly(D-lactic acid) as a Rheological Modifier of Poly(L-lactic acid): Shear and Biaxial Extensional Flow Behaviour", *J.Rheol.*, **48(3)**, 599-609 (2004)

Yu, L., K. Dean, and L. Li, " Polymer Blends and Composites from Renewable Resources", *Prog. Polym. Sci.* **31**, 576–602 (2006)

Zahavich, A., "The Effect of Multiple Extrusion Passes During the Recycling of High Density Polyethylene", PhD Thesis, McMaster University, Hamilton, ON, (1995)

Zahavich, A., B. Latto, E. Takacs, and J. Vlachopoulos, "The Effect of Multiple Extrusion Passes During Recycling of High Density Polyethylene", *Adv.inPolym.Techn.* **16,** 11-24 (1997)

Zhang, J-F. and X. Sun, "Mechanical Properties of Poly(lactic acid)/Starch Composites Compatibilized by Maleic Anhydride", *Biomacromol.* **5**, 1446-1451 (2004)

Zhang, J-F. and X. Sun, "Poly(lactic acid)-based Bioplastics" Chapter 10 in R.Smith (Ed.) "Biodegradable Polymers for Industrial Applications", Woodhead Publishing Ltd., Cambridge, England (2005), p. 251

Zuideveld, M., C. Gottschalk, H. Kropfinger, R. Thomann, M. Rusu, and H. Frey, "Miscibility and Properties of Linear Poly(L-lactide)/Branched Poly(L-lactide) Copolyester Blends", *Polymer* **47**, 3740–3746 (2006)

APPENDIX A

EXPERIMENTAL DATA FROM PARALLEL PLATE RHEOMETRY

Table A1. Frequency, complex viscosity, storage and loss moduli data for PLA 4042D at 180°C and strain 4 %

Freq rad/s	η^* Pa-s	G' Pa	G" Pa
0.10	3374.52 ± 67.16	-	337.45 ± 6.73
0.15	3319.24 ± 102.61	16 ± 3.24	486.94 ± 15.19
0.22	3163.83 ± 98.31	26.26 ± 2.38	681.12 ± 21.28
0.32	3157.24 ± 171.83	44.5 ± 4.9	997.42 ± 54.58
0.46	3098.65 ± 156.44	73.94 ± 8.51	1436.36 ± 73.1
0.68	3116.24 ± 138.68	141.42 ± 1.67	2118.35 ± 94.58
1.00	3083.25 ± 104.17	247.54 ± 18.28	3073.29 ± 103.02
1.47	3028.61 ± 116.34	472.78 ± 21.85	4420.18 ± 169.4
2.15	2975.49 ± 110.89	867.17 ± 48.94	6351.58 ± 234.41
3.16	2910.24 ± 103.17	1615.01 ± 56.11	9060.17 ± 321.39
4.64	2844.89 ± 122.45	2921.66 ± 173.89	12877.5 ± 543.3
6.81	2764.24 ± 143.16	5155.54 ± 360.57	18113.1 ± 911.2
10.00	2660.7 ± 135.94	8704.34 ± 494.48	25143 ± 1267.3
14.68	2512.48 ± 117.88	14035.4 ± 633	34102.9 ± 1610.5
21.54	2325.98 ± 92.21	21804.8 ± 785.3	45119 ± 1826.9
31.62	2106.16 ± 71.38	32630.4 ± 1085.2	58061.9 ± 1979.2
46.42	1868.81 ± 54.84	47321.5 ± 1445	72697.7 ± 2096.7
68.13	1621.72 ± 41.8	66322.4 ± 1871.1	88366.4 ± 2156.2
100.00	1378.74 ± 31.84	89982.2 ± 2395.3	104460 ± 2140

Table A2 Frequency, complex viscosity, storage and loss moduli data for PLA 4042D at 190°C and strain 10 %

Freq rad/s	η* Pa-s	G' Pa	G" Pa
0.1	1554.63 ± 19.62	-	155.42 ± 1.97
0.13	1543.73 ± 47.01	-	194.29 ± 6.27
0.16	1535.67 ± 46.76	-	243.34 ± 7.41
0.2	1532.86 ± 46.67	4.56 ± 0.24	305.82 ± 9.31
0.25	1525.15 ± 46.44	8.09 ± 0.42	383.02 ± 11.66
0.32	1513.78 ± 46.09	11.5 ± 0.6	478.56 ± 14.57
0.4	1500.96 ± 45.7	15.8 ± 0.83	597.34 ± 18.18
0.5	1496.22 ± 45.34	26.39 ± 1.43	748.21 ± 21.83
0.63	1488.78 ± 41.1	40.74 ± 1.44	936.96 ± 24.95
0.79	1480.82 ± 40.68	55.67 ± 4.18	1173.04 ± 30.82
1	1472.47 ± 38.7	79.97 ± 2.84	1467.92 ± 36.92
1.26	1464.66 ± 33.72	116.95 ± 3.25	1837.22 ± 40.22
1.58	1461.1 ± 28.47	179.15 ± 5.81	2305 ± 43.09
1.99	1452.97 ± 32.76	259.14 ± 7.62	2882.78 ± 61.63
2.51	1452.78 ± 33.09	410 ± 10.41	3620.13 ± 78.25
3.16	1450.37 ± 30.35	595.73 ± 19.89	4540.11 ± 88.89
3.97	1452.39 ± 31.03	876.63 ± 31.59	5705.74 ± 113.47
5	1455.75 ± 29.34	1279.11 ± 45.82	7171.02 ± 132.78
6.3	1451.57 ± 29.28	1803.98 ± 68.02	8964.2 ± 164.11
7.93	1440.08 ± 28.54	2507.5 ± 95.45	11141.7 ± 197.57
9.98	1419.42 ± 26.71	3447.29 ± 133.4	13745.37 ± 225.33
12.57	1389.56 ± 25.5	4687.68 ± 177.9	16824.07 ± 263.09
15.82	1351.69 ± 22.94	6321.3 ± 226.35	20432.3 ± 285.25
19.92	1306.34 ± 20.81	8449.32 ± 292.24	24612.03 ± 307.62
25.08	1253.32 ± 17.95	11181.3 ± 356.45	29374.03 ± 308.89
31.57	1195.32 ± 15.05	14651.67 ± 425.8	34776.63 ± 290.86
39.75	1132.1 ± 12.9	18987.8 ± 506.01	40792.53 ± 274.59
50	1057.74 ± 20.12	24056.77 ± 948.21	47093.7 ± 646.58
62.95	987.73 ± 17.19	30442.63 ± 1100.42	54205.23 ± 624.12
79.24	916.16 ± 14.63	38081.87 ± 1262.94	61803.33 ± 585.3
100.00	842.94 ± 11.88	47026.4 ± 1403.61	69707 ± 485.15

Table A3. Frequency, complex viscosity, storage and loss moduli data for PLA 4042D at 200°C and strain 12 %

Freq rad/s	η* Pa-s	G' Pa	G" Pa
0.22	871.36 ± 43.94	-	187.57 ± 9.28
0.32	872.38 ± 76.42	-	275.76 ± 24.19
0.46	869.21 ± 43.48	5.42 ± 2.96	403.41 ± 20.15
0.68	852.96 ± 63.45	15.4 ± 1.62	580.91 ± 43.2
1	847.34 ± 62.68	29.64 ± 4.36	846.82 ± 62.56
1.47	841.11 ± 59.66	58.04 ± 9.87	1233.22 ± 87.19
2.15	836.88 ± 60.45	115.34 ± 10.4	1799.31 ± 129.84
3.16	835.43 ± 54.3	220.63 ± 18.64	2632.62 ± 170.75
4.64	829.87 ± 51.64	429.28 ± 29.87	3827.92 ± 237.82
6.81	828.23 ± 49.29	841.02 ± 57.54	5579.65 ± 330.95
10	829.05 ± 48.04	1539.61 ± 120.61	8146.28 ± 466.07
14.68	820.3 ± 48.86	2710.96 ± 235.34	11731.1 ± 681.65
21.54	797.68 ± 48.04	4572.47 ± 399.31	16565.85 ± 963.57
31.62	760.39 ± 44.92	7504.51 ± 636.35	22844.3 ± 1286.23
46.42	711.69 ± 40.62	11996.15 ± 975.6	30777.55 ± 1643.53
68.13	652.56 ± 36.05	18600.8 ± 1427.51	40379.25 ± 2046.86
100.00	582.5 ± 25.61	26335.5 ± 211.99	49811.85 ± 37.83

Table A4. Frequency, complex viscosity, storage and loss moduli data for PLA 7000 D at 180°C and strain 5 %

Freq rad/s	η* Pa-s	G' Pa	G" Pa
0.11	4276.18 ± 53.49	-	460.51 ± 5.8
0.16	4063.81 ± 56.29	-	640.91 ± 8.44
0.23	4095.38 ± 33.39	-	950.16 ± 7.84
0.34	4070.37 ± 79.03	72.63 ± 3.95	1384.64 ± 27.16
0.5	3998.06 ± 62.82	131.64 ± 10.4	1994.67 ± 31.52
0.73	3965.19 ± 56.54	259.48 ± 10.6	2898.45 ± 40.88
1.08	3909.8 ± 57.23	475.69 ± 5.45	4184.76 ± 61.72
1.58	3842.1 ± 54.05	897.68 ± 18.02	6008.2 ± 84.17
2.32	3764.3 ± 38.86	1640.25 ± 15.96	8580.79 ± 90.16
3.41	3680.07 ± 32.91	2953.14 ± 55.82	12183.2 ± 105.3
5	3584.37 ± 44.07	5174.62 ± 81.77	17158.5 ± 209.45
7.34	3437.67 ± 38.76	8594.12 ± 171.6	23719.97 ± 253.71
10.77	3231.21 ± 38.02	13681.27 ± 307.05	32005.27 ± 339.79
15.81	2969.89 ± 36.47	21026.97 ± 451.9	41986.73 ± 441.58
23.21	2670.9 ± 34.59	31220.4 ± 638.52	53549.17 ± 569.27
34.06	2355.09 ± 31.21	44926.77 ± 840.12	66464.93 ± 720.26
50	2032.55 ± 27	62465.83 ± 1100.22	80163.07 ± 855.08
73.39	1719.19 ± 22.87	84081.7 ± 1412.93	94071.1 ± 988.23

Table A5. Frequency, complex viscosity, storage and loss moduli data for PLA 7000 D at 190°C and strain 4 %

Freq rad/s	η* Pa-s	G' Pa	G" Pa
0.16	2622.91 ± 132.34	-	414.65 ± 20.96
0.23	2560.53 ± 67.54	-	593.76 ± 15.27
0.34	2531.9 ± 112.25	27.13 ± 13.85	861.98 ± 38.15
0.5	2488.08 ± 140.33	62.62 ± 7.12	1242.44 ± 70.24
0.73	2460.16 ± 117.3	114.45 ± 3.55	1801.88 ± 86.06
1.08	2442.83 ± 110.63	216.49 ± 18.09	2622.53 ± 118.1
1.58	2409.22 ± 113.48	406.25 ± 33.08	3787.56 ± 177.06
2.32	2362.27 ± 108.89	754.39 ± 57.55	5430.16 ± 247.29
3.41	2310.87 ± 105.76	1374.25 ± 105.39	7750.92 ± 347.51
5	2249.37 ± 106.08	2472.57 ± 207.35	10971.4 ± 497.13
7.34	2192.53 ± 118.62	4415.34 ± 403.59	15472.73 ± 790.48
10.77	2121.26 ± 115.16	7530.75 ± 589.05	21573.33 ± 1110.31
15.81	2010.86 ± 99.01	12193.67 ± 777.3	29362.7 ± 1377.88
23.21	1863.21 ± 82.11	18916.03 ± 1059.15	38883.5 ± 1617.17
34.06	1686.98 ± 67.26	28310.83 ± 1420.32	50007.43 ± 1854.79
50	1493.73 ± 55.2	40935.33 ± 1910.11	62466.63 ± 2090.85
73.39	1295.95 ± 45.03	57295.43 ± 2462.15	75912.47 ± 2345.4

Table A6. Frequency, complex viscosity, storage and loss moduli data for PLA 7000 D at 200°C and strain 3 %

Freq rad/s	η* Pa-s	G' Pa	G" Pa
0.34	1490.89 ± 44.41	-	507.77 ± 15.16
0.5	1504.77 ± 30.39	-	752.22 ± 15.09
0.73	1447.38 ± 51.18	-	1061.06 ± 37.29
1.08	1449.5 ± 37.48	85.66 ± 6.12	1559.07 ± 40.16
1.58	1433.76 ± 40.1	165.34 ± 8.63	2260.93 ± 62.96
2.32	1413.62 ± 36.83	317.27 ± 23.04	3265.32 ± 83.87
3.41	1390.3 ± 35.43	590.03 ± 33.36	4699.06 ± 117.76
5	1357.15 ± 36.04	1083.93 ± 51.53	6698.56 ± 174.66
7.34	1319.06 ± 35.47	1948.06 ± 93.93	9482.44 ± 248.46
10.77	1275.51 ± 33.26	3448.13 ± 157.91	13300.17 ± 332.46
15.81	1231.64 ± 27.25	6014.25 ± 210.32	18521.77 ± 393.56
23.21	1180.9 ± 20.67	10050.34 ± 296.56	25496.57 ± 416.38
34.06	1107.89 ± 18.3	15930.17 ± 459.76	34212.3 ± 500.67
50	1013.62 ± 16.28	24145.97 ± 674.8	44558 ± 617.04
73.39	905.22 ± 14.6	35263.97 ± 937.27	56300.3 ± 780.04

Table A7. Frequency, complex viscosity, storage and loss moduli data for Ecoflex F BX at 180°C and strain 10 %

Freq rad/s	η* Pa-s	G' Pa	G" Pa
0.1	2511.93 ± 385.88	23.79 ± 4.57	249.45 ± 38.4
0.13	2447.98 ± 365.77	32.42 ± 7.76	305.73 ± 45.41
0.16	2363.82 ± 294.6	41.07 ± 10	371.46 ± 45.92
0.2	2338.55 ± 307.71	50.5 ± 10.51	462.74 ± 60.48
0.25	2290.86 ± 293.93	67.42 ± 14.78	570.08 ± 72.44
0.32	2253.05 ± 278.59	92.93 ± 19.28	704.66 ± 86.13
0.4	2222.04 ± 273.35	129.46 ± 21.11	872.95 ± 106.64
0.5	2171.46 ± 264.04	174.77 ± 32.36	1071.53 ± 128.53
0.63	2118.47 ± 256.4	239.24 ± 43.88	1311.8 ± 156.1
0.79	2067.25 ± 251.92	322.17 ± 57.44	1606.11 ± 192.14
1	2010.9 ± 242.96	430.82 ± 75.04	1959.23 ± 231.73
1.26	1951.18 ± 232.41	579.63 ± 96.93	2380.91 ± 276.89
1.58	1888.92 ± 223.15	771.09 ± 128.55	2885.2 ± 331
1.99	1823.64 ± 213.89	1016.74 ± 161.05	3484.53 ± 396.65
2.51	1759.94 ± 204.82	1342.11 ± 198.32	4200.97 ± 475.58
3.15	1695.63 ± 193.69	1755.97 ± 259.35	5052.65 ± 557
3.97	1633.82 ± 184.46	2286.19 ± 319.92	6072.61 ± 662.63
5	1574.22 ± 172.91	2953.76 ± 385.76	7295.66 ± 776.84
6.29	1510.89 ± 162.06	3770.6 ± 475.77	8730.8 ± 906.17
7.92	1445.51 ± 153.22	4756.96 ± 583.05	10420.18 ± 1069.05
9.98	1374.78 ± 143.35	5927.14 ± 710.68	12367.97 ± 1246.18
12.56	1301.52 ± 133.92	7315.24 ± 856.58	14617.87 ± 1453.36
15.81	1226.5 ± 124.21	8966.63 ± 1031.83	17194.73 ± 1678.04
19.91	1151.02 ± 114.84	10916.11 ± 1230.15	20143.3 ± 1934.97
25.06	1076.29 ± 105.86	13222.53 ± 1465.13	23506.9 ± 2221.03
31.55	1003.75 ± 97.74	15945.1 ± 1743.69	27358.1 ± 2554.49
39.72	932.82 ± 89.13	19147.7 ± 2043.87	31715.97 ± 2903.08
50	863.91 ± 81.31	22905.57 ± 2407.96	36621.13 ± 3291.7
62.95	797.7 ± 74.2	27312.3 ± 2822.61	42133.27 ± 3738.87
79.24	734.36 ± 67.67	32468.07 ± 3311.66	48293.3 ± 4237.96
100	604.98 ± 0	34189.3 ± 0	49736.9 ± 0

Table A8. Frequency, complex viscosity, storage and loss moduli data for Ecoflex F BX at 190°C and strain 3 %

Freq rad/s	η* Pa-s	G' Pa	G" Pa
0.15	1730.72 ± 54.69	-	252.97 ± 7.31
0.22	1709.64 ± 10.64	-	368.15 ± 2.42
0.32	1671.75 ± 130.52	39.48 ± 5.81	527.18 ± 40.95
0.46	1653.95 ± 81.03	99.08 ± 0.2	761.28 ± 37.93
0.68	1601.39 ± 6.15	171.51 ± 9.54	1077.45 ± 5.69
1	1539.89 ± 7.81	289.11 ± 4.51	1512.5 ± 8.8
1.47	1480.77 ± 4.86	466.98 ± 5.52	2122.72 ± 8.49
2.15	1395.99 ± 15.75	761.77 ± 1.03	2909.51 ± 35.31
3.16	1312.46 ± 11.5	1183.72 ± 8.73	3977.97 ± 35.36
4.64	1227.56 ± 4.72	1853.93 ± 18.67	5387.78 ± 29.54
6.81	1136.6 ± 0.28	2795.19 ± 35.94	7221.45 ± 11.77
10	1041.58 ± 1.65	4105.05 ± 44.03	9572.77 ± 0.7
14.68	953.86 ± 5.92	6018.56 ± 105.56	12641.2 ± 46.39
21.54	872.33 ± 10.86	8734.24 ± 217.91	16641 ± 150.54
31.62	795.29 ± 11.13	12424.2 ± 250.03	21866 ± 263.19
46.42	716.85 ± 7.52	17268.7 ± 189.15	28441.2 ± 293.45
68.13	638.94 ± 4.54	23516.3 ± 127.7	36632 ± 286.02
100	563.06 ± 2.86	31681.3 ± 126.93	46547.9 ± 259.86

Table A9. Frequency, complex viscosity, storage and loss moduli data for Ecoflex F BX at 200°C and strain 11.5 %

Freq rad/s	η* Pa-s	G' Pa	G" Pa
0.13	1422.68 ± 138.35	-	178.87 ± 17.72
0.16	1363.23 ± 78.63	6.92 ± 4.09	215.92 ± 12.6
0.2	1372.71 ± 58.11	15.58 ± 2.11	273.45 ± 11.49
0.25	1321.38 ± 84.67	23.6 ± 2.33	331.07 ± 21.49
0.32	1300.59 ± 40.05	31.41 ± 2.33	410.08 ± 12.53
0.4	1283.63 ± 62.26	46.96 ± 3.48	508.86 ± 24.57
0.5	1257.28 ± 58.82	67.56 ± 2.07	626.5 ± 29.43
0.63	1233.15 ± 75.46	94.45 ± 5.14	772.31 ± 47.34
0.79	1213.91 ± 70.32	131.01 ± 2.78	955.29 ± 56
1	1189.84 ± 67.15	183.18 ± 4.32	1175.65 ± 67.28
1.26	1164.29 ± 70.75	253.25 ± 8.44	1443.7 ± 88.95
1.58	1136.76 ± 67.15	346.93 ± 9.29	1767.9 ± 106.63
2	1107.21 ± 68.08	472.02 ± 16.68	2158.14 ± 135.41
2.51	1077.62 ± 64.35	635.83 ± 17.34	2631.08 ± 162.12
3.16	1044.08 ± 65.1	847.71 ± 29.93	3190.96 ± 205.05
3.98	1012.1 ± 63.65	1130.32 ± 41.1	3867.42 ± 251.99
5.01	979.75 ± 61.4	1493.16 ± 51.71	4677.77 ± 306.56
6.31	949.43 ± 61.28	1969.06 ± 75.11	5657.51 ± 383.26
7.94	917.75 ± 59.81	2562.56 ± 105.06	6824.58 ± 468.01
10	885.58 ± 58.86	3296.04 ± 147.83	8219.44 ± 574.86
12.59	849.87 ± 57.94	4180 ± 200.89	9848.65 ± 707.18
15.85	811.96 ± 56.33	5244.67 ± 257.21	11751.15 ± 862.74
19.95	771.24 ± 53.9	6516.44 ± 334.81	13940 ± 1030.68
25.12	729.83 ± 51.45	8038.51 ± 430.2	16475.8 ± 1227.96
31.62	687.27 ± 49.08	9850.6 ± 550.84	19372.4 ± 1461.17
39.81	644.6 ± 46.7	11996.35 ± 698.69	22684.7 ± 1733.83
50.12	603.27 ± 44.33	14567.9 ± 884.59	26493.8 ± 2049.05
63.1	561.81 ± 41.65	17592.1 ± 1094.88	30773.85 ± 2401.41
79.43	521.55 ± 39.09	21165.4 ± 1353.69	35613.2 ± 2807.92
100	482.48 ± 36.52	25374.45 ± 1677.19	41036.3 ± 3256.93

Table A10 Shear rate, shear viscosity, and normal stress differences data for PLA 4042D at 180°C

Rate s-1	η Pa-s	N_1-N_2 Pa
0.1	3187.83 ± 109.96	-
0.15849	3148.64 ± 97.98	-
0.25119	3130.88 ± 97.43	-
0.39811	3095.07 ± 96.32	-
0.63096	3082.51 ± 95.93	87.77 ± 36.44
1	3041.41 ± 94.65	216.96 ± 34.09
1.58489	3008.55 ± 111.86	603.61 ± 103.79
2.51189	2910.55 ± 117.95	1502.3 ± 227.04
3.98107	2479.58 ± 108.73	3143.58 ± 155.69

Table A11 Shear rate, shear viscosity, and normal stress differences data for PLA 4042D at 190°C

Rate s-1	η Pa-s	N_1-N_2 Pa
0.13	1596.62 ± 59.62	3.61 ± 0
0.2	1563.78 ± 62.11	4.7 ± 0
0.32	1536.94 ± 60.07	12.17 ± 0
0.5	1514.92 ± 59.35	9.84 ± 0
0.79	1498.58 ± 56.18	23.73 ± 3.78
1.26	1482.19 ± 54.91	71.36 ± 0.93
1.99	1458.86 ± 50.5	225.65 ± 18.88
3.15	1423.57 ± 39.87	621.83 ± 107.36
5	1333.11 ± 1.41	1553.84 ± 280.66

Table A12 Shear rate, shear viscosity, and normal stress differences data for PLA 4042D at 200°C

Rate s-1	η Pa-s	N_1-N_2 Pa
0.13	786.04 ± 69.24	8.04 ± 2.95
0.2	785.62 ± 62.85	1.69 ± 2.31
0.32	778 ± 66.35	2.14 ± 2.75
0.5	771.08 ± 59.57	13.59 ± 18.26
0.79	755.13 ± 52.23	10.94 ± 15.06
1.26	742.15 ± 49.75	5.6 ± 6.93
1.99	729.14 ± 42.63	18.24 ± 3.72
3.15	715.71 ± 43.93	74.14 ± 10.08
5	698.83 ± 38.02	265.93 ± 11.39

Table A13 Shear rate, shear viscosity, and normal stress differences data for PLA 7000D at 180°C

Rate s-1	η Pa-s	N_1-N_2 Pa
0.11	4394.33 ± 18.58	-
0.16	4375.28 ± 5.64	2.92 ± 3.8
0.23	4367.09 ± 11.69	10.79 ± 8.92
0.34	4358.69 ± 9.66	45.69 ± 9.18
0.5	4319.69 ± 15.87	100.42 ± 3.67
0.73	4283.5 ± 10.1	284.72 ± 15.49
1.08	4228.86 ± 16.89	633.16 ± 39.16
1.58	4136.59 ± 1.81	1352.35 ± 52.5
2.32	3902.32 ± 18.49	2786.81 ± 103.23
3.41	3136.93 ± 11.78	5290.89 ± 169.41
5	2114.89 ± 73.93	8255.08 ± 81.52

Table A14 Shear rate, shear viscosity, and normal stress differences data for PLA 7000D at 190°C

Rate s-1	η Pa-s	N_1-N_2 Pa
0.16	2638.07 ± 132.65	-
0.23	2622.19 ± 121.93	-
0.34	2609.4 ± 139.69	-
0.5	2590.84 ± 146.83	-
0.73	2577.28 ± 151.28	-
1.08	2551.47 ± 153.5	198.25 ± 59.65
1.58	2525.35 ± 151.26	457.87 ± 88.88
2.32	2479.33 ± 143.25	988.55 ± 132.23
3.41	2400.31 ± 128.76	2086.81 ± 217.52
5	2162.94 ± 118.26	4356.15 ± 414.72

Table A15 Shear rate, shear viscosity, and normal stress differences data for PLA 7000D at 200°C

Rate s-1	η Pa-s	N_1-N_2 Pa
0.16	1631.9 ± 85.02	-
0.23	1620.21 ± 71.72	-
0.34	1635.14 ± 46.13	-
0.5	1618.53 ± 38.81	-
0.73	1601.52 ± 42.82	-
1.08	1592.88 ± 47.88	81.48 ± 6.44
1.58	1570.98 ± 39.86	194.63 ± 9.36
2.32	1552.22 ± 39.77	436.11 ± 19.7
3.41	1522.53 ± 38.6	898.6 ± 69.01
5	1480.19 ± 32.55	1879.96 ± 161.75

Table A16 Shear rate, shear viscosity, and normal stress differences data for Ecoflex F BX at 180°C

Rate s-1	η Pa-s	N_1-N_2 Pa
0.1	2327.62 ± 254.15	-
0.13	2282.34 ± 265.41	102.96 ± 30.65
0.16	2242.43 ± 254.58	114.69 ± 22.55
0.2	2213.66 ± 247.79	150.32 ± 23.26
0.25	2175.12 ± 246.04	186.22 ± 22.51
0.32	2133.56 ± 252.9	243.87 ± 24.43
0.4	2088.47 ± 261.28	323.42 ± 38.73
0.5	2039.83 ± 261.77	402.43 ± 43.6
0.63	1989.63 ± 266.32	535.1 ± 46.71
0.79	1940.77 ± 286.39	724.16 ± 84.72
1	1888.74 ± 280.07	952.62 ± 92.85
1.26	1803.92 ± 271.11	1276.85 ± 185.13
1.58	1689.66 ± 286.55	1655.79 ± 337.67
1.99	1511.37 ± 247.49	2340.2 ± 259.42
2.51	1266.74 ± 244.39	3022.3 ± 294.53
3.15	977.9 ± 158.68	3579.16 ± 398.29

Table A17 Shear rate, shear viscosity, and normal stress differences data for Ecoflex F BX at 190°C

Rate s-1	η Pa-s	N_1-N_2 Pa
0.13	1804.07 ± 52.81	14.09 ± 6.35
0.2	1737.5 ± 45.19	25.34 ± 6.68
0.32	1680.08 ± 49.46	61.93 ± 2.51
0.5	1624.4 ± 28.75	138.56 ± 14.91
0.79	1579.64 ± 9.05	326.39 ± 26.7
1.26	1496.33 ± 20.01	687.54 ± 55.89
1.99	1410.11 ± 32.55	1403.1 ± 96.24
3.15	1278.51 ± 83.05	2806.54 ± 208.38

Table A18 Shear rate, shear viscosity, and normal stress differences data for Ecoflex F BX at 200°C

Rate s-1	η Pa-s	N_1-N_2 Pa
0.13	1372.43 ± 15.14	11.88 ± 4.05
0.2	1376.91 ± 47.62	20.38 ± 1.33
0.32	1345.02 ± 37.72	48.54 ± 0.56
0.5	1306.87 ± 20.56	90.77 ± 5.87
0.79	1276.8 ± 19.74	204.22 ± 16.37
1.26	1251.74 ± 24.25	444.26 ± 18.61
1.99	1205.55 ± 44.53	935.08 ± 57.41
3.15	1149.98 ± 53.39	1916.19 ± 167.55

Table A19. Frequency, complex viscosity, and storage modulus data obtained at 180°C and strain 5 % for PLA 7000 D after a single pass in Haake

Freq rad/s	η* Pa-s	G' Pa
0.32	2184.94 ± 19.77	17.4 ± 1.58
0.46	2160.83 ± 30.71	33.51 ± 0.31
0.68	2127.15 ± 28.79	73.73 ± 2.25
1	2107.8 ± 22.03	141.09 ± 2.42
1.47	2085.25 ± 23.64	263.7 ± 3.53
2.15	2052.93 ± 24.49	500.92 ± 3.51
3.16	2017.02 ± 19.79	935.42 ± 0.6
4.64	1984.51 ± 21.26	1760.25 ± 24.66
6.81	1958.06 ± 38.79	3230.04 ± 108.77
10	1921.59 ± 45.52	5610.86 ± 162.04
14.68	1840.06 ± 44	9194.95 ± 212.19
21.54	1723.36 ± 38.06	14530.4 ± 270.11
31.62	1578.25 ± 33.69	22230.15 ± 397.46
46.42	1416.66 ± 30.03	32962.55 ± 585.7
68.13	1246.04 ± 24.94	47328.85 ± 799.95
100	1073.07 ± 21.28	65718.05 ± 1153.36

Table A20. Frequency, complex viscosity, and storage modulus data obtained at 190°C and strain 8 % for PLA 7000 D after a single pass in Haake

Freq rad/s	η* Pa-s	G' Pa
0.32	1285.84 ± 3.52	9.09 ± 0.3
0.46	1289.03 ± 6.24	14.65 ± 2.49
0.68	1270.68 ± 6.25	29.44 ± 4.14
1	1262.6 ± 3.61	57.13 ± 2.34
1.47	1251.35 ± 3.14	110.31 ± 0.65
2.15	1239.32 ± 4.61	214.79 ± 0.36
3.16	1226.16 ± 5.9	407.92 ± 0.76
4.64	1218.62 ± 2.74	806.42 ± 48.49
6.81	1214.54 ± 1.01	1526.58 ± 34.18
10	1210.69 ± 3.58	2751.88 ± 27.87
14.68	1182 ± 0.12	4660.15 ± 3.72
21.54	1129.81 ± 2.11	7648.6 ± 8.57
31.62	1058.82 ± 3.68	12202.15 ± 30.33
46.42	973.51 ± 4.48	18931 ± 61.52
68.13	877.27 ± 4.7	28436.65 ± 118.86
100	774.05 ± 4.61	41301.45 ± 183.92

Table A21. Frequency, storage modulus, and complex viscosity data obtained at 190°C and strain 11 % for Ecoflex F BX 7011 after a single pass in Haake mixer

Freq rad/s	G' Pa	η* Pa-s
0.32	9.79 ± 0.36	784.68 ± 16
0.46	22.35 ± 0.91	763.12 ± 7.98
0.68	36.39 ± 0.63	760.66 ± 5.35
1	63.26 ± 0.79	752.28 ± 5.51
1.47	119.58 ± 1.87	737.27 ± 4.2
2.15	213.17 ± 1.74	722.47 ± 4.05
3.16	377.97 ± 5.32	704.2 ± 3.9
4.64	644.59 ± 9.93	680.82 ± 3.41
6.81	1085.72 ± 19.66	657.76 ± 3.39
10	1796.47 ± 33.81	637.39 ± 4.41
14.68	2823.62 ± 43.45	611.15 ± 4.37
21.54	4291.87 ± 54.24	578 ± 4.12
31.62	6349.26 ± 68.99	538.52 ± 3.71
46.42	9191.69 ± 83.2	494.92 ± 3.04
68.13	13126.2 ± 102.43	449.94 ± 2.45
100	18485.4 ± 123.02	404.16 ± 1.85

Table A22. Frequency, storage modulus, and complex viscosity data obtained at 180°C and strain 8 % for blend P90E10 (90 wt% PLA content)

Freq rad/s	G' Pa	η* Pa-s
0.10	23.47 ± 0.73	3744.81 ± 32.47
0.15	46.39 ± 0.98	3555.77 ± 14.56
0.22	64.6 ± 1.57	3399.58 ± 45.74
0.32	106.7 ± 2.73	3291.56 ± 43.22
0.46	171.89 ± 0.8	3227.05 ± 37.59
0.68	291.37 ± 3.97	3142.77 ± 29.88
1.00	499.22 ± 6.22	3045.59 ± 31.05
1.47	849.51 ± 2.71	2924.01 ± 32.21
2.15	1413.28 ± 7.25	2796.67 ± 34.36
3.16	2285.74 ± 3.9	2679.03 ± 36.06
4.64	3690.68 ± 10.61	2584.55 ± 33
6.81	5713.13 ± 22.69	2474.55 ± 28.88
10.00	8647.89 ± 20.93	2335.92 ± 27.45
14.68	12918.3 ± 4.38	2171.32 ± 26.81
21.54	19098.9 ± 49.92	1985.94 ± 26.35
31.62	27788.95 ± 145.28	1787.41 ± 25.44
46.42	39625.95 ± 314.7	1580.85 ± 24.62
68.13	55133.9 ± 565.05	1372.88 ± 23.08
100.00	74746.45 ± 940.49	1171.11 ± 20.94

Table A23. Frequency, storage modulus, and complex viscosity data obtained at 190°C and strain 8 % for blend P90E10 (90 wt% PLA content)

Freq rad/s	G' Pa	η* Pa-s
0.1	13.4 ± 0.49	2498.9 ± 180.37
0.15	19.17 ± 2.66	2370.64 ± 152.64
0.22	35.62 ± 0.55	2262.17 ± 52.79
0.32	59.5 ± 1.47	2213.93 ± 29.83
0.46	96.37 ± 0.54	2156.23 ± 7.07
0.68	161.54 ± 2.57	2101.38 ± 2.62
1	269.91 ± 3.53	2046.93 ± 5.96
1.47	461.68 ± 7.42	1991.17 ± 0.96
2.15	787.66 ± 15.58	1918.76 ± 7.66
3.16	1337.3 ± 45.57	1856.18 ± 18.38
4.64	2227.98 ± 77.27	1801.4 ± 23.3
6.81	3503.02 ± 90.96	1740.41 ± 25.51
10	5352.71 ± 102.63	1661.5 ± 24.67
14.68	8065.13 ± 118.24	1565.99 ± 21.93
21.54	12113.35 ± 137.25	1457.42 ± 17.94
31.62	18072.2 ± 187.38	1338.33 ± 14.61
46.42	26514.2 ± 257.53	1208.47 ± 12.11
68.13	38129.45 ± 378.8	1073.05 ± 9.93

Table A24. Frequency, storage modulus, and complex viscosity data obtained at 180°C and strain 8 % for blend P10E90 (10 wt% PLA content)

Freq rad/s	G' Pa	η* Pa-s
0.15	-	1637.43 ± 43.92
0.22	29.82 ± 1.79	1605.82 ± 117.92
0.32	43.77 ± 4.11	1574.65 ± 40.55
0.46	81.83 ± 4.71	1545.75 ± 81.74
0.68	138 ± 5.63	1510.18 ± 56.46
1.00	244.65 ± 6.28	1460.73 ± 59.36
1.47	407.29 ± 16.63	1400.33 ± 58.58
2.15	660.22 ± 27.06	1331.1 ± 56.44
3.16	1031.9 ± 48.46	1255.61 ± 52.23
4.64	1595 ± 87.36	1183.96 ± 52.02
6.81	2505.23 ± 181.35	1126.27 ± 60.79
10.00	3843.51 ± 233.77	1072.94 ± 57.77
14.68	5697.56 ± 271.36	1010.94 ± 48.97
21.54	8246.65 ± 323.66	938.38 ± 40.41
31.62	11753.8 ± 437.92	859.63 ± 34.26
46.42	16514.83 ± 596.78	777.4 ± 29.3
68.13	23006.23 ± 819.63	696.31 ± 25.31
100.00	31690.8 ± 1125.03	616.18 ± 22.09

Table A25. Frequency, storage modulus, and complex viscosity data obtained at 190°C and strain 7 % for blend P10E90 (10 wt% PLA content)

Freq rad/s	G' Pa	η* Pa-s
0.15	16.16 ± 0.42	1285.54 ± 8.7
0.22	21.73 ± 1.69	1195.65 ± 87.36
0.32	24.86 ± 2.22	1179.56 ± 53.09
0.46	47.88 ± 2.48	1169.53 ± 61.17
0.68	90.4 ± 5.42	1142.91 ± 68.31
1	157.93 ± 13.78	1107.83 ± 76.17
1.47	273.32 ± 21.24	1074.36 ± 68.66
2.15	454.4 ± 34.31	1025.52 ± 65.55
3.16	735.26 ± 55.18	973.31 ± 61.17
4.64	1151.43 ± 64.59	918.05 ± 55.16
6.81	1748.59 ± 125.99	862.21 ± 54.61
10	2685.6 ± 260.82	813.07 ± 60.37
14.68	4105.24 ± 326.02	772.31 ± 56.16
21.54	6078.95 ± 417.6	726.99 ± 49.05
31.62	8791.5 ± 565.2	675.67 ± 42.84
46.42	12514.85 ± 782.84	618.65 ± 37.29
68.13	17582.95 ± 1082.51	559.61 ± 32.12
100	24481.45 ± 1487.26	500.69 ± 27.92

Table A26. Shear rate and shear viscosity obtained at 190°C for PLA 7000 D after a single pass in Haake

Rate s-1	η Pa-s
0.1	1443.45 ± 61.24
0.15	1401.64 ± 54.51
0.22	1363.4 ± 46.28
0.32	1327.53 ± 47.87
0.46	1315.69 ± 52.1
0.68	1307.92 ± 46.24
1	1290.07 ± 45.61
1.47	1278.74 ± 41.59
2.15	1270.46 ± 40.43
3.16	1241.42 ± 44.77

Table A27. Shear rate and shear viscosity obtained at 190°C for Ecoflex F BX 7011 after a single pass in Haake

Rate s-1	η Pa-s
0.1	880.76 ± 31.14
0.15	868.91 ± 27.65
0.22	849.39 ± 31.23
0.32	821.03 ± 29.61
0.46	799.36 ± 31.65
0.68	794.12 ± 26.95
1	783.29 ± 27.69
1.47	773.63 ± 23.52
2.15	756.36 ± 25.14

Table A28. Shear rate and shear viscosity for blend P90E10 (90 wt% PLA content) at 180°C

Rate s-1	η Pa-s
0.1	3185.93 ± 267.36
0.15	3091.57 ± 256.74
0.22	3019.4 ± 205.61
0.32	2948.92 ± 217.48
0.46	2884.08 ± 214.73
0.68	2766.34 ± 194.53
1	2524.54 ± 150.81

Table A29. Shear rate and shear viscosity for blend P90E10 (90 wt% PLA content) at 190°C

Rate s-1	η Pa-s
0.1	2298.6 ± 97.52
0.15	2231.99 ± 71.02
0.22	2204.37 ± 81.05
0.32	2143.86 ± 77.31
0.46	2095.63 ± 81.5
0.68	2016.28 ± 68.43
1	1854.53 ± 65.57

Table A30. Shear rate and shear viscosity for blend P10E90 (10 wt% PLA content) at 180°C

Rate s-1	η Pa-s
0.11	1796.25 ±37.56
0.16	1732.68 ±48.08
0.23	1671.64 ±11.77
0.34	1679.99 ±23.51
0.5	1678.54 ±23.5
0.73	1652.25 ±45.81
1.08	1529.51 ±31.96
1.58	1488.69 ±51.34
2.32	1322.4 ±36.67

Table A31. Shear rate and shear viscosity for blend P10E90 (10 wt% PLA content) at 190°C

Rate s-1	η Pa-s
0.1	1527.11 ± 62.9
0.15	1458.72 ± 30.49
0.22	1437.56 ± 39.88
0.32	1434.85 ± 49.49
0.46	1412.16 ± 29.51
0.68	1387.76 ± 29
1	1326.51 ± 27.72
1.47	1269.92 ± 26.54
2.15	1201.08 ± 41.43

APPENDIX B

EXPERIMENTAL DATA FROM CAPILLARY RHEOMETRY

Table B1. Shear rate and shear viscosity data for PLA 4042D at 180°C in a two bore capillary rheometer and dies with D = 1mm

True* shear rate 1/s	Shear viscosity Pa.s
2947.09 ± 21.55	131.07 ± 1.61
1339.2 ± 9.98	243.46 ± 2.91
907.49 ± 6.34	330.96 ± 3.51
608.62 ± 4.54	445.38 ± 5.32
390.05 ± 2.91	594.72 ± 6.19
276.54 ± 2.49	723.43 ± 7.33
125.66 ± 0.94	1005.62 ± 0.42
57.1 ± 0.43	1187.74 ± 21.18

Table B2. Shear rate and shear viscosity data for PLA 4042D at 190°C in a two bore capillary rheometer and dies with D = 1mm

True shear rate 1/s	Shear viscosity Pa.s
2862.32 ± 3.25	118.73 ± 5.04
1299.78 ± 0.65	220.93 ± 9.37
591.23 ± 0.67	380.72 ± 16.15
268.64 ± 0.31	573.33 ± 24.32
122.06 ± 0.14	736.95 ± 41.69
55.46 ± 0.06	866.18 ± 61.25

* See Chapter 3 for definitions

Table B3. Shear rate and shear viscosity data for PLA 4042D at 200°C in a two bore capillary rheometer and dies with D = 1mm

True shear rate 1/s	Shear viscosity Pa.s
2749.35 ± 9.22	111.91 ± 0.45
1249.35 ± 3.83	200.01 ± 2.48
567.22 ± 0.94	321.97 ± 4.04
257.98 ± 1.58	466.32 ± 12.17
117.22 ± 0.35	553.31 ± 5.25
53.27 ± 0.16	614.02 ± 9.96

Table B4. Shear rate and shear viscosity data for PLA 7000D at 180°C in a two bore capillary rheometer and dies with D = 1mm

True shear rate 1/s	Shear viscosity Pa.s
3232.12 ± 12.89	140.62 ± 3.91
1469.06 ± 5.76	258.57 ± 6.34
995.93 ± 3.92	348.26 ± 7.77
667.15 ± 2.4	475.61 ± 8.59
426.45 ± 1.6	669.48 ± 12.79
303.44 ± 1	847 ± 16.67
137.8 ± 0.52	1319.77 ± 28.84
62.62 ± 0.23	1766.2 ± 46.8

Table B5. Shear rate and shear viscosity data for PLA 7000D at 190°C in a two bore capillary rheometer and dies with D = 1mm

True shear rate 1/s	Shear viscosity Pa.s
3069.27 ± 51.83	132.19 ± 4.3
1394.44 ± 23.54	239.43 ± 6.22
945.55 ± 15.96	324.35 ± 7.23
633.72 ± 10.7	437.47 ± 11.16
404.88 ± 6.84	596.45 ± 17.21
287.94 ± 4.86	726.58 ± 18.43
202.44 ± 3.42	874.65 ± 25.63
130.83 ± 2.21	1043.29 ± 17.52
94.55 ± 1.59	1163.98 ± 8.38
59.45 ± 1	1293.58 ± 9.56

Table B6. Shear rate and shear viscosity data for PLA 7000D at 200°C in a two bore capillary rheometer and dies with D = 1mm

True shear rate 1/s	Shear viscosity Pa.s
2913.9 ± 19.18	116.85 ± 0.94
1324.4 ± 8.72	217.99 ± 1.36
898.05 ± 4.22	292.75 ± 1.39
601.89 ± 3.96	389.46 ± 1
385.74 ± 2.54	513.43 ± 7.87
273.78 ± 1.38	617.39 ± 3.42
192.27 ± 1.27	716.71 ± 3.01
124.26 ± 0.82	829.46 ± 0.91
89.8 ± 0.59	898.44 ± 3.1
56.47 ± 0.37	995.94 ± 14.57

Table B7. Shear rate and shear viscosity data for Ecoflex F BX at 180°C in a two bore capillary rheometer and dies with D = 1mm

True shear rate 1/s	Shear viscosity Pa.s
2029.57 ± 34.34	174.9 ± 2.91
835.4 ± 14.37	293.63 ± 10.96
343.53 ± 5.91	461.41 ± 20.24
141.47 ± 2.43	658.61 ± 38.89
58.22 ± 1.01	888.71 ± 59.61

Table B8. Shear rate and shear viscosity data for Ecoflex F BX at 190°C in a two bore capillary rheometer and dies with D = 1mm

True shear rate 1/s	Shear viscosity Pa.s
2727.28 ± 43.95	131.16 ± 2.62
1239.23 ± 19.68	206.57 ± 8.16
560.65 ± 9.38	293.91 ± 12.97
254.5 ± 5.4	408.08 ± 25.41
116.27 ± 1.85	551.1 ± 45.41
53.32 ± 0.13	748.61 ± 40.47

Table B9. Shear rate and shear viscosity data for Ecoflex F BX at 200°C in a two bore capillary rheometer and dies with D = 1mm

True shear rate 1/s	Shear viscosity Pa.s
2697.35 ± 4.19	119.53 ± 5.76
1225.43 ± 1.65	185.62 ± 11.61
557.08 ± 2.09	269.19 ± 20.67
253.12 ± 0.45	372.13 ± 40.23
115.01 ± 0.21	472.03 ± 45.54
52.26 ± 0.09	583.82 ± 60.52

Table B10. Extensional rate and extensional viscosity data for PLA 4042D at 180°C in a two bore capillary rheometer and dies with D = 1mm

Extension rate 1/s	Extensional viscosity kPa.s
215.37 ± 3.14	4.71 ± 0.15
170.86 ± 2.74	4.68 ± 0.17
132.1 ± 7.82	4.83 ± 0.58
94.27 ± 2.85	5.12 ± 0.33
73.35 ± 1.63	5.16 ± 0.27
36.49 ± 0.42	5.97 ± 0.23
16.49 ± 0.2	7.12 ± 0.06

Table B11. Extensional rate and extensional viscosity data for PLA 4042D at 190°C in a two bore capillary rheometer and dies with D = 1mm

Extension rate 1/s	Extensional viscosity kPa.s
234.23 ± 1.11	3.4 ± 0.18
135.39 ± 2.74	3.62 ± 0.02
69.48 ± 1.91	4.28 ± 0.04
31.43 ± 2.62	5.58 ± 0.6

Table B12. Extensional rate and extensional viscosity data for PLA 4042D at 200°C in a two bore capillary rheometer and dies with D = 1mm

Extension rate 1/s	Extensional viscosity kPa.s
241.87 ± 24.3	2.71 ± 0.56
137.95 ± 14.21	2.77 ± 0.59
67.9 ± 11.73	3.5 ± 1.06
25.8 ± 3.4	5.86 ± 1.55

Table B13. Extensional rate and extensional viscosity data for PLA 7000D at 180°C in a two bore capillary rheometer and dies with D = 1mm

Extension rate 1/s	Extensional viscosity kPa.s
151.4 ± 22.86	4.87 ± 1.5
115.23 ± 13.73	4.75 ± 1.17
91.46 ± 8.77	4.77 ± 0.97
50.89 ± 5.59	4.98 ± 1.12
25.03 ± 2.33	5.64 ± 1.04

Table B14. Extensional rate and extensional viscosity data for PLA 7000D at 190°C in a two bore capillary rheometer and dies with D = 1mm

Extension rate 1/s	Extensional viscosity kPa.s
129.34 ± 2.14	2.93 ± 0.19
100.6 ± 3.64	2.98 ± 0.23
76.32 ± 3.79	3.09 ± 0.34
52.96 ± 4.55	3.24 ± 0.67
38.41 ± 1.68	3.55 ± 0.46
21.8 ± 1.22	4.85 ± 0.67

Table B15. Extensional rate and extensional viscosity data for PLA 7000D at 200°C in a two bore capillary rheometer and dies with D = 1mm

Extension rate 1/s	Extensional viscosity kPa.s
88.29 ± 1.92	2.97 ± 0.08
66.27 ± 0.25	3.02 ± 0
45.43 ± 1.28	3.11 ± 0.21
31.89 ± 0.14	3.56 ± 0.09
18.57 ± 0.29	4.6 ± 0.01

Table B16. Extensional rate and extensional viscosity data for Ecoflex F BX at 180°C in a two bore capillary rheometer and dies with D = 1mm

Extension rate 1/s	Extensional viscosity kPa.s
487.55 ± 29.37	4.92 ± 0.43
255.1 ± 16	5.56 ± 0.45
129.06 ± 10.65	6.2 ± 0.66
63.87 ± 3.67	6.69 ± 0.44
30.14 ± 1.74	7.27 ± 0.44

Table B17. Extensional rate and extensional viscosity data for Ecoflex F BX at 190°C in a two bore capillary rheometer and dies with D = 1mm

Extension rate 1/s	Extensional viscosity kPa.s
350.09 ± 21.34	4 ± 0.32
188.75 ± 15.48	4.49 ± 0.48
94.46 ± 11.96	5.26 ± 0.92
47.35 ± 7.62	6.04 ± 1.31

Table B18. Extensional rate and extensional viscosity data for Ecoflex F BX at 200°C in a two bore capillary rheometer and dies with D = 1mm

Extension rate 1/s	Extensional viscosity kPa.s
386.92 ± 8.61	2.9 ± 0.09
209.92 ± 7.47	3.16 ± 0.06
109.13 ± 5.61	3.51 ± 0.09
54.39 ± 4.14	4.03 ± 0.22

Table B19. Shear rate and extrudate swell data for PLA 4042D at 180°C in a stainless steel die with D = 2 mm and L/D = 16

Apparent shear rate 1/s	Swell Ratio D/D_0	Swell %
50	1.086	8.6 ± 0.74
100	1.1315	13.15 ± 1.9
136	1.1655	16.55 ± 1.25
150	1.17	17 ± 2.3
200	1.193	19.3 ± 2.45
300	1.225	22.5 ± 1.8
400	1.27	27 ± 0.4

Table B20. Shear rate and extrudate swell data for PLA 7000D at 180°C in a stainless steel die with D = 2 mm and L/D = 16

Apparent shear rate 1/s	Swell Ratio D/D_0	Swell %
50	1.178	17.8 ± 0.47
100	1.2	20 ± 0.54
136	1.233	23.25 ± 0.44
150	1.249	24.85 ± 0.41
200	1.265	26.45 ± 0.35
300	1.278	27.75 ± 0.66
400	1.294	29.4 ± 0.25

Table B21. Shear rate and extrudate swell data for Ecoflex F BX at 180°C in a stainless steel die with D = 2 mm and L/D = 16

Apparent shear rate 1/s	Swell Ratio D/D_0	Swell %
50	1.227	22.7 ± 0.4
100	1.292	29.2 ± 0.4
136	1.299	29.9 ± 0.25
150	1.313	31.3 ± 0.3
200	1.328	32.8 ± 0.25
300	1.34	34 ± 0.3

Table B22. Shear rate and shear stress data for PLA 4042D at 180°C in a stainless steel die with D = 1 mm and L/D = 16

Apparent shear rate 1/s	Apparent shear stress kPa
20.0 ± 0	38.28 ± 1.12
44.01 ± 0	74.38 ± 3.59
96.86 ± 0	135.16 ± 2.5
159.88 ± 0.66	180.12 ± 2.2
213.18 ± 0.66	212.66 ± 0.47
300.68 ± 0	247.34 ± 0.16
469.18 ± 0	290 ± 0
699.58 ± 0.66	325.47 ± 0.94
1032.37 ± 0	358.13 ± 1.41
2271.88 ± 0.66	438.28 ± 1.25
5001.76 ± 1.32	526.56 ± 3.28

Table B23. Shear rate and shear stress data for PLA 7000D at 180°C in a stainless steel die with D = 1 mm and L/D = 16

Apparent shear rate 1/s	Apparent shear stress kPa
20 ± 0	51.51 ± 0.57
30 ± 0	72.22 ± 1.45
50 ± 0	107.23 ± 2.9
75 ± 0	139.71 ± 2.67
100 ± 0	167.04 ± 2.57
200 ± 0.66	241.93 ± 1.87
300 ± 0.66	278.59 ± 4.63
400 ± 0.66	303.37 ± 4.61
600 ± 0.51	341.29 ± 1.67
800 ± 0.54	368.17 ± 4.55
900 ± 0.54	381.65 ± 4.31
1000 ± 0.66	389.96 ± 5.18
1200 ± 0	413.38 ± 12.28
1500 ± 0.66	448.16 ± 14.44
2000 ± 1.98	487.2 ± 12.04
3000 ± 0	533.06 ± 15.92

Table B24. Shear rate and shear stress data for Ecoflex F BX at 180°C in a stainless steel die with D = 1 mm and L/D = 16

Apparent shear rate 1/s	Apparent shear stress kPa
75 ± 0	98.24 ± 0.8
100 ± 0	118 ± 1.4
249.95 ± 0	201.32 ± 5.07
499.9 ± 0.93	282.6 ± 7.29
749.38 ± 0.46	338.76 ± 6.58
999.79 ± 0.54	381.23 ± 10.37
1499.69 ± 0.54	442.95 ± 7.3
2000.52 ± 0.66	486.34 ± 13
3500.21 ± 1.32	573.85 ± 5.8
5000.83 ± 1.07	637.07 ± 1.01
7501.24 ± 1.86	711.88 ± 0.96
9999.79 ± 1.32	773.53 ± 37.34

Table B25. Shear rate and shear viscosity data for LDPE LF-Y819-A at 180°C in a two bore capillary rheometer and dies with D = 1mm

True shear rate 1/s	Shear viscosity Pa.s
1517.75 ± 3.17	116.13 ± 0.71
689.45 ± 1.66	200.89 ± 0.69
312.92 ± 0.51	337.08 ± 0.69
142.34 ± 0.34	550.88 ± 0.57
64.68 ± 0.16	892.34 ± 5.84
29.49 ± 0.04	1430.81 ± 2.96

Table B26. Shear rate and shear viscosity data for LLDPE LL 1107x94 at 180°C in a two bore capillary rheometer and dies with D = 1mm

True shear rate 1/s	Shear viscosity Pa.s
1689.22 ± 15.2	194.1 ± 3.88
768.38 ± 4.61	423.73 ± 0.93
349.13 ± 1.75	797.44 ± 1.44
158.63 ± 0.71	1274.93 ± 3.06
72.08 ± 0.5	1815.1 ± 50.82
32.75 ± 0.29	2349.4 ± 72.83

Table B27. Extensional rate and extensional viscosity data for LDPE LF-Y819-A at 180°C in a two bore capillary rheometer and dies with D = 1mm

Extension rate 1/s	Extensional viscosity kPa.s
82.77 ± 0.59	19.53 ± 0.08
39.67 ± 0.64	30.38 ± 0.74
18.3 ± 0.21	49.31 ± 0.86

Table B28. Extensional rate and extensional viscosity data for LLDPE LL 1107x94 at 180°C in a two bore capillary rheometer and dies with D = 1mm

Extension rate 1/s	Extensional viscosity kPa.s
105.87 ± 0.85	4.34 ± 0.07
63.25 ± 1.27	4.01 ± 0.1
33.39 ± 0.23	4.23 ± 0.04

Table B29. Shear rate and extrudate swell data for LDPE LF-Y819-A at 180°C in a stainless steel die with D = 2 mm and L/D = 16

Apparent shear rate 1/s	Swell Ratio D/D_0	Swell %
50	1.88	88 ± 0.12
100	1.98	98 ± 0.06
136	1.99	99 ± 0.15
150	2.02	102 ± 0.08
200	2.08	108 ± 0.1
300	2.17	117 ± 0.09

Table B30. Shear rate and extrudate swell data for LLDPE LL 1107x94 at 180°C in a stainless steel die with D = 2 mm and L/D = 16

Apparent shear rate 1/s	Swell Ratio D/D_0	Swell %
50	1.27	27 ± 0.15
100	1.39	39 ± 0.04
136	1.41	41 ± 0.04
150	1.44	44 ± 0.02
200	1.47	47 ± 0.01
300	1.52	52 ± 0.03

Table B31. Shear rate and shear viscosity data for PLA 7000 D after a single pass in Haake, obtained at 190°C in a two bore capillary rheometer and dies with D = 1mm

True shear rate 1/s	Shear viscosity Pa.s
3596.93 ± 22.02	95.68 ± 2.71
2724.2 ± 38.31	119.56 ± 3.04
1238.78 ± 17.84	213.88 ± 6.35
839.25 ± 11.57	275.79 ± 7.8
561.36 ± 8.51	349.79 ± 7.42
359.36 ± 4.96	442.11 ± 9.38
255.57 ± 3.52	518.59 ± 10.27
116.12 ± 1.6	684.72 ± 19.37
52.77 ± 0.73	775.05 ± 27.4

Table B32. Shear rate and shear viscosity data for Ecoflex F BX 7011 after a single pass in Haake, obtained at 190°C in a two bore capillary rheometer and dies with D = 1mm

True shear rate 1/s	Shear viscosity Pa.s
3526.5 ± 17.01	88.64 ± 1.83
2670.02 ± 11.71	106.71 ± 2.9
1213.55 ± 6.44	159.01 ± 4.32
822.89 ± 3.85	188.55 ± 5.13
549.32 ± 1.03	222.19 ± 7.2
352.35 ± 0.88	259.97 ± 8.59
250.59 ± 1.17	287.87 ± 9.71
113.86 ± 0.53	356.15 ± 12.45
51.74 ± 0.24	471.93 ± 15.89

Table B33. Shear rate and shear viscosity data for blend P90E10 (90 wt% PLA content) obtained at 180°C in a two bore capillary rheometer and dies with D = 1mm

True shear rate 1/s	Shear viscosity Pa.s
2843.93 ± 11.09	117.5 ± 0.51
1291.48 ± 5.85	211.9 ± 1.44
876.14 ± 3.42	276.05 ± 2.18
586.03 ± 2.28	355.44 ± 4
373.99 ± 3.11	457.88 ± 4.74
266.51 ± 0.63	541.32 ± 7.69
121.23 ± 0.47	719.28 ± 10.28
55.09 ± 0.22	862.79 ± 11.7

Table B34. Shear rate and shear viscosity data for blend P90E10 (90 wt% PLA content) obtained at 190°C in a two bore capillary rheometer and dies with D = 1mm

True shear rate 1/s	Shear viscosity Pa.s
2703.04 ± 36.76	106.08 ± 23.43
1228.05 ± 16.7	180.89 ± 56.65
832.73 ± 11.33	227.51 ± 38.85
558.1 ± 7.58	280.44 ± 43.86
348.99 ± 10.72	328.52 ± 19.98
247.66 ± 7.6	370.87 ± 19.12
112.78 ± 3.46	450.32 ± 27.43
51.25 ± 1.58	535.58 ± 10.98

Table B35. Shear rate and shear viscosity data for blend P10E90 (10 wt% PLA content) obtained at 180°C in a two bore capillary rheometer and dies with D = 1mm

True shear rate 1/s	Shear viscosity Pa.s
2690.18 ± 11.44	119.93 ± 2.88
1222.46 ± 5.56	189.73 ± 5.19
828.94 ± 3.77	233.32 ± 3.06
555.57 ± 2.52	276.8 ± 7.12
354.94 ± 1.61	333.97 ± 5.56
252.43 ± 1.15	377.08 ± 4.6
114.7 ± 0.52	488.48 ± 2.59
52.12 ± 0.24	600.88 ± 0.59

Table B36. Shear rate and shear viscosity data for blend P10E90 (10 wt% PLA content) obtained at 190°C in a two bore capillary rheometer and dies with D = 1mm

True shear rate 1/s	Shear viscosity Pa.s
2674.64 ± 3.27	106.62 ± 1.96
1215.64 ± 1.48	162.27 ± 2.52
824.31 ± 1	193.93 ± 5.49
553.56 ± 3	230.78 ± 4.89
351.87 ± 0.34	274.1 ± 5.81
251.02 ± 0.3	307.02 ± 6.08
114.06 ± 0.14	387.7 ± 9.6
51.83 ± 0.06	494.73 ± 13.99

Table B37. Shear rate and shear stress data for blend P90E10 (90 wt% PLA content), obtained at 180°C in a stainless steel die with D = 1 mm and L/D = 16

Apparent shear rate 1/s	Apparent shear stress kPa
50	64 ± 0.74
100	100 ± 0.65
250	173 ± 1.61
480	230 ± 2.4
750	278 ± 1.2
1000	304 ± 2.2
1500	342 ± 3.1
2000	360 ± 5.2
3000	390 ± 4.4
3400	400 ± 4.84
3800	420 ± 5.14
4500	432 ± 6.3
5000	450 ± 7.12
6000	478.5 ± 6.29

Table B38. Shear rate and shear stress data for blend P10E90 190 wt% PLA content), obtained at 160°C in a stainless steel die with D = 1 mm and L/D = 16

Apparent shear rate 1/s	Apparent shear stress kPa
250	161.27 ± 4.5
500	232.2 ± 7.04
1000	314.22 ± 0.89
1500	370.79 ± 4.75
2000	421.32 ± 9.89
3000	481.49 ± 11.03
4000	534.28 ± 0
5000	570 ± 1.86
6000	604.22 ± 9.84
6750	635 ± 3.53
7000	644.77 ± 6.43
7600	670 ± 7.1
8000	677 ± 2.7
9000	705.23 ± 4.4

APPENDIX C

WALL SLIP DATA

Table C1. Apparent shear rate and wall shear stress data for PLA 4042 D at 180°C and stainless steel dies with different diameters and L/D = 16

Die 16 x 1 mm		Die 24 x 1.5 mm		Die 32 x 2 mm	
App. Shear Rate 1/s	Wall Shear Stress kPa	App. Shear Rate 1/s	Wall Shear Stress kPa	App. Shear Rate 1/s	Wall Shear Stress kPa
1993.07 ± 12.9	379.97 ± 14.67	2000.09 ± 0.55	424.65 ± 0.75	1500.28 ± 0.16	397.98 ± 1.63
1327.24 ± 0.47	343.66 ± 12.17	1327.08 ± 0	383.08 ± 0.81	928.47 ± 0.16	357.46 ± 1.66
876.22 ± 5.12	307.34 ± 13.63	881.17 ± 0.14	347.72 ± 1.08	574.6 ± 0	319.75 ± 2.07
584.84 ± 0.46	269.35 ± 15.4	584.84 ± 0.13	313.41 ± 1.21	355.72 ± 0	279.68 ± 1.56
388.42 ± 0.47	230.44 ± 16.07	386.43 ± 2.34	277.95 ± 0.53	220.16 ± 0	236.87 ± 1.69
257.51 ± 0.44	192.37 ± 16	257.62 ± 0	240.41 ± 0.03	136.26 ± 0	193.33 ± 1.54
170.94 ± 0.23	152.72 ± 12.96	171.2 ± 0	202.17 ± 0.1	84.36 ± 0	151.2 ± 1.54
113.5 ± 0	118.52 ± 10.2	113.55 ± 0.14	165.29 ± 0.36	52.13 ± 0	113.85 ± 1.16
75.33 ± 0	87.47 ± 6.8	75.35 ± 0	130.37 ± 0.46	32.32 ± 0.04	82.72 ± 0.89
50 ± 0	62.45 ± 5.24	50.01 ± 0.07	99.94 ± 0.43	20.01 ± 0	59.15 ± 0.49

Table C2. Apparent shear rate and wall shear stress data for PLA 7000 D at 180°C and stainless steel dies with different diameters and L/D = 16

Die 16 x 1 mm		Die 24 x 1.5 mm		Die 32 x 2 mm	
App. Shear Rate 1/s	Wall Shear Stress kPa	App. Shear Rate 1/s	Wall Shear Stress kPa	App. Shear Rate 1/s	Wall Shear Stress kPa
1327.01 ± 0.66	392.63 ± 6.57	1327.47 ± 0.49	420.46 ± 9.98	1500.04 ± 0.08	433.6 ± 0.23
875.99 ± 7.9	350.9 ± 5.88	880.93 ± 0.07	377.13 ± 8.95	928.35 ± 0	379.5 ± 1
585.08 ± 0.66	309.8 ± 5.78	584.75 ± 0	341.28 ± 8.1	574.49 ± 0.08	339.48 ± 1.71
387.73 ± 0.66	266.9 ± 5.83	388.09 ± 0.39	309.54 ± 6.43	355.67 ± 0.04	301.19 ± 2.73
258.1 ± 0.33	223.28 ± 4.49	257.62 ± 0	273.93 ± 6.99	220.1 ± 0.04	259.11 ± 4.4
170.83 ± 0.66	177.5 ± 3.61	171.15 ± 0.2	236.43 ± 7.82	136.32 ± 0.04	214.15 ± 5.74
113.5 ± 0	142.38 ± 1.34	113.64 ± 0	198.05 ± 7.77	84.36 ± 0	171.34 ± 5.18
75.33 ± 0	113.26 ± 2.08	75.3 ± 0	160.58 ± 6.8	52.13 ± 0.08	132.8 ± 3.19
50 ± 0	89.17 ± 1.9	49.99 ± 0.1	124.94 ± 6.58	32.29 ± 0	99.32 ± 0.99
20 ± 0	47.45 ± 1.48	20 ± 0	63.78 ± 4.3	19.99 ± 0.02	70.68 ± 0.09

Table C3. Apparent shear rate and wall shear stress data for Ecoflex F BX at 180°C and stainless steel dies with different diameters and L/D = 16

Die 16 x 1 mm		Die 24 x 1.5 mm		Die 32 x 2 mm	
App. Shear Rate 1/s	Wall Shear Stress kPa	App. Shear Rate 1/s	Wall Shear Stress kPa	App. Shear Rate 1/s	Wall Shear Stress kPa
1993.77 ± 11.64	398.82 ± 6.27	1999.72 ± 0.4	408.48 ± 5.09	1499.92 ± 0.06	375.63 ± 7.97
1327.7 ± 0.47	341.55 ± 6.75	1327.82 ± 0.39	350.26 ± 2.95	928.35 ± 0.02	308.16 ± 6.54
878.55 ± 4.83	285.1 ± 5.9	880.98 ± 0.1	295.51 ± 2.15	574.83 ± 0.04	249.48 ± 5.29
584.61 ± 0.76	235.34 ± 3.93	584.2 ± 4.59	245.94 ± 0.82	355.72 ± 0.05	198.41 ± 4.21
388.19 ± 0.76	192.04 ± 2.53	387.81 ± 3.02	201.29 ± 0.13	220.16 ± 0.03	155.46 ± 3.3
257.86 ± 0.38	154.46 ± 1.53	254.86 ± 1.95	161.95 ± 0.42	136.26 ± 0.07	119.92 ± 4.24
171.06 ± 0.27	122.72 ± 2.1	171.01 ± 0.1	129.95 ± 0.13	84.25 ± 0.02	91.79 ± 3.25
113.5 ± 0	95.79 ± 2.66	113.36 ± 0.2	102.42 ± 0.38	52.25 ± 0.01	69.83 ± 2.96
75.33 ± 0	74.55 ± 2.15	75.44 ± 0.05	80.97 ± 0.45	32.35 ± 0.02	53.04 ± 2.25
50 ± 0	57.68 ± 1.94	49.92 ± 0.05	64.06 ± 0.69	20.01 ± 0.01	40.32 ± 1.71